

**UNCOVERING THE MOLECULAR BASIS FOR FATTY ACID SYNTHASE  
PRODUCT SPECIFICITY: STRUCTURAL AND KINETIC EVALUATION OF  
THIOESTERASE I AND THIOESTERASE II**

BY

**Melissa Kay Ritchie**

A Dissertation Submitted to the Graduate Faculty of  
WAKE FOREST UNIVERSITY GRADUATE SCHOOL OF ARTS AND SCIENCES

In Partial Fulfillment of the Requirements

For the Degree of

DOCTOR OF PHILOSOPHY

Biochemistry and Molecular Biology

December 2013

Winston-Salem, North Carolina

Approved by:

W. Todd Lowther, Ph.D., Advisor

Examining Committee:

Steve Kridel, Ph.D., Chairperson

Douglas S. Lyles, Ph.D.

Thomas Hollis, Ph.D.

Leslie Poole, Ph.D.

## **Acknowledgements**

I am very grateful to my advisor, Dr. W. Todd Lowther, for accepting me into his research group and for providing me the opportunity to advance my training as a research scientist at Wake Forest School of Medicine. His expertise, mentorship, and faithful dedication toward maintaining a collaborative work environment were fundamental to my success as a graduate student. His enthusiasm and motivation toward his entire research staff are invaluable assets, and enhance the reputation of the Biochemistry Department.

I want to thank all of the former and current students of the Lowther Lab with whom I had the pleasure to conduct research. As well, I would like to extend many thanks to all of the Biochemistry Department professors who played fundamental roles in my success. The diversity of expertise in the Biochemistry Department is a great resource for all graduate students, and many of you provided critical insights when I needed advice. I want to specifically thank my committee members who provided guidance and support throughout my research efforts over the past few years. Their commitment toward my Ph.D. training has also been an invaluable asset.

I finally want to thank all of my family and friends who have whole-heartedly supported my decision to earn my Ph.D. For my mother, I am thankful for every phone call answered, no matter the time of day, for every word of encouragement, and for each time you entertained my 'alternative ambitions'. For Joseph, I am thankful for your love and commitment and for providing a foundation with which I could always lean on. My friends have become my family, and so to my family, I am blessed to share with you all of my success.

## Table of Contents

<b>Acknowledgements</b>	ii
<b>List of Illustrations</b>	vi
<b>List of Tables</b>	vii
<b>List of Abbreviations</b>	viii
<b>Abstract</b>	xi
<b>Chapter 1 Introduction</b>	1
1.1 Cellular Lipids	2
1.2 FASN Upregulation in cancer	2
1.3 Type I versus Type II Fatty Acid Synthase Assemblies	3
1.3.1 Structure of the Mammalian Type I FASN	4
1.3.2 Mammalian Type I FASN Mechanism	7
1.4 Products of Type I and Type II FASN	9
1.4.1 Type II FASN Product Distribution	9
1.4.2 Type I FASN Product Distribution	10
1.5 FASN-like Modular Synthases: Polyketide Synthase (PKS) and Non-ribosomal Peptide Synthetase (NRPS)	11
1.5.1 Polyketide Synthase Assembly and Catalytic Mechanism	13
1.5.2 Non-ribosomal Peptide Synthetase Assembly and Catalytic Mechanism	15
1.6 Efficiency of Product Turnover by FASN, PKS, and NRPS	18
1.7 Type II Thioesterases	20
1.8 Central Role of the Carrier Protein in Multifunctional Enzyme Complexes	21
1.9 Interactions between Carrier Protein Domains and Thioesterase Activities are Promising Targets for Therapeutic Development	24
References	27
<b>Chapter 2 Crystal Structure of Human Thioesterase II: Insights into the Molecular Basis for the Novel Modulation of Fatty Acid Synthase Activity</b>	41
Abstract	42
2.1 Introduction	44
2.2 Experimental Procedures	47
2.2.1 Purification of human ACP	47
2.2.2 Purification of human TE2	48
2.2.3 Purification of HAAS+His	49
2.2.4 Purification of <i>S. coelicolor</i> phosphopantetheinyl transferase (Loader+His)	49
2.2.5 Synthesis and purification of 4'PP-ACP (ACPSH)	49
2.2.6 Synthesis and purification of acyl-ACP	50
2.2.7 KDH-coupled assay for monitoring acyl-CoA hydrolysis	51
2.2.8 Inhibition Assay	51
2.2.9 Quantitative MALDI-TOF MS discontinuous assay for	

	monitoring acyl-ACP hydrolysis	52
	2.2.10 Crystallization of TE2	53
	2.2.11 Data Collection and Structure Determination	53
2.3	Results	54
	2.3.1 TE2 is an $\alpha/\beta$ serine hydrolase related to PKS/NRPS type II thioesterases	54
	2.3.2 TE1 and TE2 differential activity toward acyl substrates and inhibition via $\beta$ -lactone natural products suggest unique active site architectures and ACP interactions	57
	2.3.2A Kinetic evaluation of TE1 and TE2 hydrolysis of acyl-CoA substrate mimetics	57
	2.3.2B Evaluation of $\beta$ -lactone congeners on TE1 and TE2 hydrolase activity	59
	2.3.2C Kinetic evaluation of TE1 and TE2 hydrolysis of C16-ACP	61
	2.3.3 The 2.62 Å crystal structure of Human TE2 revealed strong homology to PKS/NRPS type II thioesterases and is in a closed conformation with sub-optimal active site geometry	65
	2.3.3A Crystal structure of Human TE2	65
	2.3.3B Comparisons of TE2 Structural Homologues	71
2.4	Discussion	75
2.5	Conclusions	80
	References	81

### **Chapter 3: Alternative acyl-ACP synthetic strategies and crystallization experiments** 92

3.1	Introduction	93
3.2	Experimental Procedures	97
	3.2.1 Purification of MBP-CoA A, MBP-CoA D, and MBP-CoA E	97
	3.2.2 Purification of Sfp+His	97
	3.2.3 Purification of human $\Delta N5\Delta C16$ ACP (nACP)	98
	3.2.4 Synthesis of <i>O</i> -acyl-ACP and <i>O</i> -acyl-nACP (acyl- <sub>crypto</sub> ACP and acyl- <sub>crypto</sub> nACP)	99
	3.2.5 Purification of iodoacetamide derivatized <i>S</i> -acyl-ACP (acyl- <sup>AA</sup> ACP)	100
	3.2.6 Quantitative MALDI-TOF MS discontinuous assay	100
	3.2.7 Purification of human TE2 (TE2-MBP)	101
	3.2.8 Purification of human $\Delta N9$ TE2 (nTE2)	102
	3.2.9 Purification of the S2308A-H2481A double mutants of TE1 or ACP-TE1 (TE1 DM; ATE DM)	102
	3.2.10 Crystallization of WT or Selenomethionine (SeMet) TE2 and nTE2	103
	3.2.11 Co-crystallization trials	104
	3.2.12 Data collection and processing	105
3.3	Results	105
	3.3.1 acyl- <sub>crypto</sub> ACP and acyl- <sub>crypto</sub> nACP syntheses	105

3.3.2	ESI-MS and ESI-MS/MS analyses of crypto substrates	106
3.3.3	Kinetic evaluation of TE1 and TE2 against C14- <sup>AA</sup> ACP and C16- <sup>AA</sup> ACP	118
3.3.4	WT and SeMet TE2-MBP crystal data	118
3.3.5	Co-crystallization experiments	122
3.4	Discussion	124
3.5	Conclusions	128
	References	129
<b>Chapter 4: Conclusions and Future Direction</b>		<b>140</b>
4.1	Conclusions	141
4.2	Future Directions	146
	References	150
<b>Curriculum Vitae</b>		<b>159</b>

## List of Illustrations

1.1	The 3.2 Å crystal structure of mammalian FASN	5
1.2	Reaction scheme for mammalian fatty acid biosynthesis	8
1.3	Biosynthetic modules for 6-deoxyerythronolide B synthase	14
1.4	Biosynthetic modules of surfactin A synthetase	17
1.5	2.8 Å crystal structure of recombinant human TE1 domain of FASN inhibited by Orlistat	24
2.1	Sequence alignment of TE1 and TE2	55
2.2	Sequence alignment for type II thioesterases from FASN, PKS and hybrid PKS/NRPS assemblies	56
2.3	Results of TE1 and TE2 kinetic evaluations against acyl-CoA substrate mimetics	58
2.4	Results of TE1 and TE2 inhibition by β-lactone congeners Orlistat and Ebelactone B	60
2.5	Synthesis and analysis of acyl-ACP substrates	62
2.6	Validation experiments for quantitative MALDI-TOF MS kinetic analyses of TE1 and TE2 hydrolysis of acyl-ACP substrates	64
2.7	Results of MALDI-TOF MS kinetic evaluation of TE1 and TE2 hydrolysis of C16-CoA	66
2.8	Current $2F_o-F_c$ electron density map with TE2 active site residues and conserved water molecule	69
2.9	2.62 Å crystal structure of human TE2	70
2.10	Comparison of TE2 structural homologues	72
2.11	Analysis of the hydrophobic content at the interface between the hydrolase cores and capping domains of TE1 and TE2	74
2.12	Electrostatic surface representation of TE1, TE2 and RedJ	76
3.1	Crystal structure of human ACP	95
3.2	MALDI-TOF MS results for crypto substrate loading of ACP	108
3.3	MALDI-TOF MS results for crypto substrate loading of nACP	110
3.4	Comparison of ESI-MS analyses of cC12-cC18 substrates	112
3.5	Results of ESI-MS for C12 crypto-substrate (cC12)	113
3.6	Comparison of ESI-MS/MS fragmentation analyses of the cC12 315 m/z species and related species for cC14-cC18	114
3.7	Analyses of ESI-MS/MS fragmentation of the 315 m/z species from cC12	115
3.8	Comparison of ESI-MS/MS fragmentation analyses of the cC12 427 m/z species and related species for cC14-cC18	116
3.9	Analyses of the MS/MS fragmentation of the 427 m/z species from cC12	117
3.10	MALDI-TOF results of IAA-treated ACP and synthesis of <i>S</i> -acyl- <sup>AA</sup> ACP substrates	119
3.11	Representative TE2-MBP crystals and sample diffraction image to 3.0 Å resolution	120
3.12	Initial crystal hits from co-crystallization experiments	123

## List of Tables

2.1	Data collection and refinement statistics	68
3.1	Substrate molecular weights and corresponding acyl- <sub>crypto</sub> ACP products	107
3.2	Substrate molecular weights and corresponding acyl- <sub>crypto</sub> nACP products	109
3.3	Summary of data collection statistics	121

## List of Abbreviations

4'PP	4'-phosphopantetheinyl
6-DEBS	6-deoxyerythronolide B synthase
6dEB	6-dexoyerythronolide
$\alpha$ -KG	$\alpha$ -ketoglutarate
A	Adenylation
<sup>AA</sup> ACP	Iodoacetamide derivatized Acyl Carrier Protein
<sup>AA</sup> ACPSH	4'-phosphopantetheinyl iodoacetamide derivatized Acyl Carrier Protein
ACC	Acetyl CoA Carboxylase
ACL	Acetyl CoA Lyase
ACN	Acetonitrile
ACP	Acyl Carrier Protein
ACPSH	4'-phosphopantetheinyl-Acyl Carrier Protein
Acyl- <sub>crypto</sub> ACP	<i>O</i> -linked acyl-4'-phosphopantetheinyl-Acyl Carrier Protein
Acyl- <sub>crypto</sub> nACP	<i>O</i> -linked acyl-4'-phosphopantetheinyl- $\Delta$ N5 $\Delta$ C16 Acyl Carrier Protein
AT	Acyl transferase
ATE DM	ACP-TE1 S2308A H2481 double mutant
ATP	Adenosine triphosphate
C14- <sup>AA</sup> ACP	Myristoyl-4'PP- iodoacetamide derivatized Acyl Carrier Protein
C16- <sup>AA</sup> ACP	Palmitoyl-4'PP- iodoacetamide derivatized Acyl Carrier Protein
C	Condensation
CCD	Charge-coupled detector
C12	Laurate
C14	Myristate
C16	Palmitate
C18	Stearate
C10-ACP	decanoyl-Acyl Carrier Protein
C12-ACP	Lauryl-4'PP- Acyl Carrier Protein
C14-ACP	Myristoyl-4'PP- Acyl Carrier Protein
C16-ACP	Palmitoyl-4'PP- Acyl Carrier Protein
C18-ACP	Stearoyl-4'PP- Acyl Carrier Protein
CoA	Coenzyme A
CoA A	Pantothenate kinase
CoA D	Phosphopantetheine transferase
CoA E	Phosphopantothenoylcysteine decarboxylase
DH	Dehydratase
DEBS1	Deoxyerythronolide synthase complex I
DEBS2	Deoxyerythronolide synthase complex II
DEBS3	Deoxyerythronolide synthase complex III
DMSO	Dimethyl sulfoxide
DTNB	5,5'-dithiobis-(2-nitrobenzoic acid)
DTT	Dithiothreitol
E	Epimerization
EDTA	Ethylenediamine tetraacetic acid



ER	Enoyl reductase
ESI-MS	Electrospray ionization mass spectrometry
ESI-MS/MS	Electrospray ionization tandem mass spectrometry
FASN	Fatty Acid Synthase
HAAS+His	<i>Holo</i> acyl-Acyl Carrier Protein Synthase
HEPES	4-(2-hydroxyethyl) piperazine-1-ethanesulfonic acid
IAA	Iodoacetamide
IPTG	Isopropyl $\beta$ -D-1-thiogalactopyranoside
KCl	Potassium chloride
KDH	$\alpha$ -keto glutarate dehydrogenase
K <sub>2</sub> HPO <sub>4</sub>	Di-potassium monohydrogen phosphate
KR	Keto reductase
KS	Keto synthase
LCFA	Long chain fatty acid
LD	Linker domain
Loader+His	<i>S. coelicolor</i> phosphopantetheinyl transferase
M	N-methylation
MALDI-TOF	Matrix-assisted laser desorption ionization-time of flight
MAT	Malonyl-acetyl transferase
MBP	Maltose binding protein
MCFA	Medium chain fatty acid
MgCl <sub>2</sub>	Magnesium chloride
MPD	Methyl propanediol
MWCO	Molecular weight cut-off
m/z	mass/charge
nACP	$\Delta$ N5 $\Delta$ C16 Acyl Carrier Protein (residues 2123-2196)
NaCl	Sodium chloride
NAD <sup>+</sup>	Nicotinamide adenine dinucleotide (oxidized)
NADH	Nicotinamide adenine dinucleotide (reduced)
NADP <sup>+</sup>	Nicotinamide adenine dinucleotide phosphate (oxidized)
NADPH	Nicotinamide adenine dinucleotide phosphate (reduced)
NaH <sub>2</sub> PO <sub>4</sub>	Sodium dihydrogen phosphate
NaNO <sub>3</sub>	Sodium nitrate
NaOAc	Sodium Acetate
(NH <sub>4</sub> ) <sub>2</sub> SO <sub>4</sub>	Ammonium Sulfate
NRP	Non-ribosomal peptide
NRPS	Non-Ribosomal Peptide Synthetase
nTE2	$\Delta$ N9 TE2
$\Psi$ ME	Pseudo methyltransferase
$\Psi$ KR	Pseudo keto reductase
PCP	Peptidyl carrier protein
PEG	Polyethylene glycol
PKS	Polyketide Synthase
PMSF	Phenylmethylsulfonyl fluoride
PUFA	Poly-unsaturated fatty acid
RFU	Relative fluorescence unit

SeMet	Selenomethionine
Sfp+His	<i>B. subtilis</i> phosphopantetheinyl transferase
Surf A	Surfactin A synthetase complex A
Surf B	Surfactin A synthetase complex B
Surf C	Surfactin A synthetase complex C
Surf S	Surfactin A synthetase
T	Thiolation
TCA	Tricarboxylic Acid
TE	Thioesterase
TEV	Tobacco etch virus
TE1	Thioesterase I
TE1 DM	TE1 S2308A H2481A double mutant
TE2	Thioesterase II
TE2-MBP	TE2 cleaved from N-terminal 6X His-tag-MBP fusion
TPP	Thiamine pyrophosphate
Tris	2-amino-2-hydroxymethyl-propane-1,3-diol

## Abstract

Fatty acid synthase (FASN) is a multifunctional homodimeric enzyme solely responsible for the synthesis long chain fatty acids (LCFAs) *de novo*. Fatty acids, and their lipid derivatives, are critical components of all cellular biological processes, including energy storage and utilization, membrane maintenance and expansion, post-translational modification of proteins, and intracellular signalling. FASN primarily generates palmitate (C16) and to a lesser extent stearate (C18), and this strict product distribution is dictated by the acyl chain-length selectivity of the endogenous thioesterase (TE1) domain. With the exception of lactating breast, liver and adipose tissues, FASN expression is essentially absent in normal cells since these cells obtain lipids from the diet. In lactating breast, the product distribution of FASN is modulated by a monofunctional type II thioesterase, called thioesterase II (TE2), to favor the medium chain fatty acids (MCFAs) laurate (C12) and myristate (C14). The TE2 interaction with FASN and its ability to outcompete TE1 for the acyl substrate tethered to the acyl carrier protein (ACP) domain is quite remarkable, yet the mechanisms of binding and catalysis are poorly understood. Moreover, there are additional implications for understanding TE1 and TE2 mechanisms of catalysis as it relates to chemotherapeutic research targeting FASN. It is widely accepted that increased lipogenesis of LCFAs via FASN is a hallmark of neoplastic transformation. Therefore, FASN has been firmly established as a target for pharmaceutical intervention in several cancers, including lung, colon, prostate, ovarian and breast. Current drug discovery strategies have succeeded in killing cancer cells *in vitro* and *in vivo* via targeting FASN through inhibition of the endogenous thioesterase (TE1) domain. The success of TE1-

targeted FASN inhibition warrants a more comprehensive understanding of the interplay between TE1 and TE2 and their relationship to FASN product distribution. Aberrant TE2 expression and activity on TE1-inactivated FASN could rescue fatty acid biosynthesis, thus negating current drug development strategies.

The data presented in this manuscript support the overarching hypothesis that the differences in tertiary structural organization, substrate specificity and ACP binding by TE1 and TE2 warrants further investigation for additional, more comprehensive thioesterase inhibitors as well as the need to explore potential antagonists targeting the ACP-TE1 or ACP-TE2 interface. The secondary structure superpositions of TE1 and TE2 reveal a conserved  $\alpha/\beta$  serine hydrolase fold with divergent subdomain architectures as well as unique substrate binding motifs in the active sites. The kinetic studies revealed only modest differences in TE1 specific activity against acyl-CoA and acyl-ACP substrates, whereas TE2 resulted with a 20-fold increase in activity against acyl-ACP compared to acyl-CoA substrates. Expanding our understanding of the ACP-TE interactions will help guide future drug discovery efforts against FASN for the treatment of cancer.

## **Chapter 1: Introduction**

## 1.1 Cellular Lipids

Lipids are essential components of every cellular organism in existence, serving fundamental roles in cell biology including membrane and organelle synthesis and organization, energy storage and utilization, and intracellular signalling (1-6). The variety of cellular lipids includes the free fatty acids present as acyl-coenzyme A (CoA) thioesters, glycerophospholipids, sphingolipids, and sterols. In eukaryotes and prokaryotes, lipids are derived from exogenous sources (i.e., diet/absorption) and endogenously via *de novo* fatty acid biosynthesis. When environmental resources are insufficient, *de novo* fatty acid biosynthesis supplements the intracellular lipid pool to maintain cellular homeostasis. In higher eukaryotes, dietary sources supply the majority of lipids utilized by cells. Therefore, the endogenous *de novo* synthetic pathway primarily serves to balance the carbon energy status of cells via transforming acetyl-CoA into saturated free fatty acids for energy storage.

## 1.2 FASN Upregulation in Cancer

In addition to their vital role in normal cellular function, fatty acids play an equally crucial role in the survival and proliferation of several cancers (7-10). In contrast to normal tissues, cancer cells do not readily absorb dietary sources of lipids to support their high metabolic needs; therefore, cancer cells are dependent on endogenous fatty acid stores generated by FASN. The link between cancer cell metabolism and FASN has been demonstrated in several publications which show upregulation of the FASN enzyme in a multitude of cancers, including lung, liver, ovarian, breast, prostate and colon (8-25). The observation that FASN expression is essentially devoid in normal tissues, with the

exceptions being liver and adipose tissue, has led the research community toward drug discovery against FASN. Moreover, since FASN is the sole enzyme responsible for *de novo* fatty acid synthesis, FASN represents an attractive target for cancer therapy.

Within the last thirty years, several FASN inhibitors have been identified. The first organic compounds discovered to inhibit the keto-synthase (KS) domain were derived from fungal sources, and several synthetic analogues soon followed (26-29). The potent antioxidant epigallocatechin (ECGC) from green tea and other heterocyclics were shown to have mild inhibitory effects as well, but the specific domain interactions have yet to be fully characterized (30-32). Similarly, one study identified the efficacy of mono- and poly-unsaturated long-chain fatty acids to attenuate FASN activity, via non-covalent interactions with the endogenous thioesterase (TE1) domain (33-34). Surprisingly, the most recent advance in FASN-targeted cancer therapy research came about when the weight-loss drug Orlistat was identified to inhibit the TE1 domain *in vitro* (35-40). Follow-up studies on recombinant enzyme, cancer cell lines, and tumor xenograft experiments in mice using Orlistat treatment resulted in complete enzyme inhibition, cancer cell death, and tumor regression, respectively. The cumulative achievements in understanding FASN catalysis, substrate recognition, and detailed structural organization continues to advance the drug discovery efforts of FASN-targeted cancer research.

### **1.3 Type I versus Type II Fatty Acid Synthase Assemblies**

Prokaryotes and eukaryotes have evolved architecturally divergent yet mechanistically similar FASN systems. In bacteria, such as *Escherichia coli*, the Type II

FASN is composed of discrete, monofunctional enzymes which coalesce to form a multi-enzyme complex (41). In contrast, the eukaryotic Type I FASN of the cytosol is a 560 kDa homodimer composed of identical  $\alpha$  subunits that contain all necessary catalytic functions (29,42). The fungal Type I FASN contains two multifunctional polypeptides that assemble into a  $\alpha_6\beta_6$  dodecamer with a mass of 2.6 MDa (43-47). A small subset of *Cornyforme* prokaryotes have evolved an  $\alpha_6$  hexameric Type I FASN of 2.0 MDa that can produce both saturated and unsaturated fatty acids products (48-49). Interestingly, there is a Type II FASN system, similar to bacteria, within the mitochondria, which is thought to be primarily responsible for the synthesis of octanoic acid for lipoic acid synthesis (50-53). Despite the various architectures and molecular assemblies, all FASNs catalyze condensation and sequential reduction of acetyl-CoA and malonyl-CoA to generate fatty acids.

### 1.3.1 Structure of the Mammalian Type I FASN

The crystal structure of the  $\alpha_2$  homodimeric porcine FASN was first published in 2006 and then later in 2008 with improved resolution (54). These structures constitute the only available crystal structures for intact FASN. The FASN homodimer organizes seven functional domains (Figure 1), of which six are catalytic, to synthesize the sixteen carbon (C16) fatty acid palmitate. The primary structural arrangement of FASN begins with the ketoacyl-synthase (KS) domain, followed by the malonyl-acetyl transferase (MAT), dehydratase (DH), enoyl reductase (ER), ketoacyl-reductase (KR), acyl carrier protein (ACP), and thioesterase (TE) domains. In order to differentiate this C-terminal TE domain from other human thioesterases, we denote the endogenous TE domain as TE1. The ACP domain is non-catalytic and functions to shuttle the growing acyl chain to the



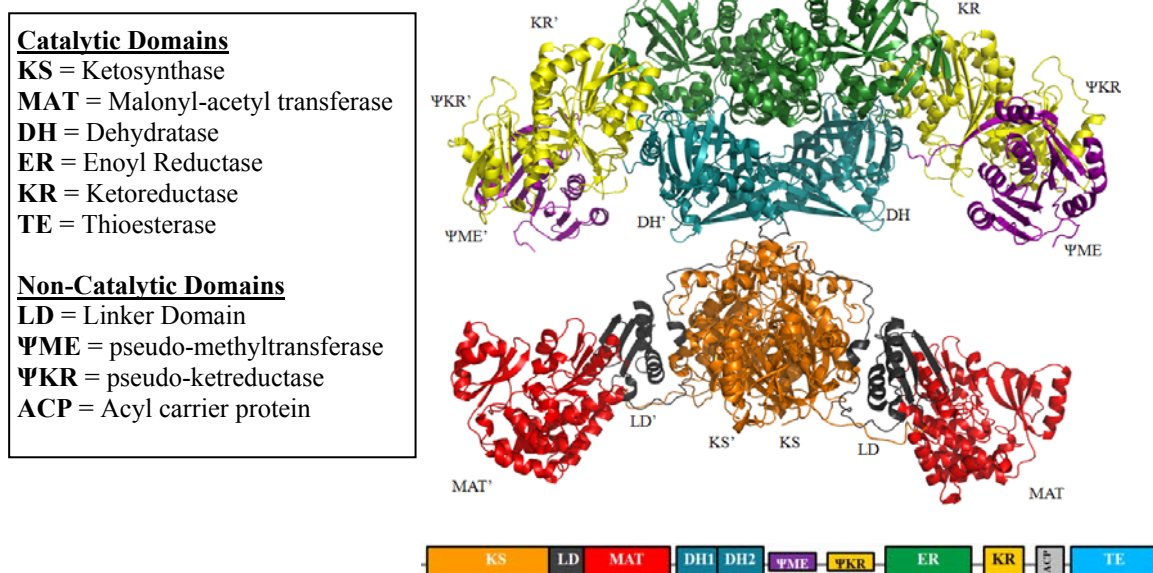


**Figure 1. The 3.2 Å crystal structure of mammalian FASN.** Five catalytic domains of FASN are modeled, and the domains are colored based on the coloring scheme for the linear peptide diagram shown below. The structure resembles a body; the condensing activities of KS and MAT form the lower body legs; the catalytic KR, DH, KR and non-catalytic ΨME and ΨKR domains makeup the upper body arms. Due to low resolution data and the inherent flexibility of the ACP-TE1 C-terminus, neither domain is modeled. Homology modeling using the equivalent monofunctional *E. coli* enzyme crystal structures revealed two unexpected ΨME and ΨKR structural features. These pseudo domains are structurally homologous to other ME and KR enzymes, but neither are active or confer additional activity for the FASN dimer, but serve to orient the catalytic domains for cooperative, iterative processing of the acyl intermediate. The only structured linker domain (LD) observed with this 3.2 Å data connects the condensing KS and MAT domains.

other domains, as described in more detail below. Importantly, only five of the seven domains are observed in FASN structure, due to the inherent flexibility of the C-terminal ACP and TE1 domains. High resolution structures of recombinantly expressed ACP or TE1 are available, but their orientation within the context of the FASN dimer is still unclear (37,55).

The crystal structure revealed that the FASN monomers are positioned along a central vertical axis in a head-to-head and tail-to-tail orientation. Consistent with their *E. coli* counterparts, the KS, DH and ER domains form dimers, and their interfaces are positioned along the central axis of the FASN body (41). In contrast, the FASN MAT and KR domains are apparently monomeric, yet the *E. coli* AT equivalent is dimeric and the *E. coli* KR is tetrameric. Interestingly, the five structured domains are architecturally separated between the condensing activities of the KS and MAT domains (lower body) and the catalytic KR, ER, and DH domains (upper body). The junction between the upper and lower body elements may serve as a pivot point, facilitating ACP shuttling of the growing acyl chain between the condensing activities of one monomer to the catalytic domains of the complementary monomer. Smith *et al.* demonstrated the cooperativity of the dimer by generating a dimer of one catalytically active monomer and a comprehensive knock-out inactive monomer (56). The mutant homodimer maintained 32% activity compared to the WT homodimer, whereas dissociated WT monomers are incapable of palmitate synthesis. The results of this study revealed the necessity of the dimeric organization for a single monomer or cooperative FASN monomers to maintain activity. An interesting observation of asymmetry for the lower body portion of FASN is seen as a slight tilt of the left-side KS-MAT domains toward the upper body region. This

asymmetry of FASN has lead researchers to consider the asynchronous activity of the enzyme. This notion is supported by cryo-electron microscopy analyses of FASN which determined that the dimer flexibility enables catalysis (57).

As described in more detail the next section, the growing acyl chain (Figure 2) is covalently tethered via a thioester linkage to the 4'-phosphopantetheinyl (4'PP) moiety attached to Ser2156 of the ACP domain. Whereas the domains upstream of ACP are responsible for the condensation and  $\beta$ -carbon processing of the growing acyl chain, the C-terminal TE1 domain functions to select and hydrolyze the mature fatty acid product from the 4'-PP moiety. The terminating activity of TE1 liberates the acyl product, regenerates the holo-ACP domain, and ensures fatty acid biosynthesis continues uninhibited.

### **1.3.2 Mammalian Type I FASN Mechanism**

Fatty acid synthesis (Figure 2) requires one mole of acetyl-CoA, seven moles of malonyl-CoA, and 14 moles of NADPH in order to generate a single mole of palmitate. Acetyl-CoA is generated from a direct siphon off of the TCA cycle, where ATP citrate lyase (ACL) hydrolyses the two-carbon substrate from citrate and generates the CoA adduct from ATP. Malonyl-CoA is synthesized from acetyl-CoA via acetyl CoA carboxylase (ACC), and is the rate-limiting step in the fatty acid synthesis cycle (58-59). Fatty acid synthesis is initiated when MAT primes the 4'PP of ACP with an acetyl moiety, which is immediately transferred to the active site cysteine of KS. MAT then loads a malonyl moiety onto holo-ACP, and concomitant decarboxylation of the malonyl moiety facilitates condensation to the acetyl group of KS, generating a 4-carbon,

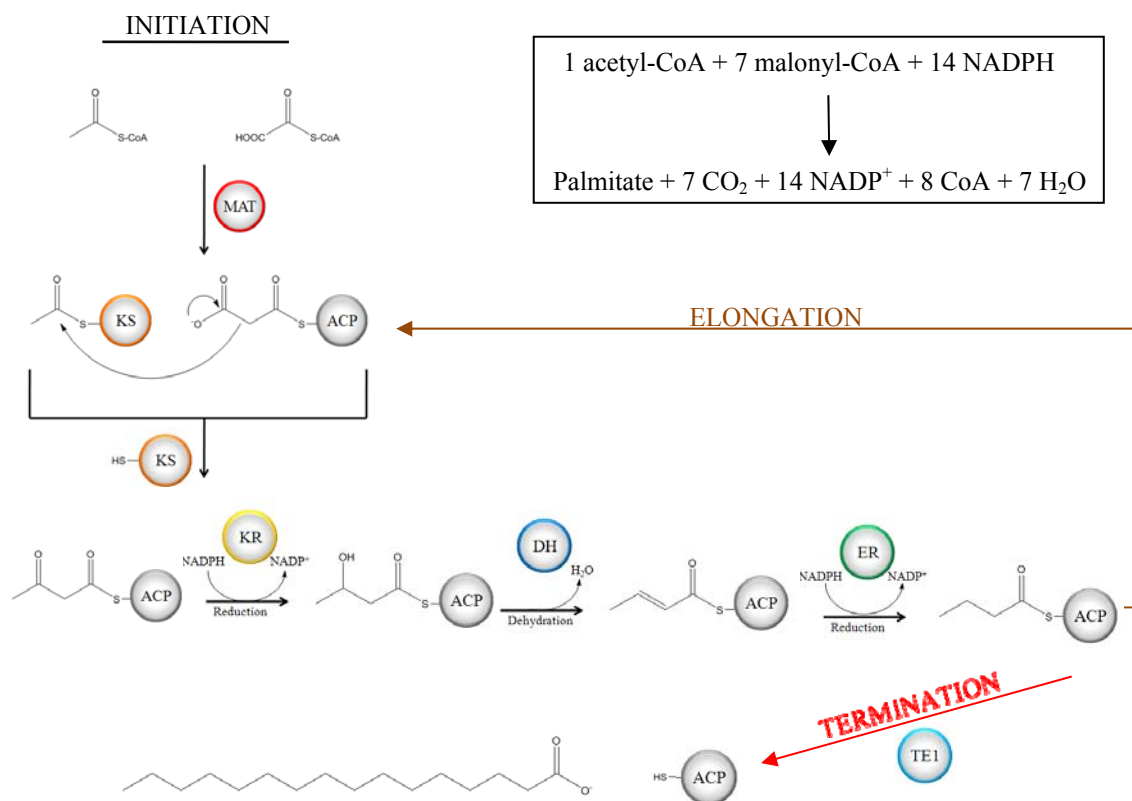


**Figure 2. Reaction scheme for mammalian fatty acid biosynthesis.** Fatty acid synthesis is initiated with the loading of acetyl from acetyl-CoA and malonyl from malonyl-CoA onto KS and ACP via MAT. Concomitant decarboxylation of malonyl facilitates non-catalytic condensation with the acetyl moiety on KS, resulting in a four-carbon,  $\beta$ -keto acyl intermediate covalently linked via a thioester to the 4'-PP cofactor of ACP.  $\beta$ -carbon processing proceeds in three steps: first, KR catalyzes a reduction reaction with a hydride from NADPH generating a  $\beta$ -hydroxy intermediate; next, DH catalyzes elimination of the  $\beta$ -hydroxy through release of a water molecule generating a  $\beta$ -enoyl intermediate; and finally, ER catalyzes the second reduction reaction with another hydride from NADPH generating the fully saturated acyl-ACP intermediate. The acyl-ACP intermediate is sequentially elongated by two carbons with six or seven cycles of  $\beta$ -carbon processing. When the palmitate or stearate products have been processed, TE1 terminates elongation by hydrolyzing the thioester bond and forms an acyl-enzyme intermediate before liberating the acylate to the cytosol. The stoichiometry of palmitate synthesis is shown in the upper right-hand inset.

$\beta$ -ketoacyl product tethered to the ACP domain. The  $\beta$ -keto functional group of this newly elongated acyl chain is then processed via reduction and elimination reactions by three domains. The first reduction reaction is catalyzed by the KR domain, where the  $\beta$ -keto group is reduced to a  $\beta$ -hydroxy by hydride transfer from NADPH. The  $\beta$ -hydroxy acyl-ACP substrate is then delivered to the DH domain, which results in the formation of a  $\beta$ -enoyl desaturation with loss of one mole of water. Finally, the  $\beta$ -enoyl acyl-ACP substrate is delivered to the ER domain where another mole of NADPH donates a hydride to generate a fully saturated acyl product. The iterative cycle of decarboxylative condensation and catalytic  $\beta$ -carbon processing continues until the growing acyl chain reaches 16 or 18 carbons in length. Only then does the C-terminal TE1 domain intervene by hydrolyzing the palmitate or stearate product from ACP, effectively terminating the FASN cycle. Liberation of free fatty acids by TE1 ensures acyl chain length specificity and maintains efficient FASN turnover. However, as described in the next sections, the distribution of acyl products varies amongst Type I and Type II enzymes, and the acyl chain distribution of human FASN can be altered by a Type II thioesterase called TE2, the primary focus of the studies presented in Chapter 2.

## **1.4 Products of Type I and Type II FASN**

### **1.4.1 Type II FASN Product Distribution**

Although the type I and type II FASN complexes share essentially identical enzyme activities, catalytic mechanisms, and tertiary structural folds of the individual functional domains, the type II FASN system is capable of generating an impressive variety of products compared to the very limited long-chain fatty acid products of the

type I system. *E. coli* FASN products include the saturated and unsaturated fatty acids of varying chain length, as well as iso- and anteisobranched-chain fatty acids. Given the dissociative nature of the type II system, the type II ACP proteins with varying intermediates can diffuse from the FASN complex and associate with alternative enzymatic activities to allow for the variety of products synthesized. In addition, research focused on manipulating the product distribution of type II FASN by harnessing the ability of FASN proteins to diffuse and associate with exogenous enzymes is a current strategy for development of antibacterial compounds (60-66).

#### **1.4.2 Type I FASN Product Distribution**

In contrast to the type II FASN system, mammalian type I FASN strictly favors the long-chain fatty acids (LCFAs) palmitate (C16) and stearate (C18) products. The specificity for LCFAs stem from the limit of the KS domain to accommodate the growing acyl chain as well as the selectivity of the TE1 domain for the fully processed acyl product (67). Early studies on native, rat FASN, where the resident TE1 domain was removed using limited trypsin digestion, revealed that the truncated enzyme continued building long-chain fatty acids with an upper limit of 22-carbons in chain length (68-69). This result revealed that product chain length specificity was dictated by the selectivity of the TE1 domain. The ability to selectively release the TE1 domain from the FASN complex allowed for further characterization of substrate specificity of TE1. *In vitro* kinetic studies using acyl-CoA substrates revealed that TE1 maintained the strict chain length specificity for palmitoyl-CoA and stearyl-CoA, with some appreciable activity for myristoyl (C14)-CoA as well (69-71). Kinetic studies on recombinant KS revealed that the catalytic efficiency of the domain dropped sharply when the substrate for

condensation reached or exceeded the length of myristate (72). Later kinetic studies on recombinant TE1 re-affirmed the high specificity for palmitate and stearate (37).

Interestingly, studies on the lipid distribution of bovine and rat milk fat revealed a higher ratio of medium chain-length fatty acids (MCFAs) to LCFAs (73-76). The primary MCFAs included laurate (C12) and myristate (C14), and to a lesser extent caprylate (C8) and caprate (C10). The seemingly aberrant acyl product distribution in milk fat was later resolved when a monofunctional type II thioesterase was identified in lactating rat mammary glands (77-82). Smith *et al.* isolated endogenous rat thioesterase II (TE2) and demonstrated its ability to modulate the product distribution of FASN to favor MFCAs. Importantly, the ability of TE2 to modulate FASN product distribution was uninhibited by the resident TE1, yet the ability of TE2 to associate with FASN was dependent on the dimer actively engaging in fatty acid synthesis. Surprisingly, the closest homologues to TE2 based on sequence identity were type II thioesterases associated with the distantly related non-ribosomal peptide synthetases (NRPS). NRPS TE2 enzymes perform non-specific editing roles, similar to the TE2 enzymes of polyketide synthases (PKS). A discussion of TE2 enzymes from related multifunctional enzyme complexes is addressed later in this chapter.

### **1.5 FASN-like Modular Synthases: Polyketide Synthase (PKS) and Non-ribosomal Peptide Synthetase (NRPS)**

Two additional enzymatic systems from prokaryotes and some fungi, polyketide synthases (PKS) and non-ribosomal peptide synthetases (NRPS), share similarity to the Type I multifunctional FASN. PKS and NRPS both adopt a multi-modular arrangement

of enzymatic activities on single peptides, and both systems utilize similar enzymes and reaction chemistries to generate their products (83-84). Whereas FASN houses all catalytic domains on a single polypeptide, PKS and NRPS systems utilize several multifunctional peptides, or modules, which coalesce in an assembly line fashion. The number of modules and domain organization of each module facilitates the incredible diversity of natural products observed from PKS and NRPS. Moreover, the ability of individual modules to diffuse and associate with alternative modular activities *in vivo* presents additional opportunities for micro-organisms to diversify natural product syntheses.

The macrolide and non-ribosomal peptide natural products from PKS and NRPS, respectively, have recently been recognized for their utility as chemotherapeutics for treating bacterial infections as well as cancer (62,85-89). Normally, these natural products serve their host micro-organisms by functioning as metal ion scavengers, quorum sensors, immunosuppressives, or cytostatic agents. Recognition of the bioactivity of natural products prompted the application of these metabolites toward antibiotic and anti-cancer research. Current chemotherapy research, as it relates to macrolides and non-ribosomal peptides, is now progressing in two parallel directions: first, a strong focus on the identification and application of naturally-occurring compounds; second, the genetic engineering of hybrid PKS and NRPS systems to exploit the chemical potential of expanding the natural products compound library.



### 1.5.1 Polyketide Synthase Assembly and Catalytic Mechanism

The PKS family of enzymes has four architecturally different yet mechanistically similar complexes: modular type I, which is most similar to type I FASN; iterative type I, which is most similar to bacterial polyunsaturated fatty acid (PUFA) synthases; type II dissociated, which is highly related to the type II FASN; and type III, which is composed of monofunctional, iteratively-acting condensing enzymes (90-93). For brevity, the widely referenced modular type I PKS model system, the 6-deoxyerythronolide B synthase (6-DEBS) is used for the discussion of PKS assembly and catalytic mechanism as it relates to type I FASN (84).

The synthesis of 6-deoxyerythronolide is achieved with twenty-nine reaction centers coordinated through seven multifunctional modules (Figure 3), including an initiating di-domain module. These seven modules are arranged as three complexes: DEBS 1; DEBS 2; DEBS 3. As in all type I PKS's, the multifunctional modules are composed of essential and non-essential catalytic domains, owing to the variety of macrolide products observed in nature. The essential catalytic components are the KS, AT, ACP, and TE domains. These domains ensure the ability of the synthase to sequester and elongate the product intermediate, as well as to liberate the fully processed product through concomitant cyclization and hydrolysis. The non-essential domains, KR, DH, and ER, provide opportunities for varying degrees of  $\beta$ -carbon processing of the macrolide precursor.

Seven condensation reactions and twenty-one  $\beta$ -carbon processing reactions by FASN produce one mole of palmitate, whereas six condensation reactions and seven  $\beta$ -

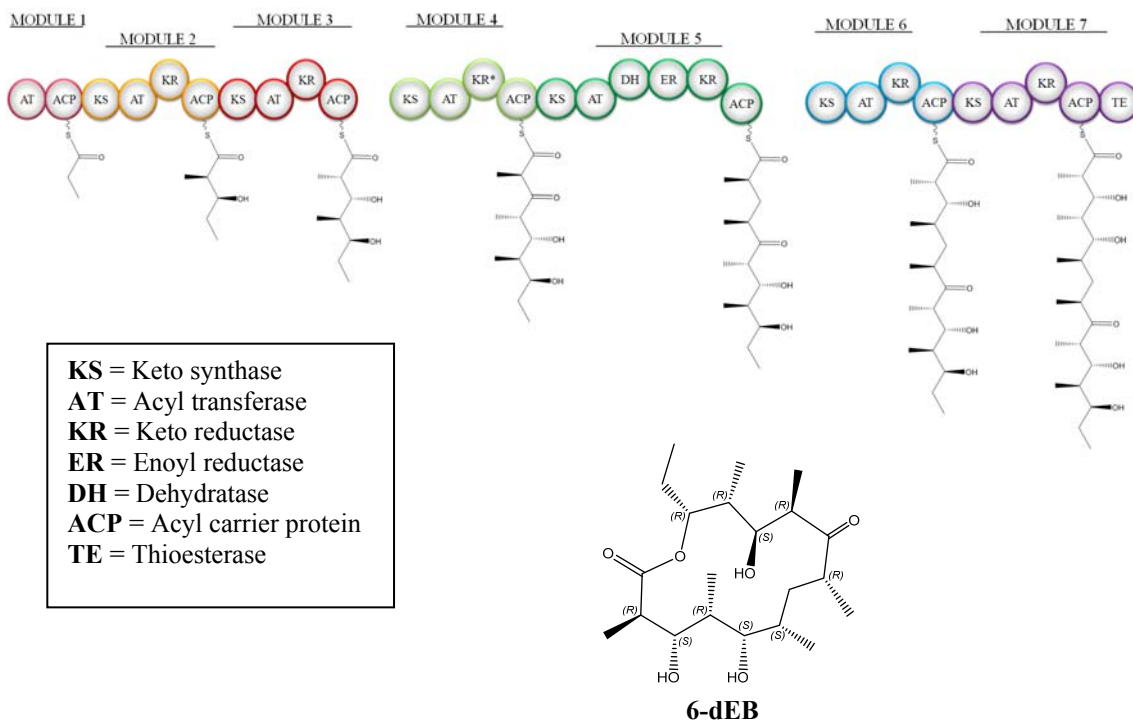


**Figure 3. Biosynthetic modules for 6-deoxyerythronolide B synthase.** Seven modules coalesce as three PKS complexes to synthesize 6-deoxyerythronolide (6-dEB). Propionyl-CoA serves as the initiator substrate for module 1, and methylmalonyl-CoA serves as the extender substrate for the other six modules. The KS, AT, and ACP domains represent the minimal activities required for PKSs. In modules 2-7, additional  $\beta$ -carbon processing domains (KR, ER, and DH) are incorporated at specific positions within the linear PKS orientation to ensure proper degree of processing is catalyzed. Interestingly, module 4 has an inactivated KR (KR\*), demonstrating the necessity of domain interactions to properly position each module within the PKS assembly. The terminating module 7 houses the resident TE domain, which terminates macrolide synthesis via macrocyclization and hydrolysis of the final product from ACP.

carbon processing reactions by 6-DEBS produce one molecule of 6DEB. The AT domain of the initiating di-domain peptides of PKS complexes exhibit varying specificities for acyl-CoA substrates, whereas the AT domains of the catalytic modules exhibit strict specificity for either the malonyl- or methylmalonyl-CoA chain-extending substrates. In the example of 6-DEBS, propionyl-CoA is loaded on the initiator di-domain, and methylmalonyl-CoA serves as the chain-extender unit. This directly contrasts with FASN, given that the MAT domain utilizes both acetyl- and malonyl-CoA substrates for either chain initiation and elongation purposes, respectively. Unlike type I FASN, where a single ACP domain shuttles the growing acyl chain to all catalytic centers, the polyketide intermediate occupies each of the six ACP domains as the macrolide is built in a linear fashion from one module to the next. As well, given the varying degree of  $\beta$ -carbon processing of the precursor, the KS of PKS systems recognize and bind  $\beta$ -keto,  $\beta$ -hydroxy and  $\beta$ -enoyl substrates, which directly contrast the substrate specificity of FASN KS for fully saturated acyl intermediates. In spite of the differences between PKS and FASN, the reaction chemistries catalyzed by the KS, AT, KR, DH, and ER domains of 6-DEBS are identical to those of the FASN dimer. When the full-length macrolide substrate is completely processed, the TE domain terminates the elongation process by hydrolyzing the thioester-linked product from ACP and catalyzes intramolecular cyclization to form the final macrolide product.

### **1.5.2 Non-ribosomal Peptide Synthetase Assembly and Catalytic Mechanism**

Three types of NRPS systems, which closely resemble the equivalently described PKS systems, have been described in the literature: type A, linear multimodular; type B, iterative; and type C, nonlinear. Both type A and B NRPS systems utilize multifunctional

polypeptides, and type C NRPS systems utilize both multimodular peptides as well as independently functioning enzymes. For brevity, the well characterized surfactin synthetase (Surf S) is used as the representative NRPS to describe how these enzymes relate to type I FASN and PKS (94).

Some important differences between NRPS and PKS/FASN systems are observed in the catalytic mechanism. To start, whereas FASN and PKS systems use short chain acyl-CoA substrates as chain extenders, NRPS systems (Figure 4) utilize aminoacyl-adenylate substrates (61-63,95). Therefore, instead of requiring the function of an AT domain, NRPS have an adenylation (A) domain. The A domain activates the amino acyl precursor with an adenylate from ATP, and each A domain from different modules confers the specificity for amino acid selection. The aminoacyl-adenylate can then be tethered to the growing peptide substrate, which is covalently tethered to the 4'-PP cofactor of the requisite peptidyl carrier (PCP) domain (or thiolation (T) domain), via the condensation (C) domain. These three domains, A, PCP, and C, represent the essential functional activities required for generating non-ribosomal peptides (NRPs). The other essential function for NRPS lies with the TE domain, present only in the last module, and functions to terminate NRP synthesis via concomittant cyclization and hydrolysis of the peptide product from PCP.

Another important difference in the catalytic mechanism of NRPS is the absence of  $\beta$ -carbon processing domains. Instead, NRPS utilize epimerization (E) domains to tailor the regiospecificity of the peptide product as well as N-methylation (M) domains. In the example of Surf S, only two of the seven modules contain E domains, and no M domains are present.

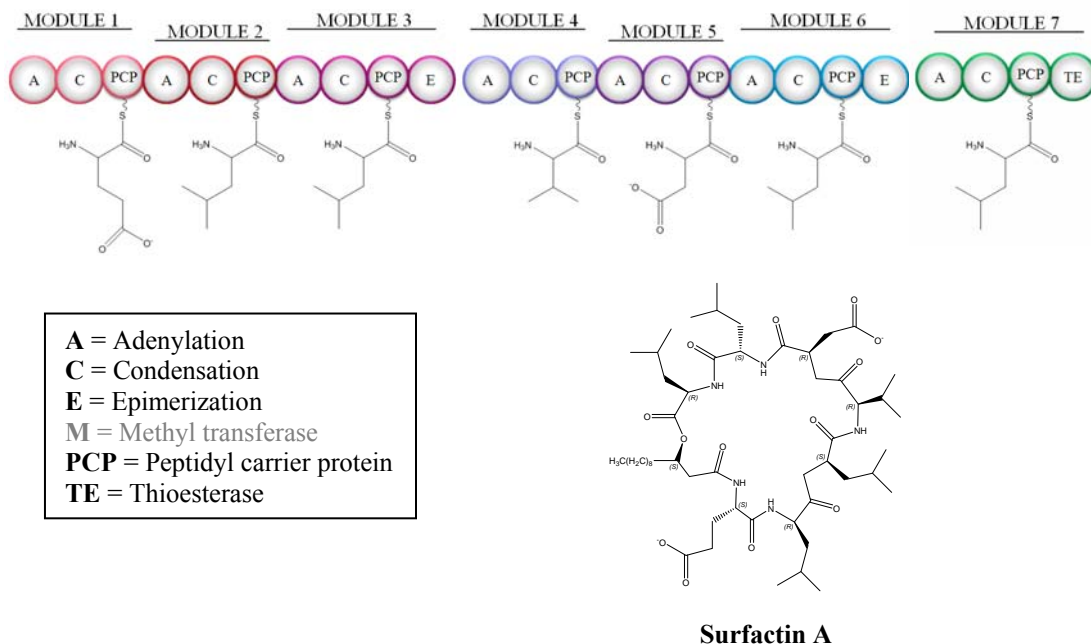


**Figure 4. Biosynthetic modules of Surfactin A synthetase (Surf S).** Seven modules coalesce as three NRPS complexes to synthesize surfactin A. The A, C, and PCP domains represent the minimal activities required for NRPSs. Each module has specificity for a particular amino acid which is used in the linear synthesis of the natural product. Activation of the selected amino acid via adenylation is required for the efficient condensation of the amino acid onto the 4'-PP cofactor of the PCP domain. Additional stereochemical or methylation processing can be catalyzed by the E and M domains, respectively, if present in the NRPS module. In the example of Surf S, only E domains are employed for accessory processing of the natural product intermediate in modules 3 and 6. The terminating module 7 houses the only TE domain, which catalyzes cyclization and hydrolysis of the fully processed natural product from PCP.

The main similarity between NRPS and FASN/PKS is demonstrated in the enzyme assembly and the use of a carrier protein domain. Surf S, in striking similarity to 6-DEBS, is composed of seven modules arranged as three complexes: Surf A; Surf B; Surf C (Figure 4). The multifunctional design of Surf S directly parallels the domain arrangement of FASN and 6-DEBS. Each aminoacyl-adenylate selected by each upstream module is condensed with downstream extenders, until the growing peptide reaches the terminal module. Therefore, in parallel with 6-DEBS, the growing peptide occupies each of the six PCP domains as the peptide is built in a linear fashion from one module to the next. Elongation is terminated via the TE domain.

### **1.6 Efficiency of Product Turnover by FASN, PKS and NRPS**

The multifunctional peptide design of FASN, PKS, and NRPS poses a challenge in defining the catalytic efficiencies of these systems. None of the catalytic domains of these synthases act independently; moreover, each domain is virtually saturated with substrate due to domain tethering.  $K_m$  and  $k_{cat}$  values are normally (and more easily) ascribed to single enzyme activities assayed against increasing substrate concentrations from well below the  $K_m$  to saturating levels. Yet, great efforts over several years have evolved kinetic characterization of the individual domains to elucidate the efficiency of product turnover for FASN, PKS and NRPS.

The results of these studies have clearly established FASN to have the fastest rate for product turnover, with the ability to generate a mole of palmitate on the order of milliseconds (67,96). Kinetic studies of individual domains resulted with  $k_{cat}$  values ranging from  $17\text{ s}^{-1}$  (KR) to  $120\text{ s}^{-1}$  (MAT) (67,96). For the TE1 domain, only an

apparent  $k_{\text{cat}}$  of  $2 \text{ s}^{-1}$  using acyl-CoA substrates was reported since substrate inhibition occurs at increasing concentrations of these detergent-like substrates. The combined results of these studies revealed that the catalytic efficiency increased by a factor of  $2 \text{ s}^{-1}$  per two-carbon additions, and the combined parameters of the individual domains activities revealed the value of FASN  $k_{\text{cat}}$  to be  $1.3 \text{ s}^{-1}$ . Importantly, the results of this kinetic study demonstrated that none of the condensing or  $\beta$ -carbon processing domains were rate-limiting in the synthesis of palmitate, and that by design, the slower turnover of TE1 ensures the proper synthesis of palmitate by minimizing opportunities for premature hydrolysis of shorter acyl products.

Similar kinetic studies have been done on the PKS and NRPS domains, and reported  $k_{\text{cat}}$  values for 6-DEBS and Surf S are  $3.4 \text{ min}^{-1}$  and  $173 \text{ min}^{-1}$ , respectively (88,97). Somewhat surprising, these catalytic efficiencies are significantly slower compared to FASN. Although the PKS and NRPS contain tethered catalytic domains, which should seemingly impart similar rates of catalysis seen for FASN, the diffusible nature of the modules appears to severely limit the efficiency of these enzyme complexes. Moreover, the complexity of extender substrates and final products utilized in PKS and NRPS catalysis, compared to FASN, contribute to the attenuated catalytic efficiency. In contrast, the LCFA and sometimes MCFA products of FASN represent some of the simplest synthetic products in nature. The ability of an accessory enzyme like TE2 to modulate FASN product distribution is an impressive observation considering the catalytic efficiency of the FASN megasynthase.

## 1.7 Type II Thioesterases

As mentioned earlier with regard to the FASN, PKS and NRPS systems can also employ type II thioesterase activities as part of the biosynthetic strategy (77,98-103). The modular design of PKS and NRPS delegates redundant enzymatic activities with varying specificities at the AT or A domains, respectively, within each module. Inherent in these redundant activities is the potential for selection of aberrant extender substrates and mis-priming of the associated carrier protein domains. When this occurs, the processivity of these synthases is stalled due to strict substrate specificity of the condensation domains or lack of carboxyl moieties required for covalent extension, or both. The editing role of the type II thioesterases catalyzes the hydrolysis of mis-primed substrates from the carrier protein domains, effectively rescuing the synthases from inactivation. The critical role of type II thioesterases in PKS and NRPS turnover has been demonstrated in several studies whereby inactivation of the editing thioesterase resulted with 30-85% loss in product turnover (100,102,104). The dissociative nature of type II thioesterases confers the ability of these enzymes to associate with a particular module when necessary, but more importantly remain dissociated during normal catalytic function so as not to inhibit the endogenous TE domain in terminating macrolide and non-ribosomal peptide synthesis. In the PKS and NRPS systems, the chain-terminating/substrate hydrolysis activities of resident TE domains are uniquely separated from the editing activities of the type II thioesterases. TE2 activity on FASN contrasts with the previous statement, due to the fact that TE2 directly intervenes with a catalytically competent multifunctional complex and effectively outcompetes the endogenous TE1 domain for the fully saturated acyl intermediate. Currently, no evidence



exists to explain the mechanisms of catalysis or substrate specificity of TE2 to relate the remarkable ability of this enzyme to associate with the dimer and modulate product specificity. The data presented in Chapter 2 address the overarching hypothesis that TE2 interactions with ACP are favored compared to TE1.

### **1.8 Central Role of the Carrier Protein in Multifunctional Enzyme Complexes**

The carrier protein domain, although devoid of any catalytic activity, furnishes an essential function for the multifunctional enzyme complexes utilized for fatty acid, polyketide, and polypeptides. The ability for these enzymatic assemblies to sequester the product intermediates via a covalent tether is paramount to the role of any single catalytic domain to achieve successful, efficient, product turnover. As a result, the carrier protein-tethered intermediates are effectively maintained at saturating levels with regard to the respective catalytic domains, which facilitates greater catalytic efficiency than would be expected of freely diffusible product intermediates.

The utility of ACP in lipogenesis ensures the ability of FASN to consistently and selectively produce palmitate and stearate, which are essential metabolites for all cell biology. Moreover, employing the utility of a carrier protein domain has allowed for the evolution of impressively diverse, yet mechanistically related synthetic complexes, which has resulted in the realization of a large family of natural products.

An inherent characteristic of carrier protein domains is that this single protein scaffold is recognized by a host of catalytic domains which allows for the binding and dissociation from several distinct protein partners. Therefore, implicit in this observation is that both substrate recognition and carrier protein domain binding are essential factors

for efficiency catalysis. Yet, it is still unclear whether substrate recognition by catalytic domains facilitates carrier protein binding, or if protein-protein interactions facilitate substrate loading into reaction centers.

### **1.9 Interactions between Carrier Protein Domains and Thioesterase Activities are Promising Targets for Therapeutic Development**

It is important to consider both factors of substrate and carrier protein interactions when exploring the therapeutic intervention of FASN, PKS and NRPS for the treatment of cancer and microbial or fungal infections, respectively. To start, the natural product industry is rapidly expanding its compound library due to the engineering of hybrid enzyme systems which mix and match PKS and NRPS modules to generate new products. However, several limitations have arisen in these efforts, stemming from slowed reaction kinetics, limitations on module specificities, and the ability for the endogenous TE domains to liberate the product. Genetic engineering can presumably overcome these limitations by tailoring the module specificities, but also the specific interactions between the carrier protein and the catalytic centers, thus affording more time for catalysis of the desired products. An alternative consideration is for drug development research aimed at antagonizing the endogenous natural product machinery. Given that some natural products act as immunosuppressants or cytostatic agents, affording microbes the ability to infect its host, inhibition of the synthetic machinery can act in an antimicrobial fashion. Antimicrobials designed to block carrier protein interactions would comprehensively inhibit catalytic activities. Similar to FASN, inhibition of either endogenous TE domain or type II thioesterase activities would severely limit the ability of the synthases to effectively generate products.

Appreciation of the interplay between ACP, TE1 and TE2 of the FASN machinery is becoming increasingly important given that pharmacological intervention of the TE1 domain of FASN is an established target for cancer treatment (35,105). The ability of TE2 to modulate FASN activity with active TE1 present represents a potential limitation in TE1-targeted FASN drug discovery. If any aberrant TE2 activity is maintained in cancer cells after treatment with TE1 inhibitors, TE2 could rescue FASN activity and cancer cell metabolism. Therefore, it is imperative that our understanding of TE1 and TE2 structural scaffolds, catalytic mechanisms, and binding modes for substrate/ligands, ACP interactions, and product hydrolysis continues to expand. Three-dimensional atomic models of cancer targets provide invaluable molecular blueprints for medicinal chemistry research and lead compound optimization.

To date, no crystallographic evidence exists to determine the interactions between the human ACP and TE1 or ACP and TE2; nor are there any structures available for TE2. Moreover, the only insight into the substrate binding mechanism is from the crystal structure of TE1 in complex with Orlistat (Figure 5). A central hypothesis governing the presented research is that TE1 and TE2 are structural homologues to the  $\alpha/\beta$  serine hydrolase family of enzymes, and that comparison of both crystal structures will reveal conserved core domain architectures but dissimilar sub-domain features. A second related hypothesis is that the differences in sub-domain architecture will demonstrate differences in ACP interactions.

Additionally, the only kinetic studies on TE1 and TE2 have employed the sub-optimal acyl-CoA substrates. While these substrate mimics provide great insight into substrate specificity; however, the absence of the ACP domain portion of the substrate is

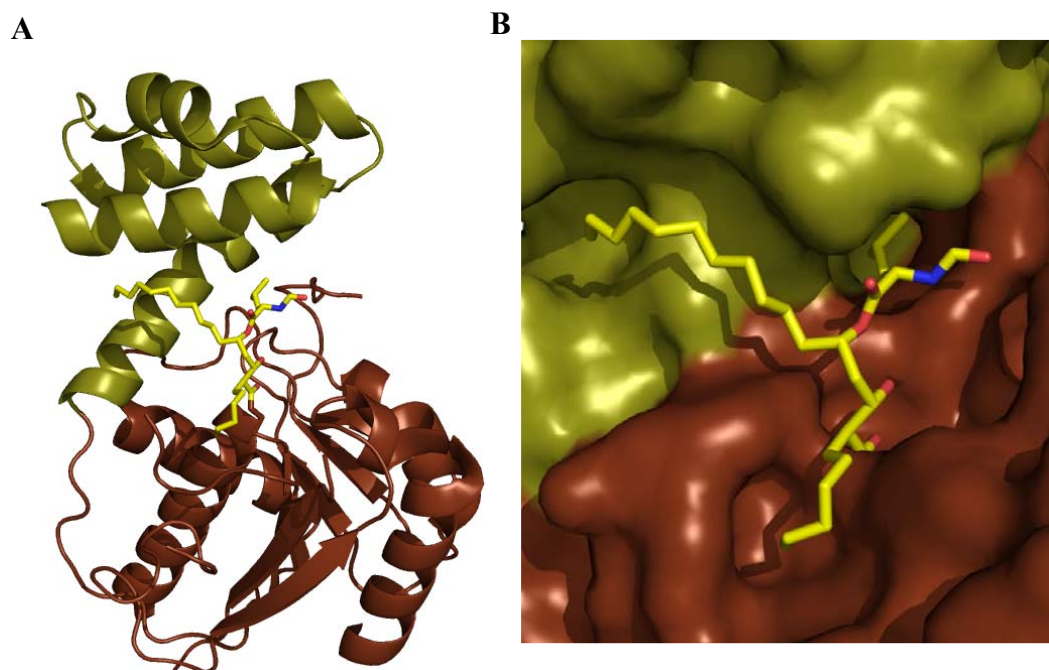


**Figure 5.** The 2.3 Å crystal structure of recombinant human TE1 domain of FASN inhibited by Orlistat. The TE1-orlistat complex was the first structure to model substrate packing into the TE1 active site. **A.** Orlistat (yellow) binds at the interface between sub-domains A (green) and B (brown) and is covalently linked to active site Ser2308. The canonical  $\alpha/\beta$  serine hydrolase fold is observed in sub-domain B. The non-canonical sub-domain A is composed of a 4  $\alpha$ -helical bundle. Both domains participate in substrate binding. **(B).** Surface representation at the sub-domain interface reveals unique binding channels. The palmitoyl-like moiety of Orlistat packs along the specificity channel, whereas the octanoyl moiety packs into a short chain pocket. Orlistat binding and orientation provided the first rationale for how to target novel therapeutics to the TE1 active site.

a glaring limitation of this kinetic characterization. The ability to compare TE1 and TE2 activities on an acyl-ACP substrate could provide additional clues into the apparent competition of TE1 and TE2 for acyl-ACP. Therefore, it is hypothesized that TE1 and TE2 will be more active toward acyl-ACP substrates compared to the standard acyl-CoA substrate mimics; i.e., ACP-TE protein-protein interactions will facilitate substrate recognition and improved catalytic efficiencies.

The data reported in this thesis addresses the above-stated hypotheses with the experimental design listed below:

1. Human TE1 and TE2 activity on acyl-CoA substrates will be determined and will report the first kinetic studies on the human enzymes.
2. Kinetic studies of TE1 and TE2 on the biologically relevant acyl-ACP substrates will reveal improved specific activities for both enzymes. Acyl-CoA substrates are freely diffusible, therefore the catalytic efficiency of both thioesterase enzymes is limited by the ability of the enzymes to scavenge the substrate and then bind and hydrolyze the thioester bond. The acyl substrate tethered to an ACP domain will facilitate protein-protein interactions, presumably increasing the rate of substrate-enzyme interactions and substrate loading into the active site.
3. Inhibition studies will reveal differences in inhibitor potency against TE1 and TE2. TE1 demonstrates strict selectivity for palmitate and stearate, whereas TE2 is expected to have a broad selectivity for MCFAs and LCFAs. These differences in specificity may be related to differences in catalytic mechanisms by way of substrate binding; therefore, it is not unreasonable to expect varying degrees of inhibition between the enzymes depending on the choice of inhibitor.

4. The TE2 crystal structure will reveal a conserved  $\alpha/\beta$  serine hydrolase fold, but the domain insertion will deviate from TE1. The differences in sub-domain architecture will explain the lack of chain-length selection of TE2. TE1 and TE2 share only 15% sequence identity, yet both enzymes recognize and hydrolyze the same acyl-ACP substrate of FASN. Therefore, these enzymes are expected to have similar structures. The interface of sub-domains A and B of TE1 generate the substrate binding channel; therefore, the expectation is that the sub-domain portion of TE2 will not provide a structured substrate binding channel, allowing for non-specific hydrolysis of varying chain-length acyl products.

## References

1. Wolken, J. J. (1968) Cellular organelles and lipids. *J Am Oil Chem Soc* **45**, 241-246
2. Wakil, S. J. (1962) Lipid metabolism. *Annu Rev Biochem* **31**, 369-406
3. Bray, G. A., Lovejoy, J. C., Smith, S. R., DeLany, J. P., Lefevre, M., Hwang, D., Ryan, D. H., and York, D. A. (2002) The influence of different fats and fatty acids on obesity, insulin resistance and inflammation. *J Nutr* **132**, 2488-2491
4. Wymann, M. P., and Schneider, R. (2008) Lipid signalling in disease. *Nat Rev Mol Cell Biol* **9**, 162-176
5. Wakil, S. J., and Abu-Elheiga, L. A. (2009) Fatty acid metabolism: target for metabolic syndrome. *J Lipid Res* **50 Suppl**, S138-143
6. Schug, Z. T., Frezza, C., Galbraith, L. C., and Gottlieb, E. (2012) The music of lipids: how lipid composition orchestrates cellular behaviour. *Acta Oncol* **51**, 301-310
7. Wang, W. Q., Zhao, X. Y., Wang, H. Y., and Liang, Y. (2008) Increased fatty acid synthase as a potential therapeutic target in multiple myeloma. *J Zhejiang Univ-Sc B* **9**, 441-447
8. Mashima, T., Seimiya, H., and Tsuruo, T. (2009) *De novo* fatty-acid synthesis and related pathways as molecular targets for cancer therapy. *Brit J Cancer* **100**, 1369-1372
9. Uddin, S., Hussain, A. R., Ahmed, M., Abubaker, J., Al-Sanea, N., AbdulJabbar, A., Ashari, L. H., Alhomoud, S., Al-Dayel, F., Bavi, P., and Al-Kuraya, K. S. (2009) High Prevalence of Fatty Acid Synthase Expression in Colorectal Cancers

- in Middle Eastern Patients and Its Potential Role as a Therapeutic Target. *Am J Gastroenterol* **104**, 1790-1801
10. Flavin, R., Peluso, S., Nguyen, P. L., and Loda, M. (2010) Fatty acid synthase as a potential therapeutic target in cancer. *Future Oncol* **6**, 551-562
  11. Shurbaji, M. S., Kalbfleisch, J. H., and Thurmond, T. S. (1996) Immunohistochemical detection of a fatty acid synthase (OA-519) as a predictor of progression of prostate cancer. *Hum Pathol* **27**, 917-921
  12. Oskouian, B. (2000) Overexpression of fatty acid synthase in SKBR3 breast cancer cell line is mediated via a transcriptional mechanism. *Cancer Lett* **149**, 43-51
  13. Pizer, E. S., Pflug, B. R., Bova, G. S., Han, W. F., Udan, M. S., and Nelson, J. B. (2001) Increased fatty acid synthase as a therapeutic target in androgen-independent prostate cancer progression. *Prostate* **47**, 102-110
  14. Wang, Y., Kuhajda, F. P., Li, J. N., Pizer, E. S., Han, W. F., Sokoll, L. J., and Chan, D. W. (2001) Fatty acid synthase (FAS) expression in human breast cancer cell culture supernatants and in breast cancer patients. *Cancer Lett* **167**, 99-104
  15. Swinnen, J. V., Roskams, T., Joniau, S., Van Poppel, H., Oyen, R., Baert, L., Heyns, W., and Verhoeven, G. (2002) Overexpression of fatty acid synthase is an early and common event in the development of prostate cancer. *Int J Cancer* **98**, 19-22
  16. De Schrijver, E., Brusselmans, K., Heyns, W., Verhoeven, G., and Swinnen, J. V. (2003) RNA interference-mediated silencing of the fatty acid synthase gene



- attenuates growth and induces morphological changes and apoptosis of LNCaP prostate cancer cells. *Cancer Res* **63**, 3799-3804
17. Qiao, S., Pennanen, P., Nazarova, N., Lou, Y. R., and Tuohimaa, P. (2003) Inhibition of fatty acid synthase expression by 1alpha-2,5-dihydroxyvitamin D3 in prostate cancer cells. *J Steroid Biochem Mol Biol* **85**, 1-8
  18. Baron, A., Migita, T., Tang, D., and Loda, M. (2004) Fatty acid synthase: a metabolic oncogene in prostate cancer? *J Cell Biochem* **91**, 47-53
  19. Wang, Y. Y., Kuhajda, F. P., Li, J., Finch, T. T., Cheng, P., Koh, C., Li, T., Sokoll, L. J., and Chan, D. W. (2004) Fatty acid synthase as a tumor marker: its extracellular expression in human breast cancer. *J Exp Ther Oncol* **4**, 101-110
  20. Lu, S., and Archer, M. C. (2005) Fatty acid synthase is a potential molecular target for the chemoprevention of breast cancer. *Carcinogenesis* **26**, 153-157
  21. Zhou, W., Han, W. F., Landree, L. E., Thupari, J. N., Pinn, M. L., Bililign, T., Kim, E. K., Vadlamudi, A., Medghalchi, S. M., El Meskini, R., Ronnett, G. V., Townsend, C. A., and Kuhajda, F. P. (2007) Fatty acid synthase inhibition activates AMP-activated protein kinase in SKOV3 human ovarian cancer cells. *Cancer Res* **67**, 2964-2971
  22. Liu, H., Liu, Y., and Zhang, J. T. (2008) A new mechanism of drug resistance in breast cancer cells: fatty acid synthase overexpression-mediated palmitate overproduction. *Mol Cancer Ther* **7**, 263-270
  23. Ogino, S., Nosho, K., Meyerhardt, J. A., Kirkner, G. J., Chan, A. T., Kawasaki, T., Giovannucci, E. L., Loda, M., and Fuchs, C. S. (2008) Cohort study of fatty

- acid synthase expression and patient survival in colon cancer. *J Clin Oncol* **26**, 5713-5720
24. Migita, T., Ruiz, S., Fornari, A., Fiorentino, M., Priolo, C., Zadra, G., Inazuka, F., Grisanzio, C., Palescandolo, E., Shin, E., Fiore, C., Xie, W., Kung, A. L., Febbo, P. G., Subramanian, A., Mucci, L., Ma, J., Signoretti, S., Stampfer, M., Hahn, W. C., Finn, S., and Loda, M. (2009) Fatty acid synthase: a metabolic enzyme and candidate oncogene in prostate cancer. *J Natl Cancer Inst* **101**, 519-532
  25. Murata, S., Yanagisawa, K., Fukunaga, K., Oda, T., Kobayashi, A., Sasaki, R., and Ohkohchi, N. (2010) Fatty acid synthase inhibitor cerulenin suppresses liver metastasis of colon cancer in mice. *Cancer Sci* **101**, 1861-1865
  26. Liu, B., Wang, Y., Fillgrove, K. L., and Anderson, V. E. (2002) Triclosan inhibits enoyl-reductase of type I fatty acid synthase *in vitro* and is cytotoxic to MCF-7 and SKBr-3 breast cancer cells. *Cancer Chemother Pharmacol* **49**, 187-193
  27. Kim, E. K., Miller, I., Aja, S., Landree, L. E., Pinn, M., McFadden, J., Kuhajda, F. P., Moran, T. H., and Ronnett, G. V. (2004) C75, a fatty acid synthase inhibitor, reduces food intake via hypothalamic AMP-activated protein kinase. *J Biol Chem* **279**, 19970-19976
  28. Rae, C., and Graham, A. (2008) Fatty acid synthase inhibitor, C75, blocks resistin-induced increases in lipid accumulation by human macrophages. *Diabetes Obes Metab* **10**, 1271-1274
  29. Pellinen, J., and Szentirmai, E. (2012) The effects of C75, an inhibitor of fatty acid synthase, on sleep and metabolism in mice. *PLoS One* **7**, e30651

30. Pandey, P. R., Okuda, H., Watabe, M., Pai, S. K., Liu, W., Kobayashi, A., Xing, F., Fukuda, K., Hirota, S., Sugai, T., Wakabayashi, G., Koeda, K., Kashiwaba, M., Suzuki, K., Chiba, T., Endo, M., Fujioka, T., Tanji, S., Mo, Y. Y., Cao, D., Wilber, A. C., and Watabe, K. (2011) Resveratrol suppresses growth of cancer stem-like cells by inhibiting fatty acid synthase. *Breast Cancer Res Treat* **130**, 387-398
31. Brusselmans, K., De Schrijver, E., Heyns, W., Verhoeven, G., and Swinnen, J. V. (2003) Epigallocatechin-3-gallate is a potent natural inhibitor of fatty acid synthase in intact cells and selectively induces apoptosis in prostate cancer cells. *Int J Cancer* **106**, 856-862
32. Pan, M. H., Lin, C. C., Lin, J. K., and Chen, W. J. (2007) Tea polyphenol (-)-epigallocatechin 3-gallate suppresses heregulin-beta1-induced fatty acid synthase expression in human breast cancer cells by inhibiting phosphatidylinositol 3-kinase/Akt and mitogen-activated protein kinase cascade signaling. *J Agric Food Chem* **55**, 5030-5037
33. Notarnicola, M., Messa, C., Refolo, M. G., Tutino, V., Miccolis, A., and Caruso, M. G. (2011) Polyunsaturated fatty acids reduce Fatty Acid Synthase and Hydroxy-Methyl-Glutaryl CoA-Reductase gene expression and promote apoptosis in HepG2 cell line. *Lipids Health Dis* **10**
34. Zhang, W., Chakravarty, B., Zheng, F., Gu, Z., Wu, H., Mao, J., Wakil, S. J., and Quioco, F. A. (2011) Crystal structure of FAS thioesterase domain with polyunsaturated fatty acyl adduct and inhibition by dihomo-gamma-linolenic acid. *Proc Natl Acad Sci USA* **108**, 15757-15762

35. Kridel, S. J., Axelrod, F., Rozenkrantz, N., and Smith, J. W. (2004) Orlistat is a novel inhibitor of fatty acid synthase with antitumor activity. *Cancer Res* **64**, 2070-2075
36. Ma, G., Zancanella, M., Oyola, Y., Richardson, R. D., Smith, J. W., and Romo, D. (2006) Total synthesis and comparative analysis of orlistat, valilactone, and a transposed orlistat derivative: Inhibitors of fatty acid synthase. *Org Lett* **8**, 4497-4500
37. Pemble, C. W. t., Johnson, L. C., Kridel, S. J., and Lowther, W. T. (2007) Crystal structure of the thioesterase domain of human fatty acid synthase inhibited by Orlistat. *Nat Struct Mol Biol* **14**, 704-709
38. Carvalho, M. A., Zecchin, K. G., Seguin, F., Bastos, D. C., Agostini, M., Rangel, A. L., Veiga, S. S., Raposo, H. F., Oliveira, H. C., Loda, M., Coletta, R. D., and Graner, E. (2008) Fatty acid synthase inhibition with Orlistat promotes apoptosis and reduces cell growth and lymph node metastasis in a mouse melanoma model. *Int J Cancer* **123**, 2557-2565
39. Zhang, W., Richardson, R. D., Chamni, S., Smith, J. W., and Romo, D. (2008) Beta-lactam congeners of orlistat as inhibitors of fatty acid synthase. *Bioorg Med Chem Lett* **18**, 2491-2494
40. Dowling, S., Cox, J., and Cenedella, R. J. (2009) Inhibition of fatty acid synthase by Orlistat accelerates gastric tumor cell apoptosis in culture and increases survival rates in gastric tumor bearing mice in vivo. *Lipids* **44**, 489-498
41. White, S. W., Zheng, J., Zhang, Y. M., and Rock, C. O. (2005) The structural biology of type II fatty acid biosynthesis. *An. Rev. Biochem.* **74**, 791-831

42. Maier, T., Jenni, S., and Ban, N. (2006) Architecture of mammalian fatty acid synthase at 4.5 Å resolution. *Science* **311**, 1258-1262
43. Stoops, J. K., and Wakil, S. J. (1981) The yeast fatty acid synthetase. Structure-function relationship and the role of the active cysteine-SH and pantetheine-SH. *J Biol Chem* **256**, 8364-8370
44. Lomakin, I. B., Xiong, Y., and Steitz, T. A. (2007) The crystal structure of yeast fatty acid synthase, a cellular machine with eight active sites working together. *Cell* **129**, 319-332
45. Jenni, S., Leibundgut, M., Maier, T., and Ban, N. (2006) Architecture of a fungal fatty acid synthase at 5 Å resolution. *Science* **311**, 1263-1267
46. Leibundgut, M., Maier, T., Jenni, S., and Ban, N. (2008) The multienzyme architecture of eukaryotic fatty acid synthases. *Curr Opin Struct Biol* **18**, 714-725
47. Maier, T., Leibundgut, M., Boehringer, D., and Ban, N. (2010) Structure and function of eukaryotic fatty acid synthases. *Q Rev Biophys* **43**, 373-422
48. Morishima, N., Ikai, A., Noda, H., and Kawaguchi, A. (1982) Structure of bacterial fatty acid synthetase from *Brevibacterium ammoniagenes*. *Biochim Biophys Acta* **708**, 305-312
49. Stuible, H. P., Wagner, C., Andreou, I., Huter, G., Haselmann, J., and Schweizer, E. (1996) Identification and functional differentiation of two type I fatty acid synthases in *Brevibacterium ammoniagenes*. *J Bacteriol* **178**, 4787-4793
50. Huxtable, R. J., and Wakil, S. J. (1971) Comparative mitochondrial oxidation of fatty acids. *Biochim Biophys Acta* **239**, 168-177

51. Zhang, L., Joshi, A. K., and Smith, S. (2003) Cloning, expression, characterization, and interaction of two components of a human mitochondrial fatty acid synthase. Malonyltransferase and acyl carrier protein. *J Biol Chem* **278**, 40067-40074
52. Witkowski, A., Joshi, A. K., and Smith, S. (2007) Coupling of the *de novo* fatty acid biosynthesis and lipoylation pathways in mammalian mitochondria. *J Biol Chem* **282**, 14178-14185
53. Bunkoczi, G., Misquitta, S., Wu, X., Lee, W. H., Rojkova, A., Kochan, G., Kavanagh, K. L., Oppermann, U., and Smith, S. (2009) Structural basis for different specificities of acyltransferases associated with the human cytosolic and mitochondrial fatty acid synthases. *Chem Biol* **16**, 667-675
54. Maier, T., Leibundgut, M., and Ban, N. (2008) The crystal structure of a mammalian fatty acid synthase. *Science* **321**, 1315-1322
55. Bunkoczi, G., Pasta, S., Joshi, A., Wu, X., Kavanagh, K. L., Smith, S., and Oppermann, U. (2007) Mechanism and substrate recognition of human *holo* ACP synthase. *Chem Biol* **14**, 1243-1253
56. Joshi, A. K., Rangan, V. S., Witkowski, A., and Smith, S. (2003) Engineering of an active animal fatty acid synthase dimer with only one competent subunit. *Chem Biol* **10**, 169-173
57. Brignole, E. J., Smith, S., and Asturias, F. J. (2009) Conformational flexibility of metazoan fatty acid synthase enables catalysis. *Nat Struct Mol Biol* **16**, 190-197
58. Waite, M., and Wakil, S. J. (1962) Studies on the mechanism of fatty acid synthesis. XII. Acetyl coenzyme A carboxylase. *J Biol Chem* **237**, 2750-2757

59. Zaidi, N., Royaux, I., Swinnen, J. V., and Smans, K. (2012) ATP citrate lyase knockdown induces growth arrest and apoptosis through different cell- and environment-dependent mechanisms. *Mol Cancer Ther* **11**, 1925-1935
60. Staunton, J., and Wilkinson, B. (2001) Combinatorial biosynthesis of polyketides and nonribosomal peptides. *Curr Opin Chem Biol* **5**, 159-164
61. Condurso, H. L., and Bruner, S. D. (2012) Structure and noncanonical chemistry of nonribosomal peptide biosynthetic machinery. *Nat Prod Rep* **29**, 1099-1110
62. Hur, G. H., Vickery, C. R., and Burkart, M. D. (2012) Explorations of catalytic domains in non-ribosomal peptide synthetase enzymology. *Nat Prod Rep* **29**, 1074-1098
63. Mootz, H. D., and Marahiel, M. A. (1999) Design and application of multimodular peptide synthetases. *Curr Opin Biotechnol* **10**, 341-348
64. Boettger, D., and Hertweck, C. (2013) Molecular diversity sculpted by fungal PKS-NRPS hybrids. *Chem Biochem* **14**, 28-42
65. Lin, S., Huang, T., and Shen, B. (2012) Tailoring enzymes acting on carrier protein-tethered substrates in natural product biosynthesis. *Methods Enzymol* **516**, 321-343
66. Zabala, A. O., Cacho, R. A., and Tang, Y. (2012) Protein engineering towards natural product synthesis and diversification. *J Ind Microbiol Biotechnol* **39**, 227-241
67. Chang, S. I., and Hammes, G. G. (1990) Structure and Mechanism of Action of a Multifunctional Enzyme - Fatty-Acid Synthase. *Accounts Chem Res* **23**, 363-369

68. Smith, S., Agradi, E., Libertini, L., and Dileepan, K. N. (1976) Specific release of the thioesterase component of the fatty acid synthetase multienzyme complex by limited trypsinization. *Proc Natl Acad Sci USA* **73**, 1184-1188
69. Lin, C. Y., and Smith, S. (1978) Properties of the thioesterase component obtained by limited trypsinization of the fatty acid synthetase multienzyme complex. *J Biol Chem* **253**, 1954-1962
70. Naggert, J., Witkowski, A., Wessa, B., and Smith, S. (1991) Expression in *Escherichia coli*, purification and characterization of two mammalian thioesterases involved in fatty acid synthesis. *Biochem J* **273 ( Pt 3)**, 787-790
71. Chakravarty, B., Gu, Z., Chirala, S. S., Wakil, S. J., and Quioco, F. A. (2004) Human fatty acid synthase: structure and substrate selectivity of the thioesterase domain. *Proc Natl Acad Sci USA* **101**, 15567-15572
72. Smith, S., Witkowski, A., and Joshi, A. K. (2003) Structural and functional organization of the animal fatty acid synthase. *Prog Lipid Res* **42**, 289-317
73. Smith, S. (1980) Mechanism of chain length determination in biosynthesis of milk fatty acids. *J Dairy Sci* **63**, 337-352
74. Smith, S. (2009) Mechanism of chain length determination in biosynthesis of milk fatty acids. 1980. *J Mammary Gland Biol Neoplasia* **14**, 245-260
75. Smith, S., and Abraham, S. (1970) Fatty acid synthetase from lactating rat mammary gland. I. Isolation and properties. *J Biol Chem* **245**, 3209-3217
76. Smith, S., and Abraham, S. (1975) Fatty acid synthase from lactating rat mammary gland. *Methods Enzymol* **35**, 65-74



77. Libertini, L. J., and Smith, S. (1978) Purification and properties of a thioesterase from lactating rat mammary gland which modifies the product specificity of fatty acid synthetase. *J Biol Chem* **253**, 1393-1401
78. Libertini, L. J., and Smith, S. (1979) Synthesis of long chain acyl-enzyme thioesters by modified fatty acid synthetases and their hydrolysis by a mammary gland thioesterase. *Arch Biochem Biophys* **192**, 47-60
79. Smith, S., and Libertini, L. J. (1979) Specificity and site of action of a mammary gland thioesterase which releases acyl moieties from thioester linkage to the fatty acid synthetase. *Arch Biochem Biophys* **196**, 88-92
80. Nolin, J. M., Thompson, B. J., and Smith, S. (1982) Localization of thioesterase II, the chain-length regulatory enzyme of milk fatty acid synthesis, in rat mammary gland epithelial cells. *J Endocrinol* **94**, 251-256
81. Pazirandeh, M., Chirala, S. S., Huang, W. Y., and Wakil, S. J. (1989) Characterization of recombinant thioesterase and acyl carrier protein domains of chicken fatty acid synthase expressed in *Escherichia coli*. *J Biol Chem* **264**, 18195-18201
82. Tai, M. H., Chirala, S. S., and Wakil, S. J. (1993) Roles of Ser101, Asp236, and His237 in catalysis of thioesterase II and of the C-terminal region of the enzyme in its interaction with fatty acid synthase. *Proc Natl Acad Sci USA* **90**, 1852-1856
83. Hutchinson, C. R. (2003) Polyketide and non-ribosomal peptide synthases: falling together by coming apart. *Proc Natl Acad Sci U S A* **100**, 3010-3012
84. Smith, S., and Tsai, S. C. (2007) The type I fatty acid and polyketide synthases: a tale of two megasynthases. *Nat Prod Rep* **24**, 1041-1072

85. Kao, C. M., Luo, G. L., Katz, L., Cane, D. E., and Khosla, C. (1994) Engineered Biosynthesis of a Triketide Lactone from an Incomplete Modular Polyketide Synthase. *J Am Chem Soc* **116**, 11612-11613
86. Kao, C. M., Luo, G. L., Katz, L., Cane, D. E., and Khosla, C. (1996) Engineered biosynthesis of structurally diverse tetraketides by a trimodular polyketide synthase. *J Am Chem Soc* **118**, 9184-9185
87. Luo, G. L., Pieper, R., Rosa, A., Khosla, C., and Cane, D. E. (1996) Erythromycin biosynthesis: Exploiting the catalytic versatility of the modular polyketide synthase. *Bioorgan Med Chem* **4**, 995-999
88. Pieper, R., EbertKhosla, S., Cane, D., and Khosla, C. (1996) Erythromycin biosynthesis: Kinetic studies on a fully active modular polyketide synthase using natural and unnatural substrates (vol 35, pg 2054, 1996). *Biochemistry* **35**, 10248-10248
89. Kao, C. M., Luo, G., Pieper, R., Cane, D. E., and Khosla, C. (1997) Structure, function and engineering of modular polyketide synthases. *Abstr Pap Am Chem S* **213**, 77-Biot
90. Pieper, R., Gokhale, R. S., Luo, G. L., Cane, D. E., and Khosla, C. (1997) Purification and characterization of bimodular and trimodular derivatives of the erythromycin polyketide synthase. *Biochemistry* **36**, 1846-1851
91. Moffet, D. A., Khosla, C., and Cane, D. E. (2006) Modular polyketide synthases: Investigating intermodular communication using 6 deoxyerythronolide B synthase module 2. *Bioorg Med Chem Lett* **16**, 213-216

92. Horsman, G. P., Van Lanen, S. G., and Shen, B. (2009) Iterative type I polyketide synthases for enediyne core biosynthesis. *Methods Enzymol* **459**, 97-112
93. Tsai, S. C., and Ames, B. D. (2009) Structural enzymology of polyketide synthases. *Methods Enzymol* **459**, 17-47
94. Finking, R., and Marahiel, M. A. (2004) Biosynthesis of nonribosomal peptides. *Annu Rev Microbiol* **58**, 453-488
95. Tang, G. L., Cheng, Y. Q., and Shen, B. (2007) Chain initiation in the leinamycin-producing hybrid nonribosomal peptide/polyketide synthetase from *Streptomyces atroolivaceus* S-140. Discrete, monofunctional adenylation enzyme and peptidyl carrier protein that directly load D-alanine. *J Biol Chem* **282**, 20273-20282
96. Smith, S. (1994) The animal fatty acid synthase: one gene, one polypeptide, seven enzymes. *FASEB J* **8**, 1248-1259
97. Weinreb, P. H., Quadri, L. E. N., Walsh, C. T., and Zuber, P. (1998) Stoichiometry and specificity of in vitro phosphopantetheinylation and aminoacylation of the valine-activating module of surfactin synthetase. *Biochemistry* **37**, 1575-1584
98. Barnes, E. M., Jr., Wakil, S. J., and Swindell, A. C. (1970) Purification and properties of a palmityl thioesterase II from *Escherichia coli*. *J Biol Chem* **245**, 3122-3128
99. Heathcote, M. L., Staunton, J., and Leadlay, P. F. (2001) Role of type II thioesterases: evidence for removal of short acyl chains produced by aberrant decarboxylation of chain extender units. *Chem Biol* **8**, 207-220

100. Kim, B. S., Cropp, T. A., Beck, B. J., Sherman, D. H., and Reynolds, K. A. (2002) Biochemical evidence for an editing role of thioesterase II in the biosynthesis of the polyketide pikromycin. *J Biol Chem* **277**, 48028-48034
101. Schwarzer, D., Mootz, H. D., Linne, U., and Marahiel, M. A. (2002) Regeneration of misprimed nonribosomal peptide synthetases by type II thioesterases. *Proc Natl Acad Sci USA* **99**, 14083-14088
102. Claxton, H. B., Akey, D. L., Silver, M. K., Admiraal, S. J., and Smith, J. L. (2009) Structure and functional analysis of RifR, the type II thioesterase from the rifamycin biosynthetic pathway. *J Biol Chem* **284**, 5021-5029
103. Whicher, J. R., Florova, G., Sydor, P. K., Singh, R., Alhamadsheh, M., Challis, G. L., Reynolds, K. A., and Smith, J. L. (2011) Structure and function of the RedJ protein, a thioesterase from the prodiginine biosynthetic pathway in *Streptomyces coelicolor*. *J Biol Chem* **286**, 22558-22569
104. Linne, U., Schwarzer, D., Schroeder, G. N., and Marahiel, M. A. (2004) Mutational analysis of a type II thioesterase associated with nonribosomal peptide synthesis. *Eur J Biochem* **271**, 1536-1545
105. Kridel, S. J., Lowther, W. T., and Pemble, C. W. (2007) Fatty acid synthase inhibitors: new directions for oncology. *Expert Opin Investig Drugs* **16**, 1817-1829

## **Chapter 2.**

### **Crystal Structure of Human Thioesterase 2: Insights into the Molecular Basis for the Novel Modulation of Fatty Acid Synthase Activity.**

**Melissa Ritchie, Jill Clodfelter, Lynnette Johnson, Steve Kridel, W. Todd Lowther**

## Abstract

Human thioesterase 2 (TE2) is a discrete, monofunctional  $\alpha/\beta$  serine hydrolase up-regulated in lactating breast and functions to modulate fatty acid synthase (FASN) acyl product distribution to favor the medium chain fatty acids (MCFAs) laurate (C12) and myristate (C14). In the absence of TE2, FASN produces palmitate (C16) and stearate (C18) long chain fatty acids (LFCAs) due to the high selectivity of the endogenous, C-terminal thioesterase 1 (TE1) domain. The acyl or fatty acid chains produced by FASN are tethered via a covalent thioester linkage to the 4'-phosphopanthetheinyl (4'PP) cofactor the acyl carrier protein (ACP) domain. Both TE1 and TE2 interact with the acyl-ACP in order to hydrolyze and liberate the free fatty acid from the FASN complex. The ability of TE2 to modulate FASN product distribution in the presence of active, ACP-tethered TE1 suggests that the interactions between TE2 and ACP are favored over the interactions between TE1 and ACP. Moreover, the differences in substrate specificity suggest that TE1 and TE2 have unique active site architectures. In this manuscript, we report the 2.62 Å crystal structure of human TE2 as well as kinetic studies on human TE1 and TE2 using acyl-CoA and acyl-ACP substrates. The secondary structure superpositions of TE1 and TE2 reveal a conserved  $\alpha/\beta$  serine hydrolase fold with divergent subdomain architectures as well as unique substrate binding motifs in the active sites. TE2 is observed in the closed conformation given that residues in loop regions block the active site region. Moreover, the catalytic triad is observed to be sub-optimally positioned for nucleophile activation. The kinetic studies revealed only modest differences in TE1 specific activity against acyl-CoA and acyl-ACP substrates, whereas

TE2 resulted with a 20-fold increase in activity against acyl-ACP compared to acyl-CoA substrates.

## 2.1 Introduction

Fatty acids are important constituents of all biological processes (1-4). Long chain fatty acids (LCFAs) serve fundamental roles in membrane synthesis, energy storage, signal transduction and post-translational modifications of proteins. Medium chain fatty acids (MCFAs) have known anti-microbial properties, and are optimal metabolites for infant absorption and nourishment (5-7). In humans, cellular lipid homeostasis is maintained via absorption of exogenous lipids and *de novo* synthesis of endogenous lipid sources. Under normal conditions, cellular absorption of lipids is favored due to the abundance of circulating lipids derived from dietary sources. In contrast, aberrant lipid metabolism in several cancers is characterized by a critical dependence for endogenously derived lipids (3,8-20). Moreover, the depletion of endogenous lipids in cancer cells represents an attractive strategy for anti-cancer research (21-38).

The type I multifunctional human fatty acid synthase (FASN) is the sole enzyme responsible for the *de novo* production of LCFAs in cells and is the primary target for anti-cancer research aimed at depleting endogenous lipid sources (39-44). FASN is a cytosolic, homodimeric enzyme with a mass of 0.54 MDa, and is composed of 7 duplicate functional domains: keto synthase (KS); malonyl-acetyl transferase (MAT); dehydratase (DH); keto reductase (KR); enoyl reductase (ER); acyl carrier protein (ACP); and thioesterase (TE1). FASN domain organization is shown in Chapter 1, Figure 1.1. The acyl product distribution of FASN is dictated by the selectivity of the endogenous, C-terminal TE1 domain, which functions to liberate free fatty acids by hydrolyzing the thioester linkage of the 4'-phosphopantetheinyl (4'PP) cofactor of ACP (45-48).



Kinetic studies using acyl-ACP mimetics have clearly demonstrated the selectivity of native or recombinant TE1 for palmitate (C16) and stearate (C18) fatty acids. However, in the lactating breast, the acyl distribution of FASN products favors MCFAs, such as laurate (C12) and myristate (C14) (49). Remarkably, this shift in acyl chain-length distribution is achieved through the interaction of human thioesterase 2 (TE2), a discrete, monomeric type II  $\alpha/\beta$  serine hydrolase with a mass of 31 kDa. The accessory function of a type II thioesterase with FASN in lactating mammary tissue was first identified in rats, and its upregulation during lactation has been identified in several mammalian systems (50-55). Kinetic studies using acyl-CoA substrates demonstrated the broad specificity of endogenous or recombinant rat TE2 for fatty acids 10-14 carbons in length, consistent with the fatty acid distribution in rat milk fat.

Human TE1 and TE2 share only 15.9 % sequence identity, yet both enzymes associate with the same acyl-ACP domain of FASN for catalysis. In fact, the closest TE2 homologues based on sequence identity are the type II thioesterases, RifR and RedJ, associated with the prokaryotic rifamycin polyketide synthase (PKS) and prodiginine hybrid PKS/non-ribosomal peptide synthetase (NRPS) multimodular assemblies, respectively (56-57). The modular arrangement of representative PKS and NRPS systems are shown in Chapter 1, Figures 1.3 and 1.4. PKS and NRPS assemblies share many similarities with FASN, including the utilization of multifunctional peptides, shared domains and chemistries, and processing of substrates (58-60). Notably, all three systems employ either an acyl (FASN and PKS) or peptidyl (NRPS) carrier protein to covalently tether the product intermediates with a 4'PP cofactor. Importantly, the carrier protein is always directly tethered to the endogenous thioesterase domain, which is

required for liberation of fatty acid, macrolide, or non-ribosomal products. Moreover, all three systems employ a type II thioesterase, yet the biological consequences of TE2 activity compared to RifR and RedJ are quite different. RifR and RedJ serve editing roles in stalled biosynthetic processes by performing hydrolysis of aberrant acyl substrates on their respective carrier protein domains; TE2 intervenes with active FASN and effectively modulates the acyl product distribution.

The implications of FASN product modulation via an accessory enzyme is relevant to current drug discovery strategies aimed at targeting TE1 to inhibit endogenous lipid sources. It is evident that both substrate and ACP interactions facilitate TE1 and TE2 catalysis, and that carrier protein-thioesterase dynamics are critical in maintaining efficient, active multifunctional enzyme assemblies. The ability of TE2 to modulate FASN product distribution in the presence of active, ACP-tethered TE1 suggests that the interactions between TE2 and ACP are favored over the interactions between TE1 and ACP. Moreover, the differences in substrate specificity suggest that TE1 and TE2 have unique active site architectures. The potential differences in substrate selection and ACP recognition by TE1 and TE2 warrants further investigation in order to better understand the molecular mechanisms facilitating fatty acid synthesis in cells. Herein, we report the first crystal structure of recombinant human TE2, solved to 2.62 Å resolution. In addition, the specific activities of recombinant human TE2 and TE1 using acyl-CoA and acyl-ACP substrates were determined. The TE2 crystal structure revealed a closed conformation over the active site and a putative substrate binding pocket composed of small hydrophobic residues. Kinetic evaluation of TE1 and TE2 against acyl-CoA substrates demonstrated TE1 to have the highest specific activity for all substrates; TE2

demonstrated 20-fold enhanced specific activity when assayed against the palmitoyl-ACP substrate, and 5-fold higher specific activity compared to TE1. These combined structural features and kinetic results suggest TE2 interactions with ACP result in sub-domain reorganization, which facilitate substrate loading into the active site and efficient hydrolase activity.

## 2.2 Experimental Procedures

### 2.2.1 Purification of human ACP

The ACP domain (residues 2118-2212) was sub-cloned into pET151 TOPO/D (Invitrogen) using the full-length human FASN gene (Origene) and forward 5'-CACCTATAGGGACAGGGACAGCCAGCGGG-3' and reverse 5'-TTAGCTGGGCCAGACCATCCTCCTT-3' primers. ACP in pET151 TOPO/D is expressed with an N-terminal 6X-His-tag and TEV protease recognition sequence (ACP+His). Protein expression in C41(DE3) *E. coli* was induced with 0.2 mM IPTG at 16 °C overnight. Clarified cell lysate containing 100 μM PMSF and benzamidine, 1 mM MgCl<sub>2</sub> and 100 μg DNase powder in 20 mM HEPES pH 7.9, 500 mM KCl, 5 mM Imidazole, 10% glycerol and 1% Triton X-100 was applied to an equilibrated nickel NTA column (Qiagen). ACP+His was eluted using a 5-250 mM imidazole gradient in 20 mM HEPES pH 7.9 and 500 mM KCl. Fractions containing ACP+His were pooled, treated with 5 mM EDTA, 2 mM DTT and 5.0 mg of 3C protease and dialyzed against 4.0 L of 20 mM HEPES pH 7.0 and 1 mM DTT. Removal of the affinity tag was confirmed with Bruker Autoflex MALDI-TOF MS (3C protease recognizes TEV and 3C protease recognition sequences), and the matrix used for sampling was a saturated sinapic acid

(Fluka Chemika) solution composed of 50% ACN and 0.1% formic acid. ACP was applied to a Q-sepharose fast-flow ion-exchange column (GE Healthcare), and eluted with a 0-500 mM NaCl in 20 mM HEPES pH 7.0 and 1 mM DTT. Fractions containing ACP were pooled, concentrated to 5 mL, and injected over a Superdex 75 gel filtration column equilibrated in 20 mM HEPES pH 7.5, 250 mM NaCl and 1 mM DTT. Highly pure ACP fractions were pooled, concentrated and aliquoted for storage at -80 °C.

### 2.2.2 Purification of human TE2

Human TE2 was sub-cloned into pET151 TOPO/D using forward 5'-CACCATGGAGAGAGGAGACCAACCTAAGAGAACC-3' and reverse 5'-TTAAAATTGGATATCGATGATACTTCTAGACACTTG-3' primers. The TE2 active site S101A mutant was generated using the QuickChange procedures (Stratagene) and the following forward and reverse primers, 5'-GCATTTTTTGGCCACGCTATGGGATCCTACATTGC-3' and 5'-GCAATGTAGGATCCCATAGCGTGGCCAAAAAATGC-3'. TE2+His protein expression in BL21(DE3) GOLD *E. coli* was induced with 0.1 mM IPTG at 16 °C overnight. NTA and Q-sepharose purification strategies are identical to methods described for ACP+His purification, except with dialysis and Q-sepharose buffers adjusted to final pH 7.5 and 5 mM DTT. Fractions containing TE2 were pooled, concentrated to 5 mL, and injected onto a Superdex 75 gel filtration column equilibrated in 20 mM HEPES pH 7.5, 100 mM NaCl and 5 mM DTT. Highly pure TE2 fractions were pooled, concentrated and aliquoted for storage at -80 °C. The cloning and purification strategies for WT TE1 and TE1 S2308A active site mutant have been previously reported (61).

### 2.2.3 Purification of HAAS+His

The *E. coli* holo acyl-ACP synthase (HAAS+His) expression construct (pET28b) was kindly donated by Dr. John Shanklin at the Brookhaven National Laboratories. HAAS+His purification strategy was slightly modified from what was previously reported (62-63). First, cell cultures were grown at 37 °C to mid-log phase, and then cooled to room temperature prior to induction. Second, highly pure HAAS+His was eluted from a NTA column with 250 mM imidazole in 50 mM Tris 8.0, 20 mM MgCl<sub>2</sub>, 2% Triton X-100. Highly purified HAAS+His was dialyzed overnight into 50 mM Tris 8.0, 20 mM MgCl<sub>2</sub> and 2% TritonX-100, and then aliquoted, flash frozen in liquid nitrogen and stored at -80 °C.

### 2.2.4 Purification of *S. coelicolor* phosphantetheinyl transferase (Loader+His)

Loader+His was subcloned into pET151 TOPO/D using forward 5'-CACCATGAGCATCATCGGGGTCGGG-3' and reverse 5'-CTATCCCTCCGCGATCACCACCG-3' primers. NTA and Q-sepharose purification strategies are identical to methods described for TE2+His; Superdex 75 methods were not necessary.

### 2.2.5 Synthesis and purification of 4'PP-ACP (ACPSH) (64)

Fifty milligrams of ACP was resuspended in 5 mL reaction buffer containing 50 mM Tris 8.0, 1 mM MgCl<sub>2</sub>, 10 mM CoA, 1.6 mg/mL Loader+His and 5 mM β-mercaptoethanol. The reaction was incubated at room temperature with intermittent stirring for 1.5 hours. ACP loading was monitored via MALDI-TOF MS until the observed ACP peak at 11184 m/z reached extinction and only the fully loaded ACPSH

peak was observed at 11524 m/z. The completed reaction was diluted with 5 mL -T/G buffer (20 mM HEPES pH 7.9, 500 mM KCl), and then applied to a NTA column equilibrated in -T/G buffer. Eluted ACPSH was manually harvested via inspection of the OD<sub>280nm</sub> chromatography trace and dialyzed overnight against 2.0 L 50 mM Tris 8.0, 1 mM DTT. Dialyzed ACPSH was concentrated using the 5,000 MWCO spin concentrators, aliquoted, and stored at -80 °C.

### **2.2.6 Synthesis and purification of acyl-ACP**

Acyl chain loading efficiency was tested on laurate, myristate, palmitate and stearate. Small scale 100 µl reactions composed of 1 mg/mL ACPSH, 0.3 mg/mL HAAS+His, 100 mM Tris 8.0, 10 mM MgCl<sub>2</sub>, 1% TritonX-100 and 3 µL of saturated acyl sodium salt in 100% methanol were incubated at room temperature for up to 2 hours. ACPSH loading was monitored via MALDI-TOF MS until the observed ACPSH peak at 11524 m/z reached extinction and only the fully loaded acyl-ACP peaks were observed at the theoretical m/z values of 11707 (C12-ACP), 11735 (C14-ACP), 11763 (C16-ACP), and 11791 (C18-ACP). Samples were desalted using C18 ZipTip (Millipore) procedures prior to MALDI-TOF MS analyses.

Synthesis was scaled proportionally to generate 20 mg of C16-ACP in 10 mL reaction buffer. MALDI-TOF MS analyses confirmed 100% loaded C16-ACP after 1.5 hours at room temperature. A 2 mL NTA column was prepared and equilibrated in 50 mM Tris 8.0 and 0.5% TritonX-100. The loaded reaction was filtered with a 0.45 µm syringe filter prior to loading onto the NTA column. The flow-through was collected and immediately dialyzed overnight into 2.0 L of 50 mM NaOAc pH 5.5 and 0.5% Tween 20

at 4 °C. Fully intact dialyzed C16-ACP was concentrated using a 5,000 MWCO spin concentrator, aliquoted and stored at -80 °C.

### **2.2.7 KDH-coupled assay for monitoring acyl-CoA hydrolysis(65)**

Thiamine pyrophosphate (TPP),  $\alpha$ -keto glutarate dehydrogenase (KDH), and  $\alpha$ -keto glutarate ( $\alpha$ KG) were purchased from Sigma Aldrich, USA. Acyl-CoA substrates were purchased from Avanti Polar Lipids, Inc. Fresh stocks of NAD<sup>+</sup> and NADPH were prepared and the concentrations measured at 260 nm ( $\epsilon=18 \text{ mM}^{-1}\text{cm}^{-1}$ ) and 340 nm ( $\epsilon=6.22 \text{ mM}^{-1}\text{cm}^{-1}$ ), respectively. All kinetic measurements were performed on a Cary Eclipse Fluorescence Spectrophotometer (Agilent Technologies) equilibrated at 30 °C. The voltage gain was manually set to achieve the maximum relative fluorescence unit (RFU) when 10  $\mu\text{M}$  NADH was measured. An NADH standard curve of 0, 1.25, 2.5, 5, and 10  $\mu\text{M}$  was measured in duplicate. 25 nM TE1 and 125 nM TE2 were assayed for 5 minutes in triplicate. Reaction rates were measured against 10-320  $\mu\text{M}$  acyl-CoA substrates, in 250 mM Na/KPO<sub>4</sub> pH 7.5, in order to validate the decision to compare thioesterase specific activity at 20  $\mu\text{M}$  substrate concentrations; substrate inhibition at increasing substrate concentrations is inherent in this assay. All reaction rates were linear within the 5 minute window of measurement. Enzyme activities were transformed from RFU/min to  $\mu\text{mol}$  acyl-CoA hydrolyzed/min by multiplying by the product of the inverse NADH standard curve slope. Specific activities (nmol/min\*mg) were calculated by dividing the enzyme activities by the total enzyme mass composition.

### **2.2.8 Inhibition Assay**

Orlistat (Sigma) and Ebelactone B (Sigma) were used to measure TE1 and TE2 inhibition employing the KDH assay described above. 25 nM TE1 and 125 nM TE2 were incubated for 30 min at 30 °C with 0, 1, 10, and 100 molar excess Orlistat or Ebelactone B prior to kinetic measurement. Stocks of Orlistat and Ebelactone B were prepared in 100% ethanol and DMSO, respectively, such that equivalent volumes of inhibitor were added to each assay for TE1 or TE2; Ethanol or DMSO were added to the control samples at the same final concentration. TE1 and TE2 were assayed in triplicate against 20  $\mu$ M palmitoyl-CoA and myristoyl-CoA, respectively.

### **2.2.9 Quantitative MALDI-TOF MS discontinuous assay for monitoring acyl-ACP hydrolysis**

Quantitative MALDI-TOF MS analyses were used to measure the specific activity of TE1 and TE2 against acyl-ACP substrates. The matrix used for sampling was a saturated sinapic acid (Fluka Chemika) solution composed of 50% ACN and 0.1% formic acid. As a control, 10  $\mu$ M ACPSH and 10  $\mu$ M C16- ACP were combined, mixed 1:10 with matrix and spotted on a MTP 384 massive plate. Positive ion mode data collection was used to iteratively collect spectra every time 50 shots were added to the sum. The relationship between measured peak intensities and number of shots produced a linear trend for both ACPSH and C16-ACP, indicating that these species do not affect the ionization or desorption of each other, and that neither species reached saturation for the mass detector. A mock activity curve was prepared and measured, composed of 0-10  $\mu$ M ACPSH and 20-10  $\mu$ M C16-ACP so that the final ACP composition in each sample is 20  $\mu$ M. The ratio of ACPSH peak intensities to the sum of observed ACPSH and C16-ACP



peak intensities was determined by the equation  $I_{ACPSH}/(I_{ACPSH} + I_{C16-ACP})$ . The ratio of intensities plotted against the concentration of ACPSH produced a linear trend.

Reaction rates were measured for 25 nM TE1 and 10 nM TE2 against 20  $\mu$ M C16-ACP in triplicate in a discontinuous fashion. All reaction rates were linear within the 10 minute window of measurement. The percent of C16-ACP hydrolyzed per minute was determined by applying the equation above to the observed MALDI-TOF MS spectra. The specific activities (nmol C16-ACP/min\*mg) were determined by multiplying the former result by 20  $\mu$ M C16-ACP and dividing by the total enzyme composition.

#### **2.2.10 Crystallization of TE2**

TE2 rod-shaped crystals were identified using commercially available crystal screening kits from Qiagen and were prepared with the Gryphon crystallization robot (ArtRobbins Instr.) by mixing equal volumes (200 nL) of protein and well solutions. Optimized TE2 crystals were grown using the hanging-drop vapor diffusion method at 22 °C in well solution containing 1.64 M  $\text{NaH}_2\text{PO}_4$ , 0.42 M  $\text{K}_2\text{HPO}_4$  and 50 mM HEPES pH 7.6 . Fresh protein stocks of 10 mg/mL TE2 and 10 mM DTT were prepared and mixed in a 1:1 ratio with well solution.

#### **2.2.11 Data collection and Structure Determination**

X-ray diffraction data were collected as 0.5° oscillation images on an in-house Rigaku RA-Micro 007 generator with a Saturn92 CCD detector. Crystals were cryoprotected in paratone. The d\*Trek software was used to process the WT TE2 dataset and PHASER within the CCP4i software suite was used to identify the initial non-

isomorphous molecular replacement (MR) solution (66-69). The closest homologue of TE2, RifR (30 %, PDB code 3FLB), was used as the initial search model. A successful MR solution was obtained when only the core  $\alpha/\beta$  hydrolase fold of RifR was used (residues 5-123, 191-248). Identical strategies using only the hydrolase domain of RedJ (PDB 3QMV) also resulted with an MR solution, however the RFZ and TFZ scores for the RifR solution were superior. No MR solutions were obtained using search models of full length TE1 or its core domain (PDB 2PX6). The TE2 structure was built using COOT and all structure refinements were performed using the PHENIX software suite (70-73). The final structure was refined in PHENIX with 20 TLS groups (4 per chain). The final model is composed of residues 17-58, 75-157, and 168-265.

## 2.3 Results

### 2.3.1 TE2 is a $\alpha/\beta$ serine hydrolase related to PKS/NRPS type II thioesterases

TE1 and TE2 do not meet the criteria for homology based strictly on sequence identity, but the conserved sequence similarities establish TE2 homology to the  $\alpha/\beta$  serine hydrolase family of enzymes (Figure 2.1) (74). In contrast, TE2 shares ~30% sequence identity and approximately 42 % sequence similarity to RifR and RedJ  $\alpha/\beta$  serine hydrolases (Figure 2.2). All four thioesterases share strong homology with the position of the catalytic serine as well as the position of the catalytic histidine of the canonical Ser-His-Asp catalytic triad found in the canonical GX SXG motif. The active site S2308A of TE1 bridges two bulky tyrosine residues, whereas the type II thioesterases active site serine residues bridge histidine and methionine residues. (75). The catalytic histidine residues are positioned at the N-terminus of a hydrophobic loop region. TE1

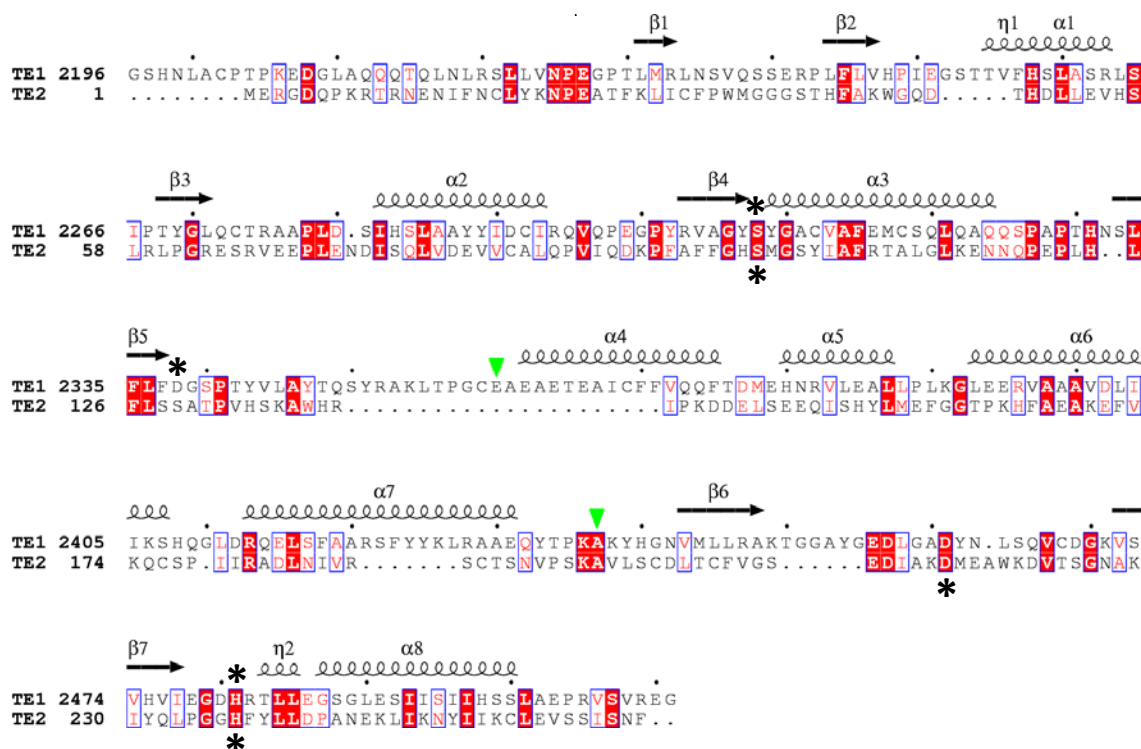


**Figure 2.1. Sequence alignment of TE1 and TE2.** The conserved residues highlighted in red represent 15.8 % sequence identity between TE1 and TE2. The active site serine residues (TE1 S2308; TE2 S101) within the canonical GX SXG motif are labeled with asterisks. Catalytic histidine (TE1 H2481; TE2 H237) and aspartate (TE1 D2338; TE2 D212) residues are also labeled with asterisks. Green arrows define the boundaries of the non-canonical loop insertion for TE1 (residues 2360-2437).

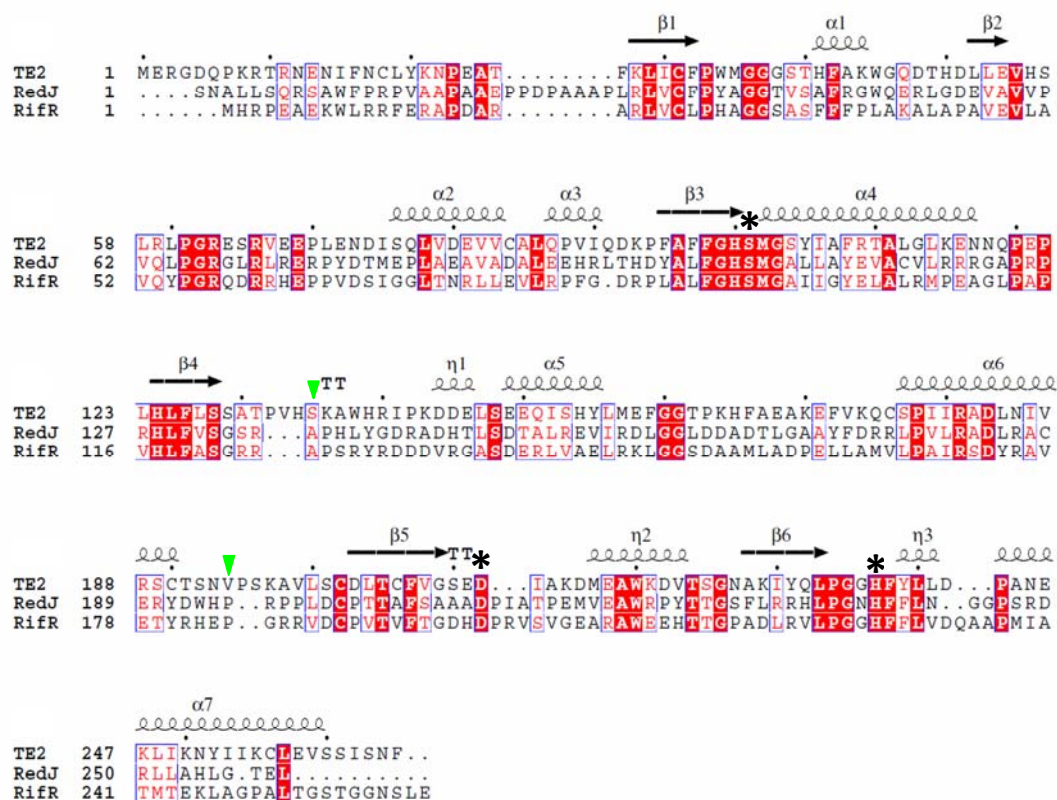


**Figure 2.2. Sequence alignment for type II thioesterases from FASN, PKS and hybrid PKS/NRPS assemblies.** TE2, RifR and RedJ share approximately 30% sequence identity. The majority of conserved amino acids lie within secondary structures present in all three crystal structures. All three catalytic residues are labeled with asterisks. The conserved active serine residues (TE2 S101; RedJ S107; RifR S94) are found within the canonical GXSSXG motif. Catalytic histidine (TE2 H237; RedJ H241; RifR H228) and aspartate (TE2 D212; RedJ D213; RifR D200) residues are also labeled with asterisks. Green arrows define the boundaries of the non-canonical loop insertions.

diverges from the type II thioesterases in its position of the catalytic aspartate, where TE2, RifR and RedJ have the acidic aspartate residue in the canonical position. Interestingly, these thioesterases have non-canonical loop insertions within the  $\alpha/\beta$  core. Loop insertions within the hydrolase fold are a common feature of several  $\alpha/\beta$  hydrolases, and gives rise to unique substrate specificities (73). The insertions in TE1, RedJ and RifR resulted with a capping domain composed of  $\alpha$ -helices observed in their respective crystal structures. Only moderate sequence similarity between TE1 and TE2 is found in the  $\alpha_6$  and  $\alpha_7$  helical elements, whereas TE2, RifR and RedJ have strong sequence identity within the loop insertion. Sequence comparison of TE2 to TE1, RifR and RedJ suggest divergent capping domain architectures comprised within structurally homologous  $\alpha/\beta$  serine hydrolase folds.

### **2.3.2 TE1 and TE2 differential activity toward acyl substrates and inhibition via $\beta$ -lactone natural products suggest unique active site architectures and ACP interactions**

#### **2.3.2A Kinetic evaluation of TE1 and TE2 hydrolysis of acyl-CoA substrate mimetics**

As seen in Figures 2.3A, TE1 and TE2 specific activities decline with increasing substrate concentrations. This observed substrate inhibition is due to the detergent-like properties of the acyl-CoA substrates; therefore, TE1 and TE2 specificity profiles were compared at 20  $\mu$ M substrates, a concentration far removed from the point of observed decline in enzyme activity. For all substrates assayed, TE1 resulted with the highest specific activity. Consistent with previously published data on endogenous TE1,

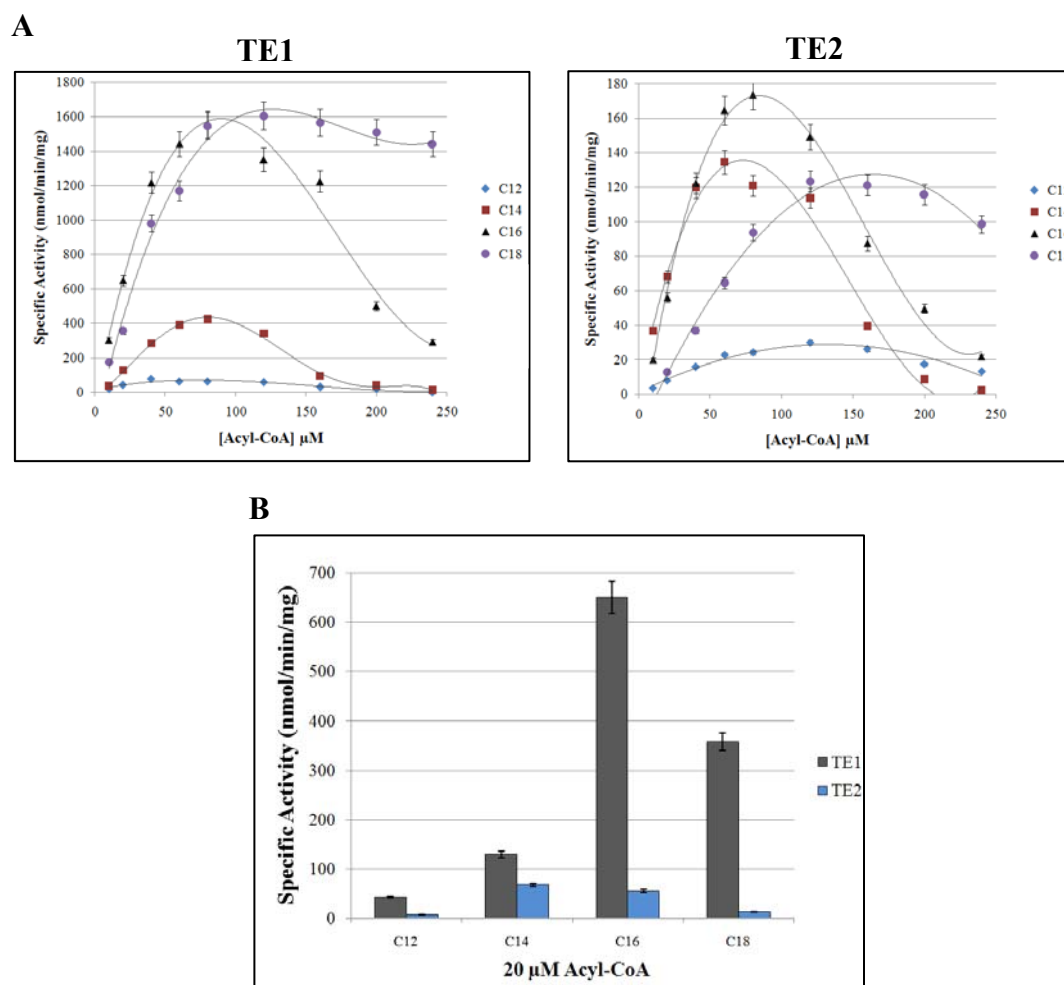


**Figure 2.3. Results of TE1 and TE2 kinetic evaluations against acyl-CoA substrate mimetics. A.** Dependence of TE1 and TE2 specific activity with increasing substrate concentrations. **B.** Comparison of TE1 and TE2 specific activities against 20  $\mu\text{M}$  acyl-CoA substrates.

recombinant TE1 demonstrated high selectivity for palmitate (C16) and stearate (C18) LCFAs (Figure 3B, gray). Previously reported activity profiles of recombinant rat TE2 demonstrated preference for MCFAs, which were consistent with the distribution of fatty acids in rat milk fat. Accordingly, the results of recombinant human TE2 activity against acyl-CoA substrates demonstrated preference for the MCFAs most abundant in human breast milk, myristate (C14) and laurate (C12) and also appreciable activity toward palmitate (Figure 3B, blue). Five hundred nM S2308A TE1 and S101A TE2 were assayed against the panel of acyl-CoA substrates, and no measurable activity was observed. The surprising result of these assays revealed a 5 to 10-fold difference in specific activities between TE1 and TE2. The differences in substrate specificity and specific activities may relate to unique structural features of the TE1 and TE2 active sites. In addition, the disproportionate specific activity of TE2 compared to TE1 is seemingly inconsistent with the increased production of MCFAs in lactating breast.

### **2.3.2B Evaluation of $\beta$ -lactone congeners on TE1 and TE2 hydrolase activity**

The differences in TE1 and TE2 active site architectures were further assessed using natural product inhibitors (Figure 2.4). Many  $\beta$ -lactone compounds are known to be susceptible to nucleophilic attack by serine hydrolases (34,76). Orlistat, a  $\beta$ -lactone compound, was previously identified as a potent inhibitor of TE1, and the crystal structure of Orlistat bound to the TE1 active site demonstrated how well Orlistat mimics the binding of a palmitoyl moiety (61). Ebelactone B was chosen for these studies because of its unique resemblance to a C14 acyl substrate. TE2 resulted with only 50% inhibition even at 100 molar excess Orlistat, whereas TE1 resulted with almost complete inhibition treated with one molar excess Orlistat. A less striking result was observed for

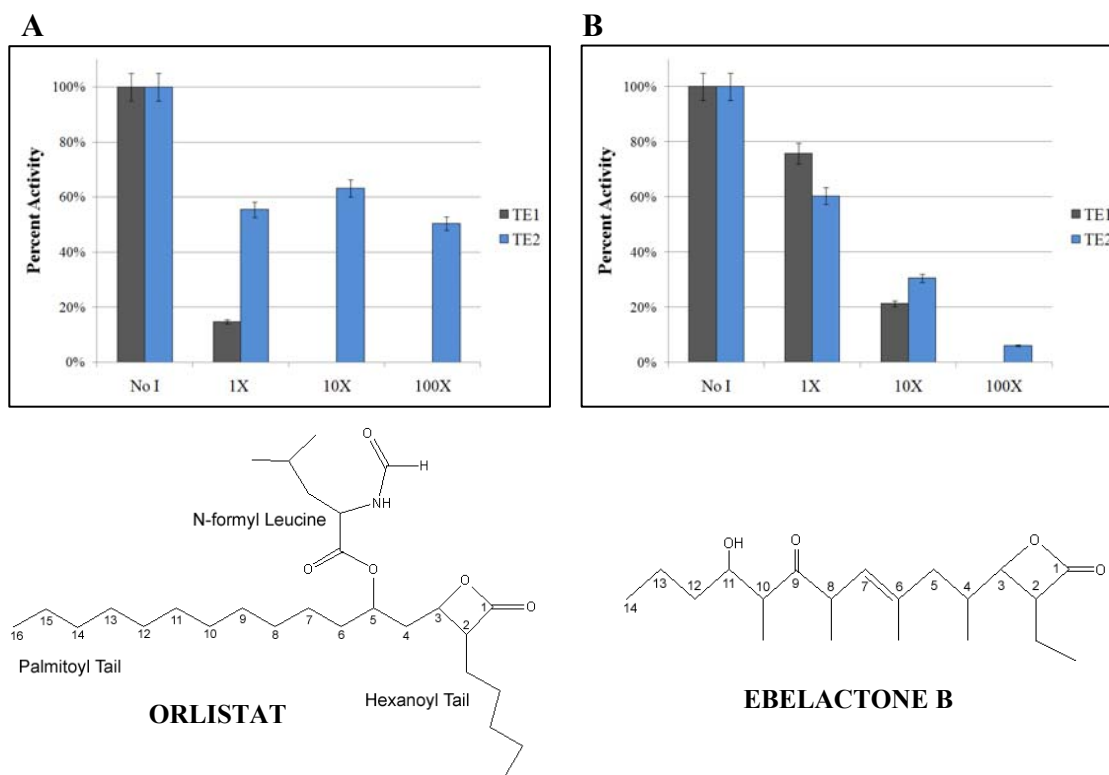


**Figure 2.4. Results of TE1 and TE2 inhibition by  $\beta$ -lactone congeners Orlistat and Ebelactone B.** **A.** Orlistat inhibition of TE1 and TE2 activity. **B.** Ebelactone B inhibition of TE1 and TE2 activity. The chemical structures of both compounds are shown below the bar graph.



Ebelactone B inhibition. Both TE1 and TE2 activities were reduced as Ebelactone B concentrations were increased; however, TE1 was almost completely inhibited at 10X ebelactone whereas TE2 never reached full inhibition even at the highest concentrations of inhibitor.

### **2.3.2C Kinetic evaluation of TE1 and TE2 hydrolysis of C16-ACP**

An efficient, reproducible and stable synthetic strategy was optimized for generating the biologically relevant acyl-ACP substrates for TE1 and TE2 kinetic experiments. Recombinant ACP was processed through a two-step synthesis to accomplish 100% conversion to acyl-ACP (Figure 2.5A). MALDI-TOF MS produced highly accurate and high resolution analyses of product intermediates; the syntheses of C12-C18 acyl-ACP substrates were prioritized to match the panel of acyl-CoA substrates (Figure 2.5B). All acyl-ACP substrates were loaded with equal efficiency.

Several key elements were crucial for optimization of acyl-ACP synthesis. First, addition of 1 % Triton-X100 detergent provided the first realization of 100% product synthesis. The aliphatic physical property of fatty acids predisposes these compounds to precipitation when suspended in an aqueous environment. Given the insolubility of these fatty acyl sodium salts in water, MeOH was used to provide high saturation solutions of each substrate. Addition of acyl substrates in MeOH to the aqueous reaction mix required slow addition with rapid mixing in order to immediately disperse the alcoholic component and minimize the potential for protein precipitation. Finally, the thioester bond tethering the acyl chain to the 4'PP cofactor is susceptible to non-enzymatic hydrolysis by nucleophilic attack of an activated water molecule at the given

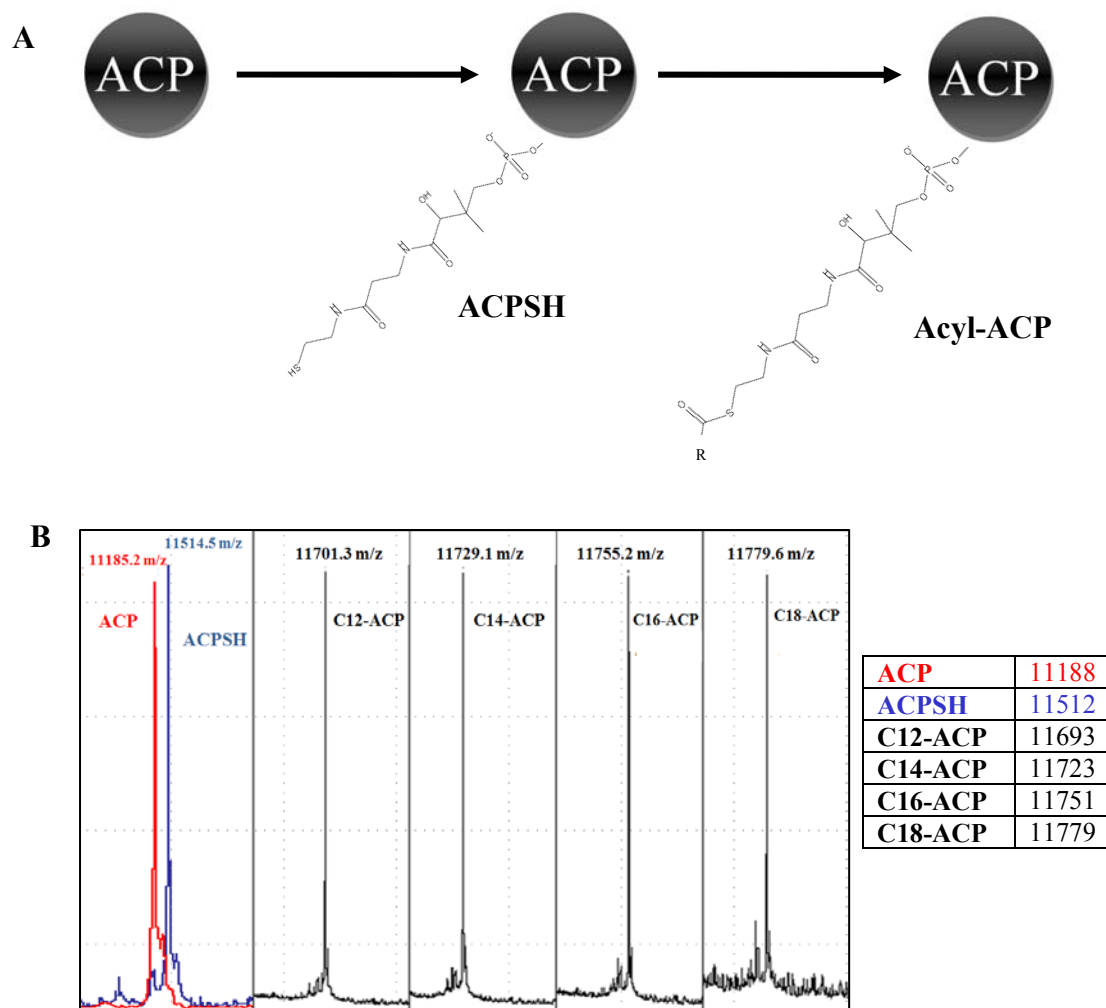


**Figure 2.5. Synthesis and analysis of acyl-ACP substrates. A. Diagram of the two-step synthetic strategy for acyl-ACP substrates.** The 4'PP cofactor attached to Ser2156 of ACP is loaded by the Loader+His enzyme in the presence of CoA and MgCl<sub>2</sub>. Acyl loading is achieved by HAAS+His in the presence of fatty acylates, MgCl<sub>2</sub> and ATP. **B. MALDI-TOF spectra representing each step of acyl-ACP syntheses.** Spectra for ACP (Red), ACPSH (Blue), and C12-C18 acyl-ACP substrates (Black) are shown. Theoretical m/z values for all samples are reported in the table.

pH of the loading reaction. Stabilization of acyl-ACP substrates was achieved by rapid buffer exchange from Tris pH 8.0 to NaOAc pH 5.5. Tween 20 detergent replaced Triton-X100 due to the ability of Triton-X100 to inhibit TE1 and TE2 activity; Tween 20 is a more favorable detergent for crystallographic purposes as well.

Generation of high milligram quantities of C16-ACP was prioritized for initial kinetic evaluations of TE1 and TE2. As will be discussed in Chapter 3 (Figure 3.10), alternative acyl-ACP synthetic strategies were also tested in parallel, but were not suitable for kinetic evaluation. Kinetic evaluation of TE1 and TE2 against the full panel of acyl-ACP substrates is proposed in Chapter 4. A novel MALDI-TOF MS discontinuous assay was developed in order to monitor acyl-ACP hydrolysis; there are no changes colorimetric or fluorescent properties with which to continuously measure thioesterase activity against acyl-ACP substrates.

A series of control MALDI-TOF MS measurements were performed to validate a method for quantitative measurement of TE1 and TE2 hydrolysis of C16-ACP (Figure 2.6). Specific challenges for using this strategy were the potential for ion-suppression of either ACPSH or C16-ACP, possible unequal sampling of substrate and product due to poor recrystallization in matrix, and limited sample detection or the potential to saturate the mass detector. ACP, ACPSH, and acyl-ACP were readily detected via MALDI-TOF MS as seen in Figure 2.5B, so sample detection was not an issue. Co-measurement of ACPSH and C16-ACP recrystallized in the same sample produced a linear result when peak intensities were plotted against the number of laser shots collected (Figure 2.6A). This result confirmed that neither ion-suppression nor saturation of the mass detector occurred. The product of TE1 or TE2 activity on C16-ACP is ACPSH; the amount of

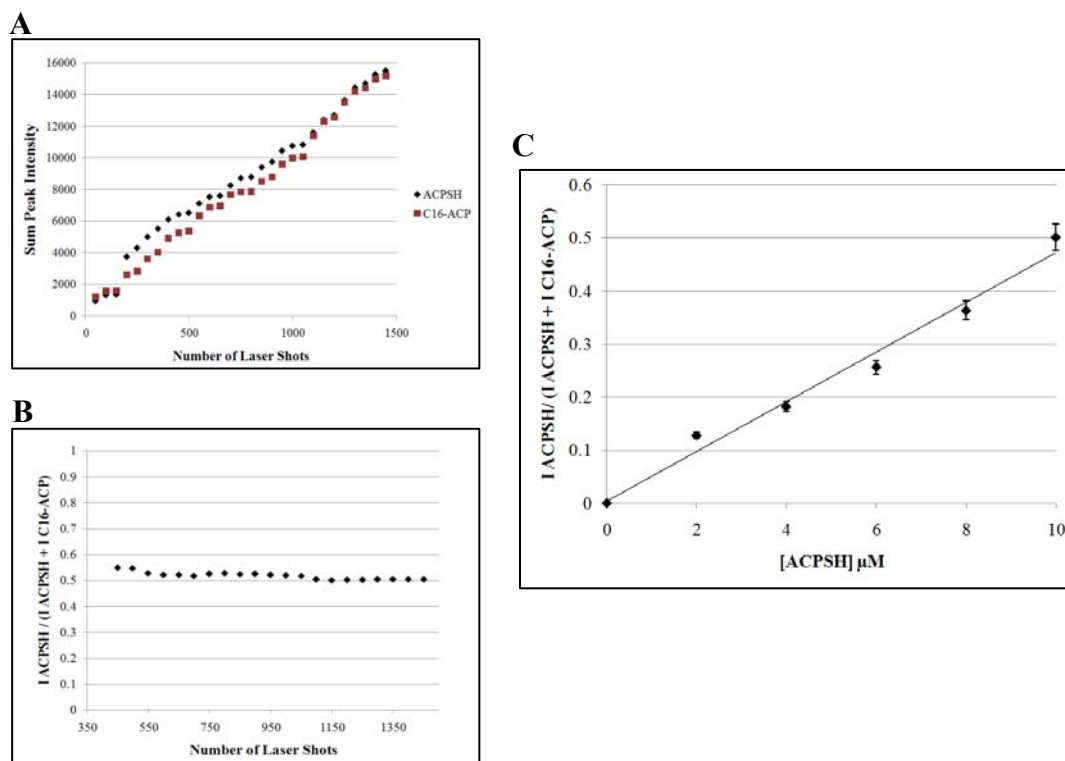


**Figure 2.6. Validation experiments for quantitative MALDI-TOF MS kinetic analyses of TE1 and TE2 hydrolysis of acyl-ACP substrates.** Quantitative analyses using MALDI-TOF methods have inherent challenges in sample ionization, ion suppression or equal sample detection per laser shot. Three control experiments were performed to address these issues. **A. Sum peak intensities plotted against number of laser shots.** Equimolar ACPSH and acyl-ACP analyses resulted with a linear trend comparing number of laser shots and the measured intensity of the observed summed peak. **B. Ratio of peak intensities plotted against number of laser shots.** The relationship between the ACPSH peak ratio to the number of laser shots resulted with a linear trend. **C. Mock activity curve.** ACPSH normalization plotted against increasing ACPSH concentrations resulted with a linear relationship.

C16-ACP decreases as ACPSH increases over time. Therefore, the ratio of these peak intensities would report the percent substrate hydrolyzed. The plot in Figure 2.6B demonstrates the independent relationship between ACPSH/C16-ACP peak intensity ratios and the number of laser shots, owing to the ability to multiply measure these samples and report equivalent proportions. The mock activity plot shown in Figure 2.6C demonstrates the linear relationship of ACPSH/C16-ACP peak intensity ratios to increasing ACPSH concentrations. The sensitivity of this assay measures 10-50% product formed.

TE1 and TE2 activity against C16-ACP was readily measured using the novel discontinuous assay (Figure 2.7). Each time point sample was quenched directly in matrix solution; TE1 and TE2 are inactivated at low pH, an inherent physical property of serine hydrolases. Quantitative MALDI-TOF analyses of TE1 and TE2 activity on C16-ACP produced a linear trend, and reaction rates and specific activities were determined. Surprisingly, TE2 demonstrated almost 5-fold higher activity toward C16-ACP compared to TE1, and 30-fold higher activity against C16-ACP compared to C16-CoA. In contrast, TE1 activity against C16-CoA and C16-ACP produced comparable rates. TE1 activity demonstrated specificity for the acyl chain, whereas TE2 activity demonstrated specificity for the ACP domain.

### **2.3.3 The 2.62 Å crystal structure of Human TE2 revealed strong homology to PKS/NRPS type II thioesterases and is in a closed conformation with sub-optimal active site geometry**

#### **2.3.3A Crystal structure of Human TE2**

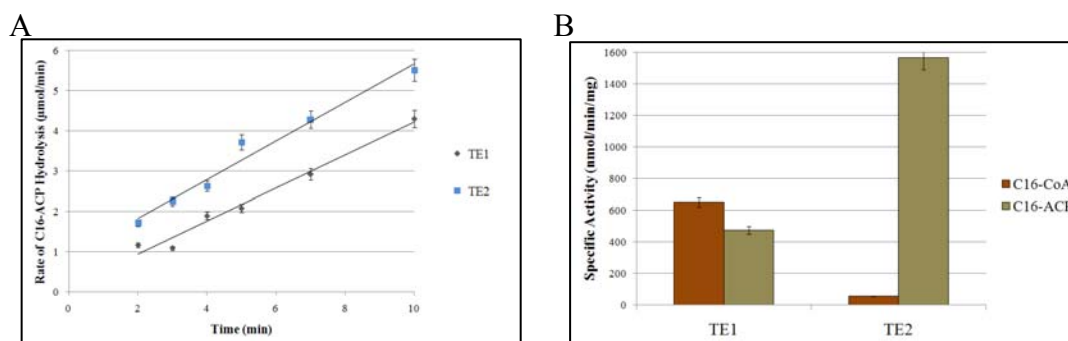


**Figure 2.7. Results of MALDI-TOF MS kinetic evaluation of TE1 and TE2 hydrolysis of C16-ACP.** **A.** Reaction rates for TE1 and TE2 hydrolysis of C16-ACP. Reaction rates for TE1 (40.8 nmol/min) and TE2 (47.8 nmol/min) were determined by linear regression analysis. **B. Graphical comparison of TE1 and TE2 specific activities against C16-CoA and C16-ACP.** Only a modest difference in specific activity, was observed for TE1 against CoA (650 nmol/min/mg) or ACP (473 nmol/min/mg) substrates. In contrast, a significant difference in specific activity was observed for TE2 against CoA (56 nmol/min/mg) or ACP (1567 nmol/min/mg) substrates.

X-ray data collection and refinement statistics are reported in Table 1. WT TE2 crystallized in the I422 spacegroup, and the dataset was scaled to 2.62 Å resolution with an  $R_{\text{merge}}$  value of 9.5 % and  $\langle I \rangle / \sigma \langle I \rangle$  value of 10.3. The dataset is 99.9 % complete with a mosaicity value of 0.54. Molecular replacement strategies using PHASER within the CCP4i suite and a search model of the RifR hydrolase core produced an initial structure solution for only the TE2 hydrolase core; the capping domain of RedJ was used to build in the TE2 capping domain. Iterative sessions of model building and refinement were performed using the PHENIX software. Final refinement strategies including individual B-factor refinement and 20 TLS groups (4 residues per group) produced the current model with refinement statistic values of 27 % and 35 % for  $R_{\text{work}}$  and  $R_{\text{free}}$ , respectively. Two variable loop regions (59-76; 158-167) as well as N-terminal residues upstream of N17 are not modeled. As seen in Figure 2.8, the electron density at the active site region of TE2 clearly defines the backbone and side-chain residues modeled.

The TE2 crystal structure confirmed its classification as a  $\alpha/\beta$  serine hydrolase enzyme (Figure 2.9A). The hydrolase core is composed of six parallel beta strands flanked by four  $\alpha$ -helices. The central  $\beta$ -sheet partially wraps around the C-terminal amphipathic helix. Consistent with hypotheses based on sequence identity, the hydrolase core of TE2 is interrupted with a loop insertion resulting in a sub-domain capping feature composed of  $\alpha$ -helices. The Ser-His-Asp catalytic triad is also shown in Figure 2.9A. Consistent with thermal factor analysis, the hydrolase core and capping domain is well ordered (Figure 2.9B). As expected, the N- and C-terminal ends of the missing variable loop regions are more disordered. In addition, the helical elements positioned on the backside relative to the active site show the highest degree of disorder.

**Table 2.1. Data collection and refinement****Data Collection**

Spacegroup	I422		
Unit cell dimensions	96.1	96.1	160.0
	90.0	90.0	90.0
Mosaicity	0.54		
Resolution Range	67.93-2.62	(2.71-2.62)	
Total number of reflections	136194		
Number of unique reflections	11637		
Average redundancy	11.7	(11.70)	
% completeness	99.9	(100.0)	
Rmerge	0.095	(0.609)	
Rmeas	0.100	(0.637)	
$\langle I \rangle / \sigma \langle I \rangle$	10.3	(2.1)	

**Refinement**

$R_{\text{work}}$	0.270
$R_{\text{free}}$	0.350
RMS(bonds)	0.009
RMS(angles)	1.340



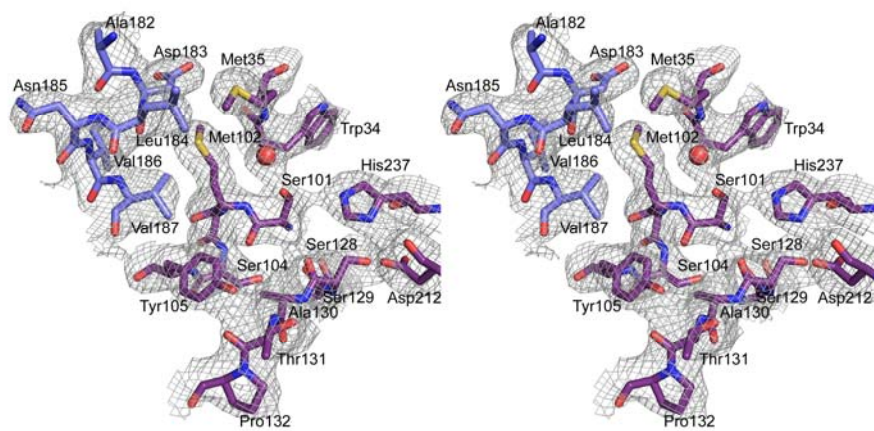


**Figure 2.8.** Current  $2F_o - F_c$  electron density map with TE2 active site residues and conserved water molecule. The map is contoured at  $1 \sigma$ .

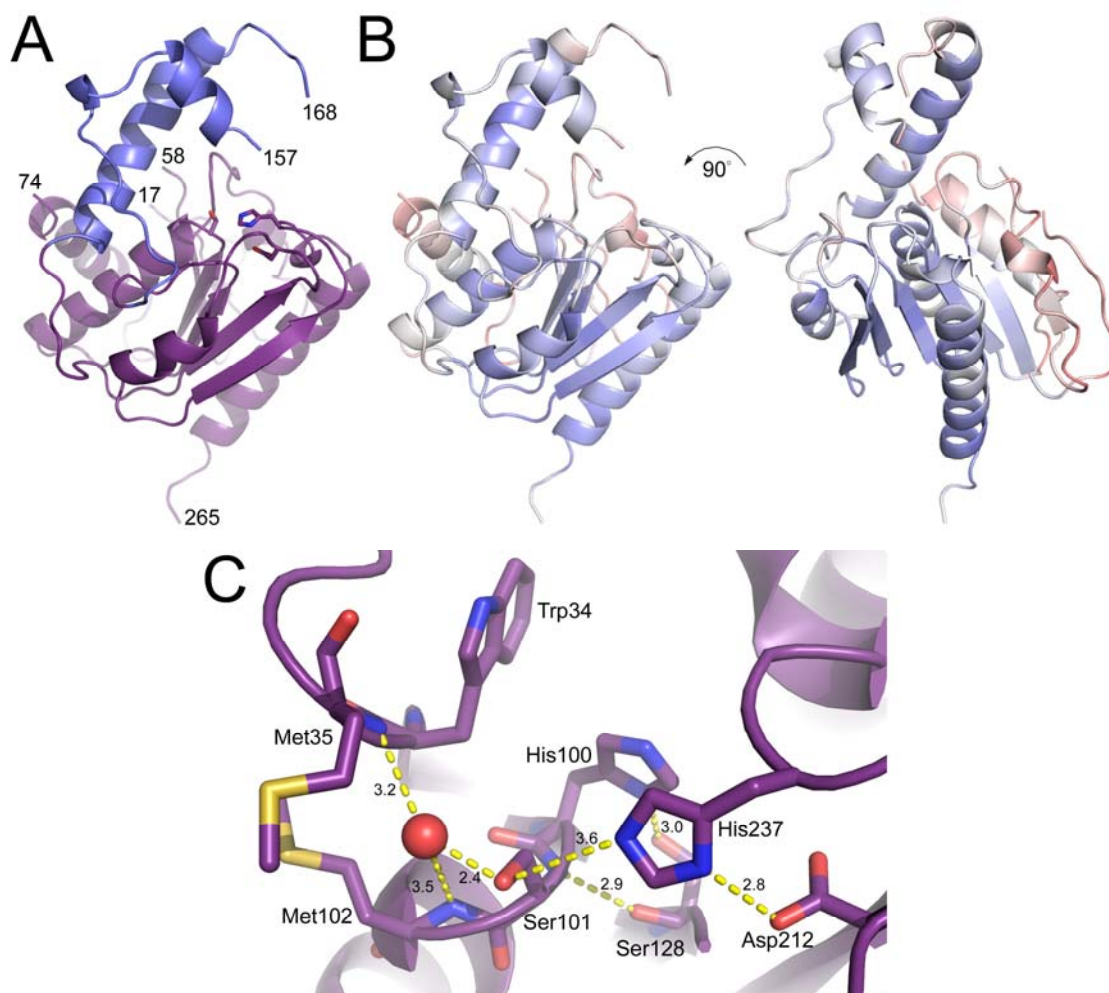


**Figure 2.9. 2.62 Å crystal structure of human TE2.** **A. Ribbon diagram of WT TE2.** The  $\alpha/\beta$  serine hydrolase core (purple) is composed of a central parallel  $\beta$ -sheet flanked by  $\alpha$ -helices. The non-canonical capping domain (slate) is a result of a loop insertion between  $\beta$ -strands 4 and 5. The Ser101-His237-Asp212 catalytic triad side chains are shown. **B. B-factor analysis of structured residues.** B-factor values from low to high are colored blue-white-red. **C. Hydrogen-bonding network of active site residues.** Ser101 is positioned too far from His237 to be activated as a nucleophile for catalysis. The well-conserved water molecule in the oxyanion hole is in hydrogen bonding with Met35 and Met102 backbone amides as well as Ser101.

The detailed hydrogen bonding network of residues at the TE2 active site is shown in Figure 2.9C. The position of Ser101 is governed by two hydrogen bonds; one hydrogen bond between the side chain and the conserved water molecule; and one hydrogen bond between its backbone amide and the side chain of Ser128. However, hydrogen bonding distances reveal that the catalytic triad of TE2 is not optimally positioned for catalysis in this conformation, with S101 3.6 Å removed from H237. The poor geometry of Ser-His-Asp catalytic triads has been described for other serine hydrolases, including trypsin, chymotrypsin and subtilisin (77). The strong electrostatic interaction between the catalytic aspartate and histidine residues forces an unfavorable geometry between the catalytic histidine and serine residues. Substrate binding relieves these restraints and facilitates efficient catalysis. Consistent with observations of the TE2 active site, slight repositioning of Ser101 and His237 is required for nucleophilic activation. The highly conserved water molecule is found in the canonical oxy-anion hole in hydrogen bonding with the active site S101 and the backbone amides of Met35 and Met102.

### **2.3.3B Comparisons of TE2 Structural Homologues**

The structural homology between TE2 and TE1, RedJ and RifR is demonstrated in Figure 2.10A. Secondary superpositions of each homologue with TE2 clearly show the highly conserved  $\alpha/\beta$  serine hydrolase core comprised of a central  $\beta$ -sheet flanked by  $\alpha$ -helices. All three TE2 homologues have loop insertions which resulted in  $\alpha$ -helical subdomain features. Inspection of each catalytic triad revealed strict positional conformity, with the exception of Asp2338 of TE1 (Figure 2.10B). RMSD statistics

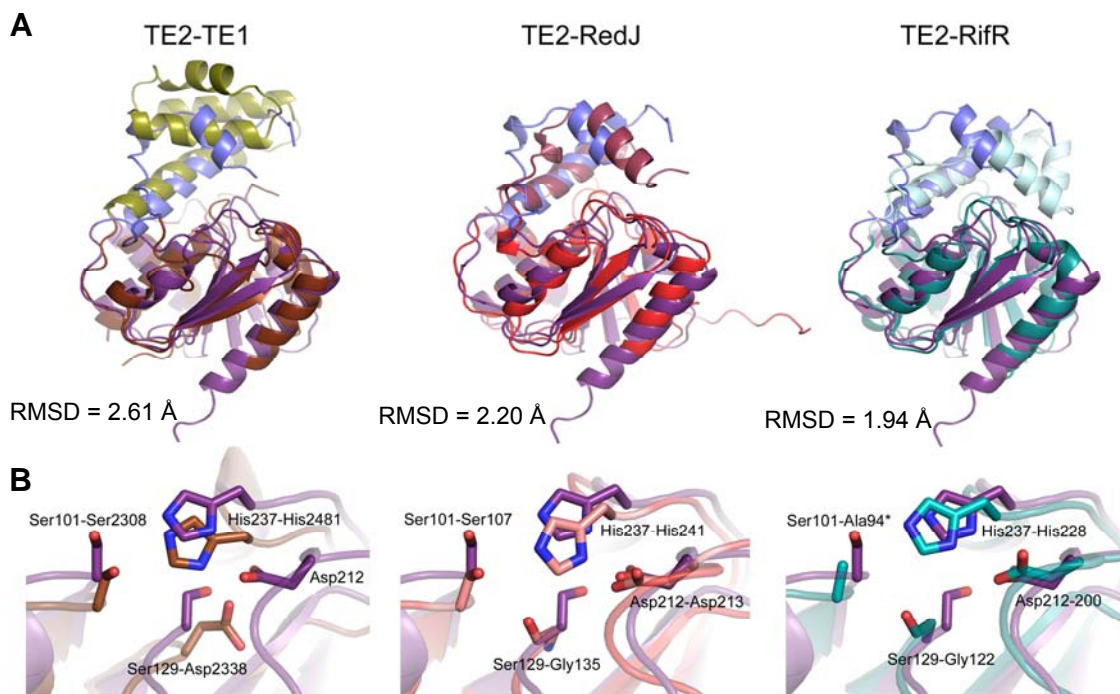


**Figure 2.10. Comparison of TE2 structural homologues. A. Secondary structure superpositions of TE2 with TE1 (brown/olive), RedJ (red/wine) and RifR (teal/cyan).** The superpositions were generated with COOT; RMSD statistics are reported in the lower left corners of each ribbon diagram. **B. Comparison of active site residues.** Positions of active site residues are highly conserved, with the exception of TE1 adopting a non-canonical position for Asp2338 (Equivalent residues for TE2, RedJ and RifR are also shown). Catalytic residues are found in loop regions connecting the secondary structural elements.

indicate TE2 and RifR have the closest structural similarity. However, visual inspection of the secondary structure overlays clearly determines RedJ to have the closest structural homology to TE2. TE2 and RedJ capping domains are equivalently composed of two helices connected by a long, disordered loop region. The capping domains of RifR and TE1 are composed of 3 and 4 helices, respectively; these additional structural elements are devoid of positional homology to TE2 or RedJ. Inasmuch, the TE1 sub-domain B structure shares the least structural homology to the capping domain structures of the three type II thioesterases.

The most common feature shared between all four thioesterase capping domains is the highly conserved  $\alpha$ -helix extending up from the hydrolase core. The interface between this helix and the hydrolase core of TE1 gives rise to the substrate specificity channel observed in the TE1-orlistat crystal complex (Figure 2.11A) (61). Hydrophobic residues from this helix as well as hydrophobic residues surrounding the TE1 active site participate in substrate binding (Figure 2.11B). Similarly, the interface between the first  $\alpha$ -helix of the TE2 capping domain and the hydrolase core produce an apparent substrate pocket comprised of hydrophobic residues (Figure 2.11C). The putative TE2 substrate binding surface is also adjacent to its active site. The TE1 substrate specificity channel is composed mostly of bulky phenylalanine and tyrosine hydrophobic residues; the putative TE2 substrate binding surface is lined with less bulky hydrophobic residues as well as some polar residues (Figure 2.11D). Given the proximity of the hydrophobic surface to the TE2 active site, it seems likely this region of the enzyme participates in substrate binding/recognition.

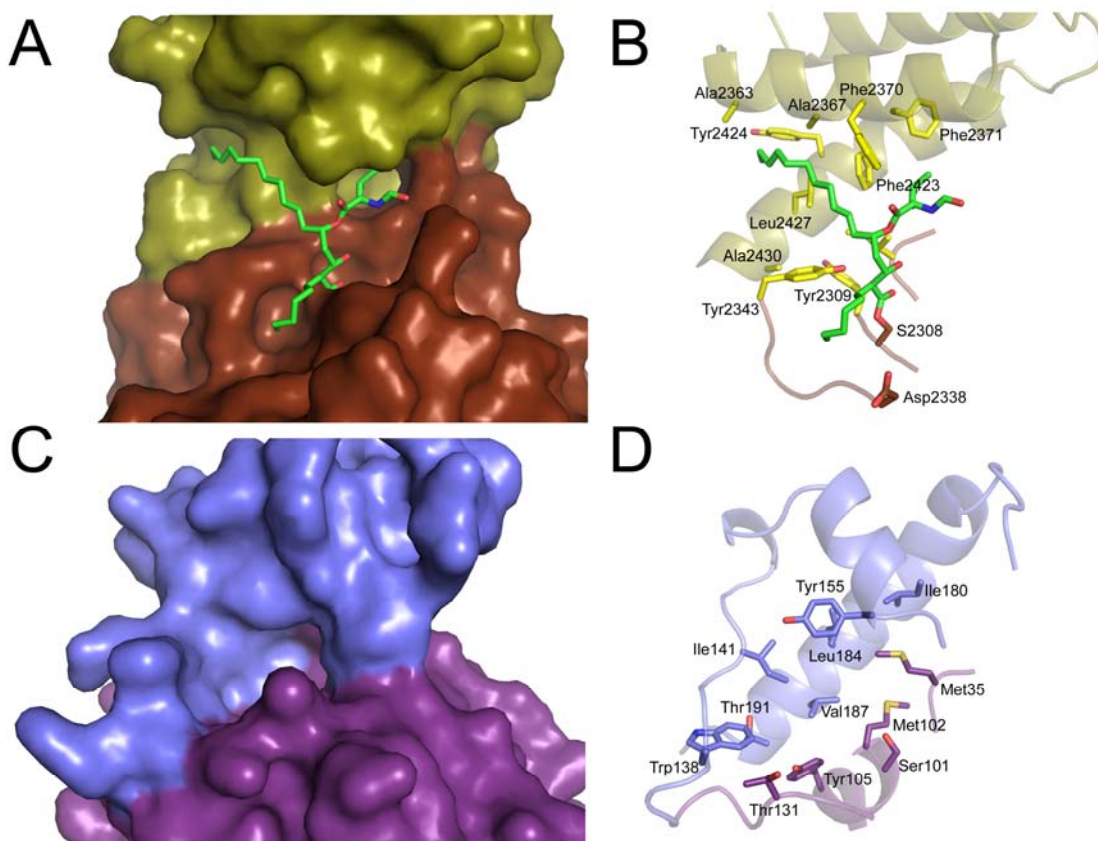


**Figure 2.11. Analysis of the hydrophobic content at the interface between the hydrolase cores and capping domains of TE1 and TE2.** The TE1-Orlistat complex revealed the position of the substrate specificity channel and the specific residues participating in substrate binding. A large pocket adjacent to the TE2 active site is located in similar orientation to the substrate specificity channel observed in TE1. **A.** Surface representation of the TE1 domain interface with Orlistat (green) covalently bound to Ser2308. **B.** Hydrophobic residues from both the hydrolase core and capping domain participate in substrate binding. **C.** Surface representation of the TE2 domain interface centered at the active site. **D.** The putative TE2 substrate binding surface is composed mostly of hydrophobic residues from both the hydrolase core and capping domain.

Further inspection of active site surfaces for TE1, TE2 and RifR show differences in active site accessibilities (Figure 2.12) (RifR is not discussed for brevity). The putative substrate binding surfaces for TE2 and RedJ are not fully accessible to solvent and are blocked by residues from both the capping domain and the hydrolase core. In contrast, the TE1 active site and substrate specificity channel are more solvent exposed and apparently unobstructed (a disordered loop extending up from the hydrolase core to the capping domain may partially block the TE1 active site). No conformational changes were observed between the native and orlistat-bound TE1 crystal structures. The observation that TE2 is in a closed conformation is consistent with the reported flexibility of capping domains described for RedJ and RifR. Re-positioning of the TE2 subdomains would allow for increased accessibility to its active site, and allow for optimal active-site positioning for catalysis.

## **2.4 Discussion**

The selection of modular synthase substrates hydrolysed by the respective type I or type II thioesterases demonstrates the critical role of thioesterases to dictate product distributions in cells and to rescue stalled synthetic modules. In eukaryotes, FASN exclusively produces palmitate and stearate LCFAs due to the selectivity of the endogenous TE1 domain. But in the presence of TE2, FASN produces a range of MCFAs and some LCFAs. In prokaryotes, the endogenous TE domains of PKS and NRPS systems determine the specificity and diversity of macrolide and non-ribosomal peptide natural products. In the absence of the housekeeping function of type II thioesterases like RifR and RedJ, these modular synthases are greatly inhibited due to utilization of aberrant metabolites for priming the carrier protein domains.



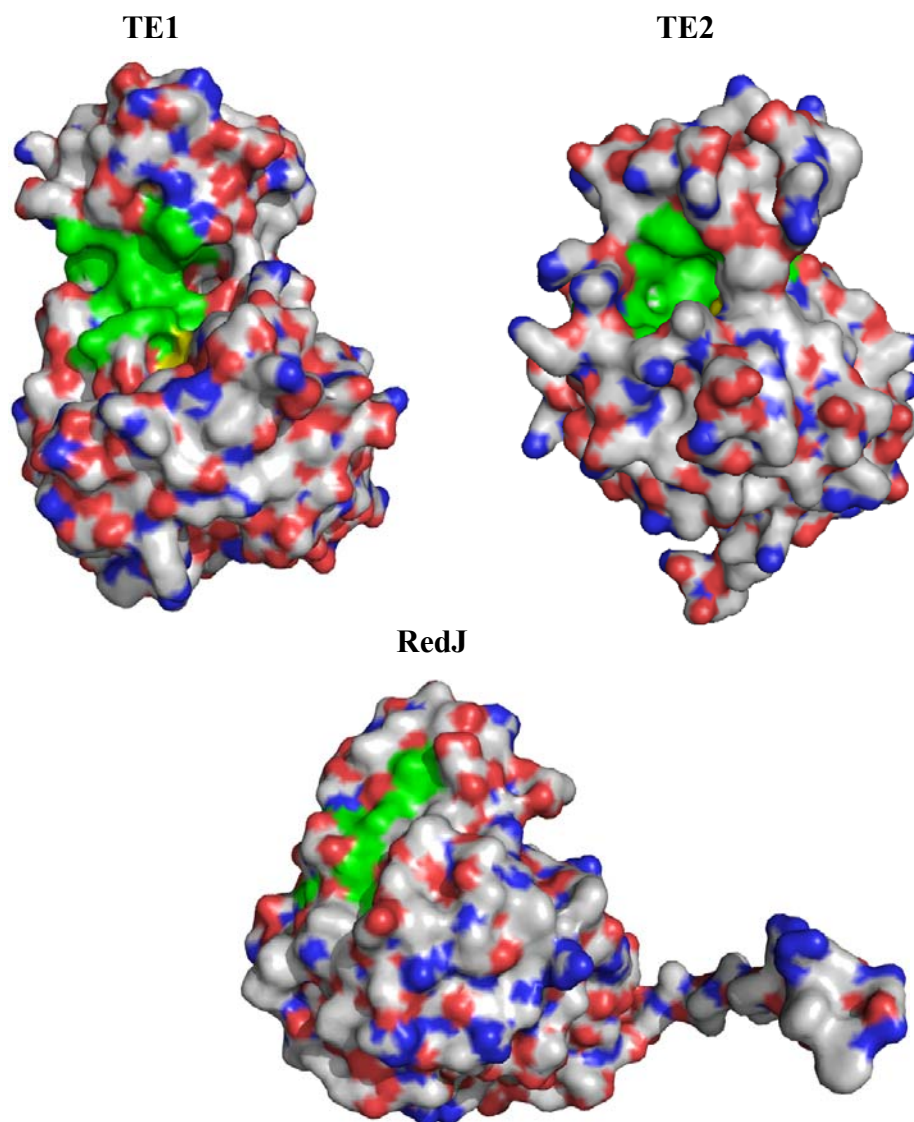


**Figure 2.12. Electrostatic surface representation of TE1, TE2 and RedJ.** The putative substrate binding surfaces for TE2 and RedJ, as well as the substrate specificity channel of TE1, are colored in green. The active site serine residues are colored yellow. The TE1 active site and substrate specificity channel are solvent exposed and fully accessible by substrates. The equivalent hydrophobic surfaces of TE2 and RedJ, as well as each active site triad, are partially blocked from solvent exposure. Both capping domains appear to adopt a closed conformation, occluding substrate access to the catalytic residues of the active site.



It is important to have highly selective terminating activities dedicated to the endogenous TE domains, due to the iterative processing of the FASN, PKS and NRPS assemblies. In all three modular synthase systems, the TE domain is directly tethered to the respective ACP or PCP domain, effectively saturating the thioesterases with a substrate binding partner. Without highly specific substrate selection, aberrant TE hydrolysis of synthetic intermediates would abolish the ability of cells to generate the necessary secondary metabolites essential for survival. The selectivity of the endogenous TE domains ensures that the desired biologic product is produced and liberated from the enzyme complex, maintaining efficient product turnover by these modular synthases. Indeed, continuous elongation and  $\beta$ -carbon processing of synthetic intermediates would likely continue in the absence of the terminating TE, effectively rendering the modular synthases inactive as the intermediates generated become less suitable substrates for the catalytic domains and/or editing type II thioesterases. This is supported by early studies on trypsin-treated FASN lacking the TE1 domains which demonstrated near inhibition of product release with a shift in acyl chain lengths favoring C20 and C22 fatty acids (45,47).

The diffusable nature of TE2, RedJ and RifR type II thioesterases requires these enzymes to have high selectivity for substrates and for their respective ACP or PCP domains, in order to carry out their biological function. Specificity for the carrier protein domains by RifR or RedJ ensures efficient restoration of stalled PKS or NRPS systems when a poorly chosen substrate is primed to the carrier protein domain. Similarly, TE2 specificity for the ACP domain of FASN ensures efficient modulation of product distribution in the presence of an active TE1 domain.

The apparent open and closed dynamics of the capping domain may prove to be an important feature of TE2. The free fatty acyl pools in cells are present as fatty acyl-CoAs. Therefore, the presence of a freely diffusable cytosolic thioesterase could jeopardize lipid homeostasis, and by extension cellular homeostasis. The apparent closed conformation of TE2 would effectively attenuate activity by limiting its access to fatty acyl-CoA metabolites present in the cell, ensuring maintenance of cytosolic lipid pools. This result is supported by the observation of a 10-fold difference in TE2 activity against acyl-CoA substrates compared to TE1. TE2 showed specificity for myristoyl-CoA, however its activity was significantly less with respect to TE1. TE2 activity was dramatically improved when presented with an acylated ACP substrate, and resulted with 5-fold higher activity against acyl-ACP compared to TE1. Differences in capping domain structures may explain differences in substrate and carrier protein recognition. The improved specific activity suggests TE2-acyl-ACP interactions facilitate changes at the TE2 active site to allow optimal alignment of the catalytic triad and improved active site accessibility.

The rigid structure of the capping domain of TE1 maintains the active site architecture for accommodating LCFAs, with strict selection for palmitate or stearate. Bulky aromatic residues constitute the active site and are thought to serve as a molecular ruler (76). In contrast, the putative TE2 substrate pocket is comprised of less-bulky hydrophobic residues and some polar residues which are more dispersed, and do not clearly establish a molecular ruler for chain-length specificity. It is not clear whether conformational changes of TE2 upon binding ACP will alter the active site register. The biological consequence of the TE2 broad substrate specificity channel can be explained

by the iterative processing of FASN. At any point in the catalytic process, 6 acyl intermediates (C4 through C16) are available for hydrolysis from ACP; therefore, the point at which TE2 binds ACP determines which acyl intermediate is subject to hydrolysis. However, it is still unclear whether TE2 exhibits any selectivity for acyl chain length. Future evaluation of TE2 activity against C12-C18-ACP substrates is needed to complement our current understanding of TE2 selectivity based on acyl-CoA substrates.

Differential inhibition of TE1 and TE2 is an important observation with respect to current drug development research targeting FASN. TE1-targeted FASN inhibition has been validated as a drug target for developing cancer treatments. However, TE1 may not be the only thioesterase activity to consider for FASN drug development. It has been demonstrated that TE2 readily modulates FASN product distribution and maintains activity when treated with concentrations of inhibitors which completely inhibit TE1. Therefore, TE2 retains the ability to rescue FASN from TE1 inhibition. Moreover, the observation that the closed conformation of TE2 confers sub-optimal alignment of catalytic residues and that the active site is blocked by the capping domain demonstrates how the potency of inhibitors may be attenuated. To date, specific upregulation of TE2 in cancer has not been identified. However, its utility as a serum marker for breast cancer was reported, but no follow up studies were done (78). TE2 expression in breast epithelial cells regardless of lactation status may explain the detection of TE2 in the serum of breast cancer patients (53,79-80).

## 2.5 Conclusions

Combined crystallographic and kinetic data firmly establish TE2 as a member of the  $\alpha/\beta$  serine hydrolase family of enzymes. TE2 homology to PKS and NRPS type II thioesterases further establish their roles in editing modular synthase activity. In the example of PKS and NRPS, type II thioesterases rescue stalled synthases and ensure efficient processing of macrolides and non-ribosomal peptides, whereas TE2 intervenes in fatty acid biosynthesis to modulate acyl product distribution. Kinetic data demonstrated the strict selection of acyl substrates by TE1 regardless of the presence of an ACP binding partner. In contrast, the novel acyl-ACP assay clearly demonstrated the requirement of the ACP domain for efficient TE2 catalysis.

Moreover, comparisons between TE1 and TE2 active site regions combined with the results of enzyme inhibition demonstrated unique active site architectures. The TE1 active site is organized and readily accessible to accommodate LCFAs. The active site region of TE2 does not have a molecular signature clearly dictating chain-length selection. In addition, the crystal structure revealed a closed conformation of the sub-domain capping feature which limits access to the active site. A more comprehensive understanding of the molecular dynamics of ACP binding by TE1 and TE2 is needed to fully understand the molecular mechanism of catalysis. This information will provide an improved foundation for FASN drug development against cancer.

## References

1. Wakil, S. J. (1962) Lipid metabolism. *Annu Rev Biochem* **31**, 369-406
2. Wolken, J. J. (1968) Cellular organelles and lipids. *J Am Oil Chem Soc* **45**, 241-246
3. Wymann, M. P., and Schneider, R. (2008) Lipid signalling in disease. *Nat Rev Mol Cell Biol* **9**, 162-176
4. Schug, Z. T., Frezza, C., Galbraith, L. C., and Gottlieb, E. (2012) The music of lipids: how lipid composition orchestrates cellular behaviour. *Acta Oncol* **51**, 301-310
5. Huang, C. B., Alimova, Y., Myers, T. M., and Ebersole, J. L. (2011) Short- and medium-chain fatty acids exhibit antimicrobial activity for oral microorganisms. *Arch Oral Biol* **56**, 650-654
6. Sun, C. Q., O'Connor, C. J., and Robertson, A. M. (2002) The antimicrobial properties of milkfat after partial hydrolysis by calf pregastric lipase. *Chem Biol Interact* **140**, 185-198
7. Petschow, B. W., Batema, R. P., and Ford, L. L. (1996) Susceptibility of *Helicobacter pylori* to bactericidal properties of medium-chain monoglycerides and free fatty acids. *Antimicrob Agents Chemother* **40**, 302-306
8. Shurbaji, M. S., Kalbfleisch, J. H., and Thurmond, T. S. (1996) Immunohistochemical detection of a fatty acid synthase (OA-519) as a predictor of progression of prostate cancer. *Hum Pathol* **27**, 917-921

9. Oskouian, B. (2000) Overexpression of fatty acid synthase in SKBR3 breast cancer cell line is mediated via a transcriptional mechanism. *Cancer Lett* **149**, 43-51
10. Wang, Y., Kuhajda, F. P., Li, J. N., Pizer, E. S., Han, W. F., Sokoll, L. J., and Chan, D. W. (2001) Fatty acid synthase (FAS) expression in human breast cancer cell culture supernatants and in breast cancer patients. *Cancer Lett* **167**, 99-104
11. Swinnen, J. V., Roskams, T., Joniau, S., Van Poppel, H., Oyen, R., Baert, L., Heyns, W., and Verhoeven, G. (2002) Overexpression of fatty acid synthase is an early and common event in the development of prostate cancer. *Int J Cancer* **98**, 19-22
12. Van de Sande, T., De Schrijver, E., Heyns, W., Verhoeven, G., and Swinnen, J. V. (2002) Role of the phosphatidylinositol 3'-kinase/PTEN/Akt kinase pathway in the overexpression of fatty acid synthase in LNCaP prostate cancer cells. *Cancer Res* **62**, 642-646
13. Rossi, S., Graner, E., Febbo, P., Weinstein, L., Bhattacharya, N., Onody, T., Bubley, G., Balk, S., and Loda, M. (2003) Fatty acid synthase expression defines distinct molecular signatures in prostate cancer. *Mol Cancer Res* **1**, 707-715
14. Baron, A., Migita, T., Tang, D., and Loda, M. (2004) Fatty acid synthase: a metabolic oncogene in prostate cancer? *J Cell Biochem* **91**, 47-53
15. Menendez, J. A., and Lupu, R. (2004) Fatty acid synthase-catalyzed *de novo* fatty acid biosynthesis: from anabolic-energy-storage pathway in normal tissues to jack-of-all-trades in cancer cells. *Arch Immunol Ther Exp (Warsz)* **52**, 414-426

16. Wang, Y. Y., Kuhajda, F. P., Li, J., Finch, T. T., Cheng, P., Koh, C., Li, T., Sokoll, L. J., and Chan, D. W. (2004) Fatty acid synthase as a tumor marker: its extracellular expression in human breast cancer. *J Exp Ther Oncol* **4**, 101-110
17. Ogino, S., Nosho, K., Meyerhardt, J. A., Kirkner, G. J., Chan, A. T., Kawasaki, T., Giovannucci, E. L., Loda, M., and Fuchs, C. S. (2008) Cohort study of fatty acid synthase expression and patient survival in colon cancer. *J Clin Oncol* **26**, 5713-5720
18. Migita, T., Ruiz, S., Fornari, A., Fiorentino, M., Priolo, C., Zadra, G., Inazuka, F., Grisanzio, C., Palescandolo, E., Shin, E., Fiore, C., Xie, W., Kung, A. L., Febbo, P. G., Subramanian, A., Mucci, L., Ma, J., Signoretti, S., Stampfer, M., Hahn, W. C., Finn, S., and Loda, M. (2009) Fatty acid synthase: a metabolic enzyme and candidate oncogene in prostate cancer. *J Natl Cancer Inst* **101**, 519-532
19. Uddin, S., Hussain, A. R., Ahmed, M., Abubaker, J., Al-Sanea, N., AbdulJabbar, A., Ashari, L. H., Alhomoud, S., Al-Dayel, F., Bavi, P., and Al-Kuraya, K. S. (2009) High Prevalence of Fatty Acid Synthase Expression in Colorectal Cancers in Middle Eastern Patients and Its Potential Role as a Therapeutic Target. *Am J Gastroenterol* **104**, 1790-1801
20. Flavin, R., Peluso, S., Nguyen, P. L., and Loda, M. (2010) Fatty acid synthase as a potential therapeutic target in cancer. *Future Oncol* **6**, 551-562
21. Pizer, E. S., Thupari, J., Han, W. F., Pinn, M. L., Chrest, F. J., Frehywot, G. L., Townsend, C. A., and Kuhajda, F. P. (2000) Malonyl-coenzyme-A is a potential mediator of cytotoxicity induced by fatty-acid synthase inhibition in human breast cancer cells and xenografts. *Cancer Res* **60**, 213-218

22. Thupari, J. N., Pinn, M. L., and Kuhajda, F. P. (2001) Fatty acid synthase inhibition in human breast cancer cells leads to malonyl-CoA-induced inhibition of fatty acid oxidation and cytotoxicity. *Biochem Biophys Res Commun* **285**, 217-223
23. Liu, B., Wang, Y., Fillgrove, K. L., and Anderson, V. E. (2002) Triclosan inhibits enoyl-reductase of type I fatty acid synthase in vitro and is cytotoxic to MCF-7 and SKBr-3 breast cancer cells. *Cancer Chemother Pharmacol* **49**, 187-193
24. Brusselmans, K., De Schrijver, E., Heyns, W., Verhoeven, G., and Swinnen, J. V. (2003) Epigallocatechin-3-gallate is a potent natural inhibitor of fatty acid synthase in intact cells and selectively induces apoptosis in prostate cancer cells. *Int J Cancer* **106**, 856-862
25. De Schrijver, E., Brusselmans, K., Heyns, W., Verhoeven, G., and Swinnen, J. V. (2003) RNA interference-mediated silencing of the fatty acid synthase gene attenuates growth and induces morphological changes and apoptosis of LNCaP prostate cancer cells. *Cancer Res* **63**, 3799-3804
26. Yeh, C. W., Chen, W. J., Chiang, C. T., Lin-Shiau, S. Y., and Lin, J. K. (2003) Suppression of fatty acid synthase in MCF-7 breast cancer cells by tea and tea polyphenols: a possible mechanism for their hypolipidemic effects. *Pharmacogenomics J* **3**, 267-276
27. Kridel, S. J., Axelrod, F., Rozenkrantz, N., and Smith, J. W. (2004) Orlistat is a novel inhibitor of fatty acid synthase with antitumor activity. *Cancer Res* **64**, 2070-2075



28. Menendez, J. A., Colomer, R., and Lupu, R. (2004) Inhibition of tumor-associated fatty acid synthase activity enhances vinorelbine (Navelbine)-induced cytotoxicity and apoptotic cell death in human breast cancer cells. *Oncol Rep* **12**, 411-422
29. Lu, S., and Archer, M. C. (2005) Fatty acid synthase is a potential molecular target for the chemoprevention of breast cancer. *Carcinogenesis* **26**, 153-157
30. Menendez, J. A., Lupu, R., and Colomer, R. (2005) Targeting fatty acid synthase: potential for therapeutic intervention in Her-2/neu-overexpressing breast cancer. *Drug News Perspect* **18**, 375-385
31. Browne, C. D., Hindmarsh, E. J., and Smith, J. W. (2006) Inhibition of endothelial cell proliferation and angiogenesis by orlistat, a fatty acid synthase inhibitor. *FASEB J* **20**, 2027-2035
32. Lupu, R., and Menendez, J. A. (2006) Targeting fatty acid synthase in breast and endometrial cancer: An alternative to selective estrogen receptor modulators? *Endocrinology* **147**, 4056-4066
33. Kridel, S. J., Lowther, W. T., and Pemble, C. W. t. (2007) Fatty acid synthase inhibitors: new directions for oncology. *Expert Opin Investig Drugs* **16**, 1817-1829
34. Richardson, R. D., Ma, G., Oyola, Y., Zancanella, M., Knowles, L. M., Cieplak, P., Romo, D., and Smith, J. W. (2008) Synthesis of novel beta-lactone inhibitors of fatty acid synthase. *J Med Chem* **51**, 5285-5296
35. Dowling, S., Cox, J., and Cenedella, R. J. (2009) Inhibition of fatty acid synthase by Orlistat accelerates gastric tumor cell apoptosis in culture and increases survival rates in gastric tumor bearing mice *in vivo*. *Lipids* **44**, 489-498

36. Murata, S., Yanagisawa, K., Fukunaga, K., Oda, T., Kobayashi, A., Sasaki, R., and Ohkohchi, N. (2010) Fatty acid synthase inhibitor cerulenin suppresses liver metastasis of colon cancer in mice. *Cancer Sci* **101**, 1861-1865
37. Notarnicola, M., Messa, C., Refolo, M. G., Tutino, V., Miccolis, A., and Caruso, M. G. (2011) Polyunsaturated fatty acids reduce Fatty Acid Synthase and Hydroxy-Methyl-Glutaryl CoA-Reductase gene expression and promote apoptosis in HepG2 cell line. *Lipids Health Dis* **10**
38. Seguin, F., Carvalho, M. A., Bastos, D. C., Agostini, M., Zecchin, K. G., Alvarez-Flores, M. P., Chudzinski-Tavassi, A. M., Coletta, R. D., and Graner, E. (2012) The fatty acid synthase inhibitor orlistat reduces experimental metastases and angiogenesis in B16-F10 melanomas. *Brit J Cancer* **107**, 977-987
39. Wakil, S. J. (1989) Fatty acid synthase, a proficient multifunctional enzyme. *Biochemistry* **28**, 4523-4530
40. Smith, S. (1994) The animal fatty acid synthase: one gene, one polypeptide, seven enzymes. *FASEB J* **8**, 1248-1259
41. Smith, S., Witkowski, A., and Joshi, A. K. (2003) Structural and functional organization of the animal fatty acid synthase. *Prog Lipid Res* **42**, 289-317
42. Maier, T., Jenni, S., and Ban, N. (2006) Architecture of mammalian fatty acid synthase at 4.5 Å resolution. *Science* **311**, 1258-1262
43. Leibundgut, M., Maier, T., Jenni, S., and Ban, N. (2008) The multienzyme architecture of eukaryotic fatty acid synthases. *Curr Opin Struct Biol* **18**, 714-725
44. Maier, T., Leibundgut, M., and Ban, N. (2008) The crystal structure of a mammalian fatty acid synthase. *Science* **321**, 1315-1322

45. Smith, S., Agradi, E., Libertini, L., and Dileepan, K. N. (1976) Specific release of the thioesterase component of the fatty acid synthetase multienzyme complex by limited trypsinization. *Proc Natl Acad Sci USA* **73**, 1184-1188
46. Dileepan, K. N., Lin, C. Y., and Smith, S. (1978) Release of two thioesterase domains from fatty acid synthetase by limited digestion with trypsin. *Biochem J* **175**, 199-206
47. Lin, C. Y., and Smith, S. (1978) Properties of the thioesterase component obtained by limited trypsinization of the fatty acid synthetase multienzyme complex. *J Biol Chem* **253**, 1954-1962
48. Chakravarty, B., Gu, Z., Chirala, S. S., Wakil, S. J., and Quioco, F. A. (2004) Human fatty acid synthase: structure and substrate selectivity of the thioesterase domain. *Proc Natl Acad Sci USA* **101**, 15567-15572
49. Jensen, R. G. (1999) Lipids in human milk. *Lipids* **34**, 1243-1271
50. Libertini, L. J., and Smith, S. (1978) Purification and properties of a thioesterase from lactating rat mammary gland which modifies the product specificity of fatty acid synthetase. *J Biol Chem* **253**, 1393-1401
51. Libertini, L. J., and Smith, S. (1979) Synthesis of long chain acyl-enzyme thioesters by modified fatty acid synthetases and their hydrolysis by a mammary gland thioesterase. *Arch Biochem Biophys* **192**, 47-60
52. Smith, S., and Libertini, L. J. (1979) Specificity and site of action of a mammary gland thioesterase which releases acyl moieties from thioester linkage to the fatty acid synthetase. *Arch Biochem Biophys* **196**, 88-92

53. Nolin, J. M., Thompson, B. J., and Smith, S. (1982) Localization of thioesterase II, the chain-length regulatory enzyme of milk fatty acid synthesis, in rat mammary gland epithelial cells. *J Endocrinol* **94**, 251-256
54. Tai, M. H., Chirala, S. S., and Wakil, S. J. (1993) Roles of Ser101, Asp236, and His237 in catalysis of thioesterase II and of the C-terminal region of the enzyme in its interaction with fatty acid synthase. *Proc Natl Acad Sci USA* **90**, 1852-1856
55. Smith, S. (1981) Medium-chain fatty acyl-S-4'-phosphopantetheine-fatty acid synthase thioester hydrolase from lactating mammary gland of rat. *Methods Enzymol* **71**, 188-200
56. Claxton, H. B., Akey, D. L., Silver, M. K., Admiraal, S. J., and Smith, J. L. (2009) Structure and functional analysis of RifR, the type II thioesterase from the rifamycin biosynthetic pathway. *J Biol Chem* **284**, 5021-5029
57. Whicher, J. R., Florova, G., Sydor, P. K., Singh, R., Alhamadsheh, M., Challis, G. L., Reynolds, K. A., and Smith, J. L. (2011) Structure and function of the RedJ protein, a thioesterase from the prodiginine biosynthetic pathway in *Streptomyces coelicolor*. *J Biol Chem* **286**, 22558-22569
58. Hutchinson, C. R. (2003) Polyketide and non-ribosomal peptide synthases: falling together by coming apart. *Proc Natl Acad Sci USA* **100**, 3010-3012
59. Smith, S., and Tsai, S. C. (2007) The type I fatty acid and polyketide synthases: a tale of two megasynthases. *Nat Prod Rep* **24**, 1041-1072
60. Hur, G. H., Vickery, C. R., and Burkart, M. D. (2012) Explorations of catalytic domains in non-ribosomal peptide synthetase enzymology. *Natural Product Reports* **29**, 1074-1098

61. Pemble, C. W., Johnson, L. C., Kridel, S. J., and Lowther, W. T. (2007) Crystal structure of the thioesterase domain of human fatty acid synthase inhibited by Orlistat. *Nat Struct Mol Biol* **14**, 704-709
62. Lambalot, R. H., and Walsh, C. T. (1995) Cloning, overproduction, and characterization of the *Escherichia coli* holo-acyl carrier protein synthase. *J Biol Chem* **270**, 24658-24661
63. Shanklin, J. (2000) Overexpression and purification of the *Escherichia coli* inner membrane enzyme acyl-acyl carrier protein synthase in an active form. *Protein Expr Purif* **18**, 355-360
64. Cox, R. J., Crosby, J., Daltrop, O., Glod, F., Jarzabek, M. E., Nicholson, T. P., Reed, M., Simpson, T. J., Smith, L. H., Soulas, F., Szafranska, A. E., and Westcott, J. (2002) *Streptomyces coelicolor* phosphopantetheinyl transferase: a promiscuous activator of polyketide and fatty acid synthase acyl carrier proteins. *J Chem Soc Perk T 1*, 1644-1649
65. Molnos, J., Gardiner, R., Dale, G. E., and Lange, R. (2003) A continuous coupled enzyme assay for bacterial malonyl-CoA:acyl carrier protein transacylase (FabD). *Anal Biochem* **319**, 171-176
66. Potterton, L., McNicholas, S., Krissinel, E., Gruber, J., Cowtan, K., Emsley, P., Murshudov, G. N., Cohen, S., Perrakis, A., and Noble, M. (2004) Developments in the CCP4 molecular-graphics project. *Acta Crystallogr D Biol Crystallogr* **60**, 2288-2294
67. McCoy, A. J. (2007) Solving structures of protein complexes by molecular replacement with Phaser. *Acta Crystallogr D Biol Crystallogr* **63**, 32-41

68. Cowtan, K., Emsley, P., and Wilson, K. S. (2011) From crystal to structure with CCP4. *Acta Crystallogr D Biol Crystallogr* **67**, 233-234
69. Winn, M. D., Ballard, C. C., Cowtan, K. D., Dodson, E. J., Emsley, P., Evans, P. R., Keegan, R. M., Krissinel, E. B., Leslie, A. G., McCoy, A., McNicholas, S. J., Murshudov, G. N., Pannu, N. S., Potterton, E. A., Powell, H. R., Read, R. J., Vagin, A., and Wilson, K. S. (2011) Overview of the CCP4 suite and current developments. *Acta Crystallogr D Biol Crystallogr* **67**, 235-242
70. Zwart, P. H., Afonine, P. V., Grosse-Kunstleve, R. W., Hung, L. W., Ioerger, T. R., McCoy, A. J., McKee, E., Moriarty, N. W., Read, R. J., Sacchettini, J. C., Sauter, N. K., Storoni, L. C., Terwilliger, T. C., and Adams, P. D. (2008) Automated structure solution with the PHENIX suite. *Methods Mol Biol* **426**, 419-435
71. Adams, P. D., Afonine, P. V., Bunkoczi, G., Chen, V. B., Davis, I. W., Echols, N., Headd, J. J., Hung, L. W., Kapral, G. J., Grosse-Kunstleve, R. W., McCoy, A. J., Moriarty, N. W., Oeffner, R., Read, R. J., Richardson, D. C., Richardson, J. S., Terwilliger, T. C., and Zwart, P. H. (2010) PHENIX: a comprehensive Python-based system for macromolecular structure solution. *Acta Crystallogr D Biol Crystallogr* **66**, 213-221
72. Emsley, P., Lohkamp, B., Scott, W. G., and Cowtan, K. (2010) Features and development of Coot. *Acta Crystallogr D Biol Crystallogr* **66**, 486-501
73. Adams, P. D., Afonine, P. V., Bunkoczi, G., Chen, V. B., Echols, N., Headd, J. J., Hung, L. W., Jain, S., Kapral, G. J., Grosse Kunstleve, R. W., McCoy, A. J., Moriarty, N. W., Oeffner, R. D., Read, R. J., Richardson, D. C., Richardson, J. S.,

- Terwilliger, T. C., and Zwart, P. H. (2011) The Phenix software for automated determination of macromolecular structures. *Methods* **55**, 94-106
74. Nardini, M., and Dijkstra, B. W. (1999) Alpha/beta hydrolase fold enzymes: the family keeps growing. *Curr Opin Struct Biol* **9**, 732-737
75. Holmquist, M. (2000) Alpha/Beta-hydrolase fold enzymes: structures, functions and mechanisms. *Curr Protein Pept Sci* **1**, 209-235
76. Zhang, W., Richardson, R. D., Chamni, S., Smith, J. W., and Romo, D. (2008) Beta-lactam congeners of orlistat as inhibitors of fatty acid synthase. *Bioorg Med Chem Lett* **18**, 2491-2494
77. Dodson, G., and Wlodawer, A. (1998) Catalytic triads and their relatives. *Trends Biochem Sci* **23**, 347-352
78. Pawlak, J., and Smith, S. (1986) Evaluation of thioesterase II as a serum marker for rat mammary cancer. *Cancer Res* **46**, 4712-4719
79. Smith, S., Pasco, D., and Nandi, S. (1983) Biosynthesis of medium-chain fatty acids by mammary epithelial cells from virgin rats. *Biochem J* **212**, 155-159
80. Thompson, B. J., and Smith, S. (1985) Biosynthesis of fatty acids by lactating human breast epithelial cells: an evaluation of the contribution to the overall composition of human milk fat. *Pediatr Res* **19**, 139-143

### **Chapter 3. Alternative acyl-ACP synthetic strategies and crystallization experiments**



### 3.1 Introduction

Research over the past six decades has expanded and refined our current understanding of FASN mechanism of catalysis, product distribution, oligomeric state, and structural organization (Figures 1.1 and 1.2) (1-9). Importantly, studies have firmly established FASN singular role in *de novo* fatty acid biogenesis, as well as its role in lactation, normal cell homeostasis, and essential requirement for tumor cell survival and proliferation (10-25). Current advances in medicinal research have established the utility for pharmacological intervention of FASN to treat microbial and fungal infections, as well as to treat a variety of cancers (26-38). Interestingly, TE1-targeted FASN inhibition via Orlistat has demonstrated strong cytotoxicity in several cancers, and has potent anti-tumor activity against prostate cancer (39-48).

Despite these advances, there still remains a sizeable gap of understanding in the molecular details of the inter-domain interactions during catalysis, and which of these interactions or the individual active sites of the six catalytic domains would be the best drug target. TE1 has emerged as an attractive target since its inhibition by Orlistat results in anti-tumor activity. Moreover, the crystal structure of TE1 with Orlistat bound in the active site was the first ligand complex for FASN published (49).

A strong interest has now developed in understanding the recognition mechanisms between TE1 and ACP. The interface between these two domains, as it relates to substrate loading and catalysis, represents an additional target for FASN drug development. However, the spatial organization of these two domains within the context of the FASN assembly is unknown. As discussed in Chapter 2, TE2 activity toward ACP

represents additional substrate and protein interactions to consider for FASN drug development. No structural evidence exists to explain the molecular recognition between ACP and TE1 or TE2. More importantly, there are no crystal structures revealing the mechanism of ACP substrate loading into the TE1 or TE2 active sites. As seen in Figure 1.1, only five of the seven functional FASN domains were modeled due to the inherent flexibility of the C-terminal ACP and TE1 domains.

Synthesis of stable, acyl-loaded ACP substrates became a priority for my research so that kinetic and crystallization experiments could be done using both TE1 and TE2. As discussed in Chapters 1 and 2, the acyl carrier protein (ACP) domain of FASN functions to shuttle the growing acyl chain to adjacent catalytic domains for reductive processing of the  $\beta$ -keto moiety to a mature hydrocarbon. ACP is a small, acidic protein comprised of a four helical bundle with an approximate molecular weight of 8 kDa (Figure 3.1). The principal function of ACP is carried out by the 4'-phosphopantetheine (4'PP) cofactor, which is covalently linked to residue Ser2156 of  $\alpha$ -helix II. The terminal sulfhydryl of 4'PP covalently tethers the acyl substrate intermediate via a thioester linkage (*S*-acyl-ACP). Apo-ACP is modified by the highly specific phosphopantetheinyl transferase (PPTase) to *holo*-ACP (ACPSH), where coenzyme A (CoA) serves as the 4'PP donor (50).

Biochemical studies have been performed on the activity of both endogenous and recombinant TE1 and TE2. Evidence supports TE1 activity to be highly selective for the long chain fatty acids palmitate (C16) and stearate (C18), whereas TE2 activity is more promiscuous against a wide range of short and medium chain fatty acids, such as caprylate (C10) and myristate (C14) (51-62). Moreover, the results reported in

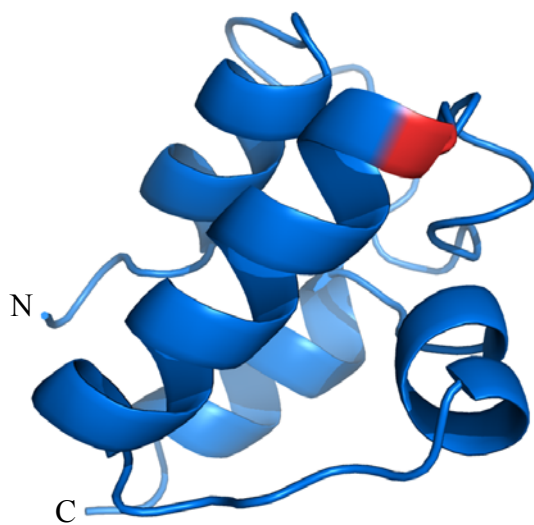


**Figure 3.1. Crystal structure of human ACP.** Ser2156 is colored in red at the C-terminal end of  $\alpha$ -helix II, and is the site of covalent attachment of the 4'PP cofactor (PDB code 2CG5).

Chapter 2, as well as previous published data on rat FASN, support the observation that TE1 has 10-fold higher specific activity against acyl-CoA substrates compared to TE2 (51-52). In contrast, the results in Chapter 2 demonstrated that TE2 has 5-fold higher activity toward C16-ACP compared to TE1. Indeed, the catalytic efficiency of TE2 was significantly improved when presented with the acyl chain substrate bound to the ACP domain. These results suggest that TE2 interactions with acyl-ACP are favored over TE1.

Much time was invested in the synthesis and optimization of the natural *S*-acyl-ACP substrates which are highly susceptible to non-enzymatic hydrolysis at physiological pH. Rapid buffer exchange to a lower pH along with the addition of detergent facilitated stabilization of the acyl-ACP substrate syntheses described in Chapter 2. However, the inherent instability of these substrates did not warrant their utilization in crystallization experiments which take several days to weeks to generate crystals. We were fortunate to collaborate with Dr. Michael Burkart of UCSD (Chemistry Department), who developed a synthetic strategy for generating the more stable, ester-linked *O*-acyl-ACP (acyl<sub>-crypto</sub>ACP) substrates (63). Acyl<sub>-crypto</sub>ACP substrates would be ideal reagents for co-crystallization experiments with TE1 S2308A or TE2 S101A. Summarized in this chapter are efforts focused on an alternative synthesis of the biologically relevant *S*-acyl-ACP substrates and the *O*-acyl-ACP substrates. In addition, alternative TE2 crystallography experiments which produced crystals and medium diffraction quality are discussed. Finally, initial crystallization experiments, which were set up in an effort to determine the interaction between acyl-CoA and TE1 or TE2 as well as the ACP-TE1 interface, are discussed.

## 3.2 Experimental Procedures

### 3.2.1 Purification of MBP-CoA A, MBP-CoA D, and MBP-CoA E

The pMal clones for CoA A, CoA D, and CoA E, enzymes of the CoA biosynthetic pathway, were kindly provided by the Burkart Laboratory (64). All three enzymes were expressed and purified using identical strategies. N-terminal MBP fused CoA A (MBP-CoA A) protein expression in C41(DE3) *E. coli* was induced with 0.1 mM IPTG at 16 °C overnight. Clarified cell lysate containing 100 μM PMSF and benzamidine, 1 mM MgCl<sub>2</sub> and DNase powder was applied to an amylose affinity column (NEB). MBP-CoA A was eluted using a 10 mM maltose buffered solution containing 50 mM Tris 8.0, 200 mM NaCl, 1 mM EDTA and 1 mM DTT. Column flow-through containing MBP-CoA A was dialyzed against 2.0 L of 20 mM HEPES pH 7.5. MBP-CoA A was applied to a Q-sepharose fast-flow ion-exchange column (GE Healthcare) and eluted with a 0-500 mM NaCl in 20 mM HEPES pH 7.5. Fractions containing highly pure MBP-CoA A were pooled, aliquoted and flash frozen in liquid nitrogen for storage at -80 °C.

### 3.2.2 Purification of Sfp+His

The clone for the N-terminal 6X His-tagged phosphopantetheinyl transferase enzyme (Sfp+His) from *B. subtilis* was kindly provided by Dr. Michael Burkart of UCSD (63-65). Sfp+His protein expression in C41(DE3) *E. coli* was induced with 0.1 mM IPTG at 16 °C overnight. Clarified cell lysate containing 100 μM PMSF and benzamidine, 1 mM MgCl<sub>2</sub> and DNase powder was applied to a nickel NTA column. Sfp+His was eluted using a 5-250 mM imidazole gradient buffered in 20 mM HEPES pH

7.9 and 500 mM KCl. Fractions containing Sfp+His were pooled, treated with 5 mM EDTA and 1 mM DTT, and dialyzed against 4.0 L of 20 mM HEPES pH 7.5 and 1 mM DTT. Sfp+His Q-sepharose purification strategies were identical to methods described for MBP-CoA A. Fractions containing highly pure Sfp+His were pooled, aliquoted and flash frozen in liquid nitrogen for storage at -80 °C.

### 3.2.3 Purification of human $\Delta N5\Delta C16$ ACP (nACP)

As an additional optimization strategy for synthesis of *O*-acyl-ACP using cryptocoacyl substrates, ACP was sub-cloned with N- and C-terminal truncations such that only the structured protein elements observed in the human phosphopantetheinyl transferase-ACP complex (PDB code 2CG5) were expressed (residues 2123-2196) (66). Implicit in this cloning strategy was the removal of the only cysteine present in the ACP clone, which would abolish any potential for formation of intermolecular ACP dimers.

The nACP variant was sub-cloned into pET151 TOPO/D (Invitrogen) using the ACP pET151 TOPO/D vector as the PCR template and forward 5'-CACCTAGAAGTACTATTCCAAGGACCAAGCCAGCGGGACCTGGTGGAGG -3' and reverse 5'-CTACTCATCCGCCTTTGAGGACAGC -3' primers. N-terminal 6X-His tag fused nACP (nACP+His with PP site) protein expression in C41(DE3) *E. coli* was induced with 0.2 mM IPTG at 16 °C overnight. Clarified cell lysate containing 100  $\mu$ M PMSF and benzamidine, 1 mM MgCl<sub>2</sub> and DNase powder was applied to a nickel NTA column. nACP+His NTA purification strategies were identical to methods described for SFP+His. Fractions containing nACP+His were pooled, treated with 5 mM EDTA, 2 mM DTT and 5.0 mg of C3 protease (a 20:1 ratio of nACP:C3) and dialyzed

against 4.0 L of 20 mM HEPES pH 7.0 and 1 mM DTT. Removal of the affinity tag was confirmed with a Bruker Autoflex MALDI-TOF MS. nACP Q-sepharose purification strategies were identical to methods described for SFP+His, except that the final pH of buffers used was 7.0. There are no aromatic residues in nACP, therefore no absorbance peak resulted from the Q-sepharose purification. MALDI-TOF MS analyses of individual fractions were used to identify nACP fractions. Fractions containing nACP were pooled, concentrated to 5 mL, and injected over a Superdex 75 gel filtration column equilibrated in 20 mM HEPES pH 7.5, 250 mM NaCl and 1 mM DTT. Highly pure nACP fractions were pooled, concentrated and aliquoted for storage at -80 °C.

### **3.2.4 Synthesis of *O*-acyl-ACP and *O*-acyl-nACP (acyl<sub>-crypto</sub>ACP and acyl<sub>-crypto</sub>nACP)**

Lauryl, myristoyl, palmitoyl, and stearoyl *O*-linked acyl-pantetheine (crypto) substrates were kindly provided by Dr. Michael Burkart from UCSD. Crypto substrates were dissolved into 100 % DMSO at 20 mM final concentrations. Loading conditions for ACP and nACP were optimized using the crypto-laurate substrate. The optimized reactions contained the following: 0.35 mg/mL ACP or nACP were treated with 5X molar excess crypto substrate (C12 –C18) in the presence of 50 mM Tris pH 8.0, 12.5 mM MgCl<sub>2</sub>, 10 mM ATP, 10% DMSO, 0.1 mg/mL MBP-CoA A, 0.11 mg/mL MBP-CoA D, 0.12 mg/mL MBP-CoA E, and 0.05 mg/mL Sfp+His at room temperature or 37 °C. Conversion of ACP to acyl<sub>-crypto</sub>ACP and nACP to acyl<sub>-crypto</sub>nACP were monitored via MALDI-TOF MS analyses.

In addition, a 1  $\mu$ M sample of each crypto substrate was suspended in 50% ACN with 0.1% formic acid and analyzed on a Bruker Esquire HCT ESI-MS to validate the chemical structures. Each substrate was analyzed using ESI-MS, and each of the three primary peaks from the parent spectrum was further analyzed using ESI-MS/MS fragmentation with the assistance of Dr. Mark Lively.

### **3.2.5 Purification of iodoacetamide derivatized *S*-acyl-ACP (acyl-<sup>AA</sup>ACP)**

As an additional strategy to overcome potential intermolecular dimerization of ACP, the single cysteine residue was covalently blocked with iodoacetamide (IAA). Moreover, DTNB quantitation of thioesterase activity on acyl-<sup>AA</sup>ACP required blocking of Cys2202 so that only the free thiol of the 4'PP cofactor was available for TNB conjugation. However, standard curve control experiments with <sup>AA</sup>ACPSH demonstrated that DTNB quantitation was not sensitive enough for kinetic evaluation.

A ten-fold molar excess of IAA was added to ACP resuspended in 100 mM Tris 8.0. MALDI-TOF MS analyses confirmed 100% covalent modification after 30 minutes at room temperature. <sup>AA</sup>ACP was dialyzed overnight against 2.0 L 50 mM Tris pH 8.0. Myristoyl (C14) and palmitoyl (C16) *S*-acyl-<sup>AA</sup>ACP substrates were synthesized using the two-step synthetic strategy described in Chapter 2.

### **3.2.6 Quantitative MALDI-TOF MS discontinuous assay**

TE1 and TE2 kinetic activities using C14-<sup>AA</sup>ACP and C16-<sup>AA</sup>ACP substrates were evaluated with the quantitative MALDI-TOF MS discontinuous assay described in Chapter 2. Only marginal thioesterase activity was detected using equimolar enzyme and substrate concentrations, and rates of hydrolysis were not obtained.



### 3.2.7 Purification of human TE2 (TE2-MBP)

WT TE2 was subcloned into a modified pET28 with Sall 5'-GACGTCGACAATGGAGAGAGGAGACCAACCTAAGAGAACC-3' and NdeI 5'-GAGCTAGCCTAAAAATTGGATATCGATGATACTTCTAGAC-3' primers. This expression construct generates an N-terminal 6X His-tag followed by a maltose binding domain (MBP) and a C3 protease recognition sequence prior to the TE2 protein. The active site Ser101 was mutated to an alanine using the QuikChange mutagenesis protocol (Stratagene) with 5'-GCATTTTTTGGCCACGCTATGGGATCCTACATTGC-3' and 5'-GCAATGTAGGATCCCATAGCGTGGCCAAAAAATGC-3' forward and reverse primers. N-terminal 6X His-tag-MBP fused TE2 (TE2+MBP) protein expression in BL21(DE3)GOLD *E. coli* was induced with 0.1 mM IPTG at 16 °C overnight. Clarified cell lysate containing 100 µM PMSF and benzamidine, 1 mM MgCl<sub>2</sub> and DNase powder was applied to a nickel NTA column. TE2+His was eluted with 20 mM HEPES pH 7.9 and 500 mM KCl buffer following a six hour on-column C3 protease digest with 3.5 mg protease and 5 mM β-mercaptoethanol. TE2-MBP column flow-through was treated with 5 mM EDTA, 2 mM DTT and dialyzed against 4.0 L of 20 mM HEPES pH 7.5 and 1 mM DTT. TE2-MBP was applied to a Q-sepharose ion-exchange column, and eluted with a 0-500 mM NaCl in 20 mM HEPES pH 7.5 and 5 mM DTT. Fractions containing TE2-MBP were pooled, concentrated to 5 mL, and injected over a Superdex 75 gel filtration column equilibrated in 20 mM HEPES pH 7.5, 100 mM NaCl and 5 mM DTT. Highly pure TE2-MBP fractions were pooled, concentrated and aliquoted for storage at -80 °C.

### 3.2.8 Purification of human $\Delta$ N9 TE2 (nTE2)

The WT TE2 protein sequence was submitted to the I-TASSER on-line server in an effort to identify potential disordered regions that could be removed to facilitate crystallization; five predicted structures resulted (66-69). These TE2 structures all had in common a disordered N-terminal region; therefore it was decided to truncate TE2 from residues 1-9 (nTE2). nTE2 was sub-cloned into pET151 TOPO/D using forward 5'-CACCTAGAAGTACTATTCCAAGGACCAACCAGGAATGAAAACATTTTCAAC TG-3' and reverse 5'-TTAAAAATTGGATATCGATGATACTTCTAGACACTTG-3' primers. N-terminal 6X-His tag fused nTE2 (nTE2+His) protein expression in BL21(DE3)GOLD *E. coli* was induced with 0.1 mM IPTG at 16 °C overnight. Clarified cell lysate containing 100  $\mu$ M PMSF and benzamidine, 1 mM MgCl<sub>2</sub> and DNase powder was applied to a nickel NTA column. nTE2+His NTA and Q-sepharose purification strategies were identical to methods described for ACP+His, except that the final pH of buffers was 7.5. nTE2 Superdex 75 purification strategies were identical to those described for TE2-MBP. Highly pure nTE2 fractions were pooled, concentrated and aliquoted for storage at -80 °C.

### 3.2.9 Purification of the S2308A-H2481A double mutants of TE1 or ACP-TE1 (TE1 DM; ATE DM)

TE1 S2308A in pET15b and ACP-TE1 S2308A in pET151TOPO/D were previously cloned in our lab. The TE1 active site H2481A mutant was generated using the QuikChange procedures (Stratagene) with forward and reverse primers 5'-GGGTGACGCCCGCACGCTGCT-3' and 5'-AGCAGCGTGCGGGCGTCACCC-3'.

The purification strategies for TE1 DM and ATE DM are identical to previously reported WT TE1 purification (49).

### **3.2.10 Crystallization of WT or Selenomethionine (SeMet) TE2 and nTE2**

WT TE2-MBP diamond-shaped crystals were identified using commercially available crystal screening kits from Qiagen. Optimized TE2-MBP crystals were grown using the hanging-drop vapor diffusion method at 4 °C in well solution containing 16% PEG 3350, 100 mM HEPES pH 7.4, 200 mM NaNO<sub>3</sub>, and 1.1 % Anapoe 80 (Avanti Polar Lipids). Fresh protein stocks of 20 mg/mL TE2-MBP and 20 mM DTT were prepared and mixed in a 1:1 ratio with well solution. S101A TE2-MBP failed to produce crystals in WT conditions; no crystallization conditions were identified from crystal screening kits. Selenomethionine was incorporated into the TE2 protein by the growth of cells in minimal media and the repression of endogenous methionine synthesis prior to induction (70). MALDI-TOF MS analyses confirmed all four methionine residues were replaced with SeMet. SeMet TE2-MBP readily produced crystals in the optimized condition described above.

nTE2 crystals of needle morphology were also identified using the commercially available crystal screening kits. These crystals were grown in well solution containing 1.8 M (NH<sub>4</sub>)<sub>2</sub>SO<sub>4</sub> and 100 mM NaOAc pH 5.5 at room temperature. Fresh protein stocks of 20 mg/mL nTE2 with 20 mM DTT were mixed in a 1:1 ratio with well solution. Subsequent optimization of crystallization conditions did not improve the crystal morphology for use in data collection.

### 3.2.11 Co-crystallization trials

Several co-crystallization experiments were performed in an effort to achieve crystal complexes, which would provide crystallographic evidence for TE1 or TE2 mechanisms of substrate binding and pantetheine and ACP recognition. In addition, nTE2 crystallization trials were set-up to obtain crystals for the native TE2 crystal structure. All co-crystallization trials were set-up using the commercially available crystal screening kits from Qiagen (seven 96-well plates):

1. 20 mg/mL TE1 S2308A or TE2 S101A + 5X molar excess C14-CoA + 20 mM DTT
2. 20 mg/mL TE1 S2308A or TE2 S101A + 5X molar excess ACPSH + 20 mM DTT
3. 10 mg/mL TE1 S2308A or TE2 S101A + ACPSH + 10 mM DTT
4. 10 mg/mL ATE S2308A +/- 10X molar excess CoA + 10 mM DTT
5. 10 mg/mL TE1+ 10 mg/mL TE2 + 10 mM DTT
6. 20 mg/mL TE1 DM or ATE DM + 5X molar excess C14-CoA or C16-CoA + 20 mM DTT
7. 20 mg/ml nTE2 + 20 mM DTT

Trays were assembled using the Gryphon crystallization robot (ArtRobbins Instr.) by mixing equal volumes (200 nL) of protein stocks listed above and well solution. Trays were initially incubated at room temperature and moved to 4 °C to promote crystal growth.

### 3.2.12 Data collection and processing

X-ray diffraction data were collected as 0.5 degree oscillation images on our in-house Rigaku RA-Micro 007 generator with a Saturn92 CCD detector. TE2-MBP or SeMet TE2 crystals were cryoprotected in aqueous mother liquor with 15% ethylene glycol. SeMet crystals with strong diffraction to 3.0 Å resolution were flash frozen in liquid nitrogen and submitted for data collection on the X-25 beam-line at NSLS in Brookhaven, NY. The d\*Trek software was used to process the WT and SeMet TE2-MBP data sets.

## 3.3 Results

### 3.3.1 acyl<sub>-crypto</sub>ACP and acyl<sub>-crypto</sub>nACP syntheses

The susceptibility of *S*-acyl-ACP substrates to non-enzymatic hydrolysis prompted our collaboration with Dr. Burkart, which provided an alternative synthetic strategy to obtain the more stable *O*-linked acyl-ACP substrates. These acyl<sub>-crypto</sub>ACP substrates would provide ideal reagents for co-crystallization experiments with the TE1 and TE2 active site mutants. Two ACP constructs were used in parallel to generate the acyl<sub>-crypto</sub>ACP/nACP substrates. Several optimizations were tested to achieve rapid conversion to product, as well as to stabilize the generated products. Optimization reactions included the addition of 10-20 % DMSO, 0.5-2.0% Triton X-100, varied enzyme concentrations, pH values ranging from 5 to 9, time dependence (hours versus overnight), reaction volume or scale, temperature (RT or 37 °C) and the molar ratio of ACP to crypto substrates. Several limitations for this synthetic scheme were observed throughout optimization trials. First, the crypto substrates for palmitate and stearate do

not readily dissolve into the aqueous reaction mix; therefore, there was a limit to the molar excess with which these crypto substrates could be used in the loading reaction. Importantly, the stearate crypto substrate was too insoluble, and no ACP/nACP loading was ever observed. Second, a limit to scale-up the reaction to generate high milligram quantities of product was observed. When reaction volumes were increased above 1 mL, the reaction kinetics was dramatically slowed, even when all reagents were scaled proportionally. Moreover, increasing the molar composition of ACP/nACP in the reaction mix resulted with heavy precipitate and incomplete conversion to product.

The most striking limitation of this synthetic strategy was the observed hydrolysis of myristoyl-<sub>crypto</sub>ACP/nACP (cC14-ACP/nACP) and palmitoyl-<sub>crypto</sub>ACP/nACP (cC16-ACP/nACP) substrates after 3 hours at room temperature; experiments conducted at 37 °C produced severe amounts of precipitate with inefficient loading. MALDI-TOF MS analyses were used throughout optimization processes to assess completion of reactions; the complete conversion of ACP/nACP to product should result with a single product peak at the expected m/z shown in Tables 3.1 and 3.2 (column 2). As seen in Figure 3.2, synthesis of cC14-ACP and cC16-ACP resulted with 2 primary peaks of m/z difference consistent with loss of the acyl chain (Tables 3.1 and 3.2, 3<sup>rd</sup> column). Identical results were observed for nACP crypto loading as seen in Figure 3.3.

### 3.3.2 ESI-MS and ESI-MS/MS analyses of crypto substrates

The surprising result of apparent acyl-<sub>crypto</sub>ACP hydrolysis raised the question of whether the substrates themselves were contaminated with CoA or pantothenic acid. If either of these impurities were present in the provided crypto substrates, the collection of

**Table 3.1. Substrate molecular weights and corresponding acyl<sub>crypto</sub>ACP products.**

Substrate	acyl <sub>crypto</sub> 4'PP	acyl <sub>crypto</sub> ACP	acyl aldehydes
C12	506.57	11692	183
C14	534.63	11720	211
C16	562.68	11748.1	239
C18	590.73	11776.1	267

The mass of the crypto substrates is reported in column 2, and the theoretical mass of acyl<sub>crypto</sub>ACP substrates is reported in column 3. The mass of the acyl chain is reported in column 4.

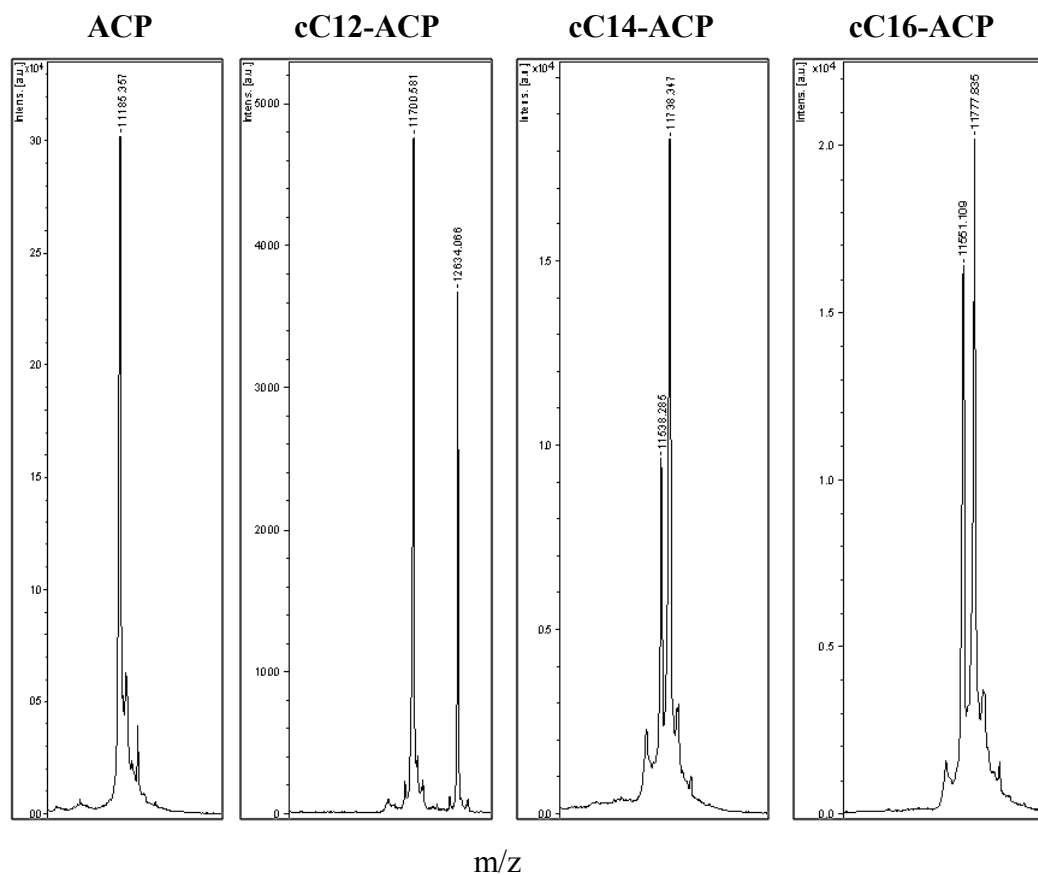


**Figure 3.2. MALDI-TOF MS results for crypto substrate loading of ACP.** MALDI-TOF MS results are shown above for ACP loading after 3 hours at room temperature. ACP incubated with reaction conditions lacking the crypto substrates produced a single peak. A single  $m/z$  species should have resulted for the conversion of ACP to acyl<sub>crypto</sub>ACP. The difference between the  $m/z$  peaks in the cC14-ACP and cC16-ACP spectra is consistent with the mass of myristate and palmitate, indicating partial hydrolysis of acyl<sub>crypto</sub>ACP products occurred. ACP was fully converted to cC12-ACP after 3 hours at room temperature and remained intact.



**Table 3.2. Substrate molecular weights and corresponding acyl-<sub>crypto</sub>nACP products.**

Substrate	acyl <sub>crypto</sub> 4'PP	acyl- <sub>crypto</sub> nACP	acyl aldehydes
C12	506.57	8908.1	183
C14	534.63	8936.4	211
C16	562.68	8964.4	239
C18	590.73	8992.5	267

The mass of the crypto substrates is reported in column 2, and the theoretical mass of acyl-<sub>crypto</sub>nACP substrates is reported in column 3. The mass of the acyl chain is reported in column 4.

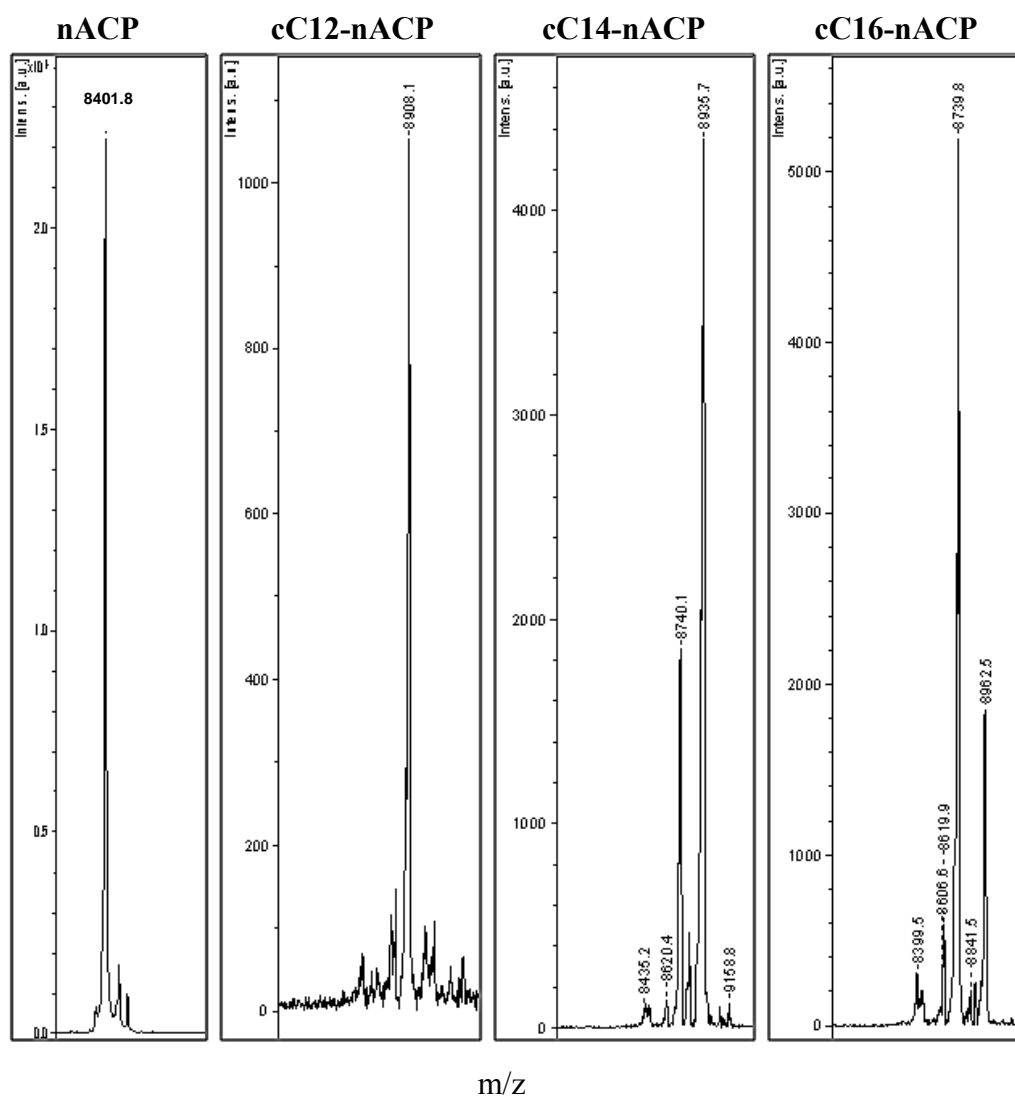


**Figure 3.3. MALDI-TOF MS results for crypto substrate loading of nACP.** nACP incubated with reaction conditions lacking the crypto substrates produced a single peak. A single  $m/z$  species should have resulted for the conversion of nACP to acyl<sub>-crypto</sub>nACP. The difference between the  $m/z$  peaks in the cC14-nACP and cC16-nACP spectra is consistent with the mass of myristate and palmitate, indicating partial hydrolysis of acyl<sub>-crypto</sub>nACP products occurred. nACP was fully converted to cC12-nACP after 3 hours at room temperature and remained intact.

pantothenate kinase enzymes along with a phosphopantetheinyl transferase would facilitate aberrant covalent modification of ACP. To determine the purity of the provided substrates, ESI-MS and ESI-MS/MS were used to provide a detailed analysis of the crypto substrates with the assistance of Mark Lively, Ph.D.

The mass analysis results for each substrate are reported in Figure 3.4. For brevity, only the cC12 substrate is discussed in detail for ESI-MS and MS/MS analyses. In Figure 3.55, the chemical composition of the primary peaks is assigned. The population of peaks in the mass spectra was consistent with two chemical species and one related potassium salt adduct; no peaks with  $m/z$  representing pantothenic acid or CoA were observed. MS/MS analyses of the 315  $m/z$  and 427  $m/z$  primary peaks were performed to validate the chemical assignment. Figures 3.6 and 3.8 show the full MS/MS analysis of the related 315  $m/z$  and 427  $m/z$  peaks for all substrates analyzed, respectively. Peaks resulting from MS/MS fragmentation of the 315  $m/z$  and 427 peaks were easily assigned to the compound shown below the spectra (Figures 3.7 and 3.9, respectively). ESI-MS analyses did not provide any evidence to suggest the crypto substrates were hydrolyzed when resuspended in aqueous solution. The combined evidence from ESI-MS analyses determined that there were no contaminating species in the substrate which could explain the secondary  $m/z$  species observed with acyl-<sub>crypto</sub>ACP/nACP loading. Altogether, the evidence suggests that crypto substrate loading of ACP or nACP is followed by hydrolysis of the acyl chain resulting in the two product peaks observed in Figures 3.2 and 3.3.

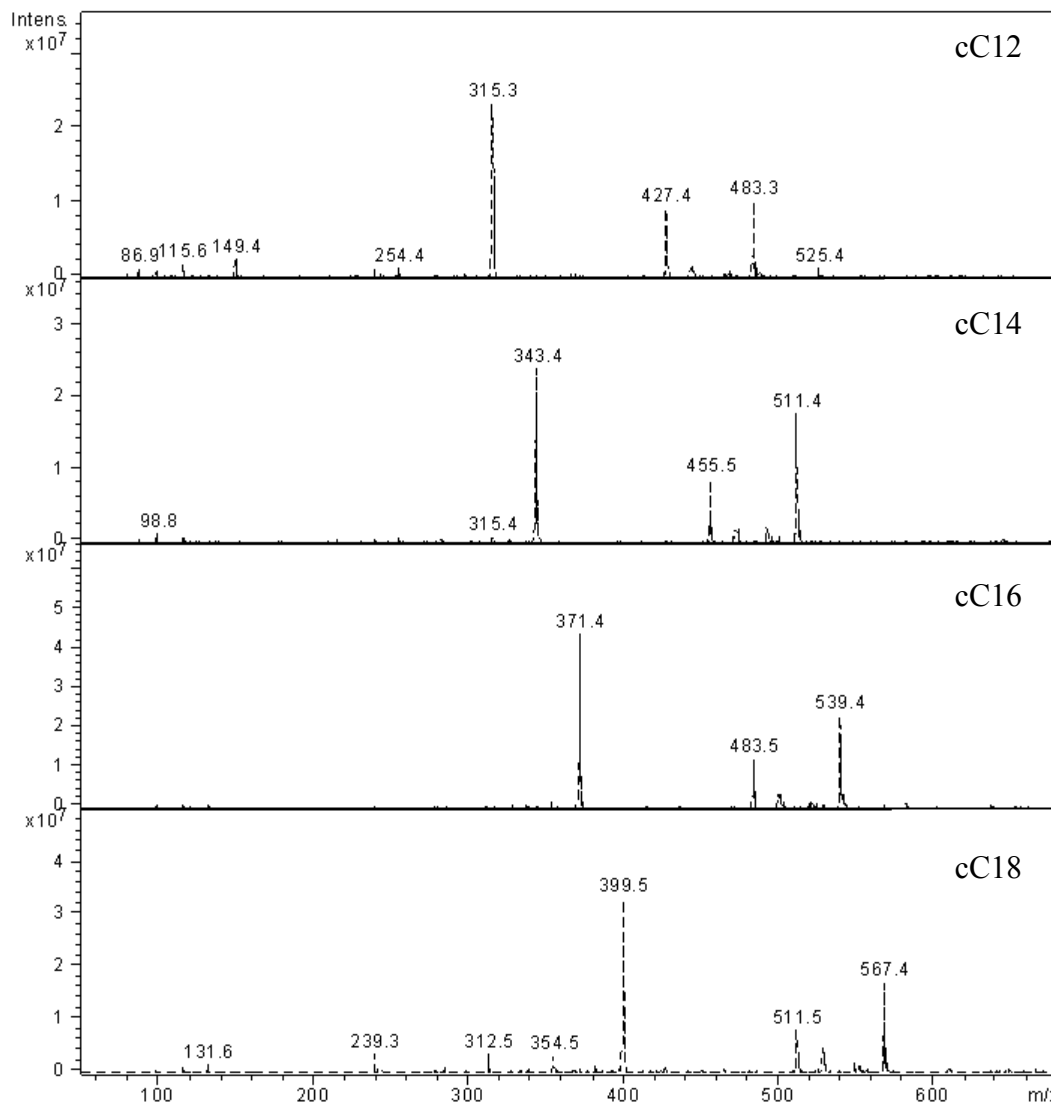


**Figure 3.4. Comparison of ESI-MS analyses of cC12-cC18 substrates.** The main peaks for each substrate are related by the expected difference of 28 m/z.

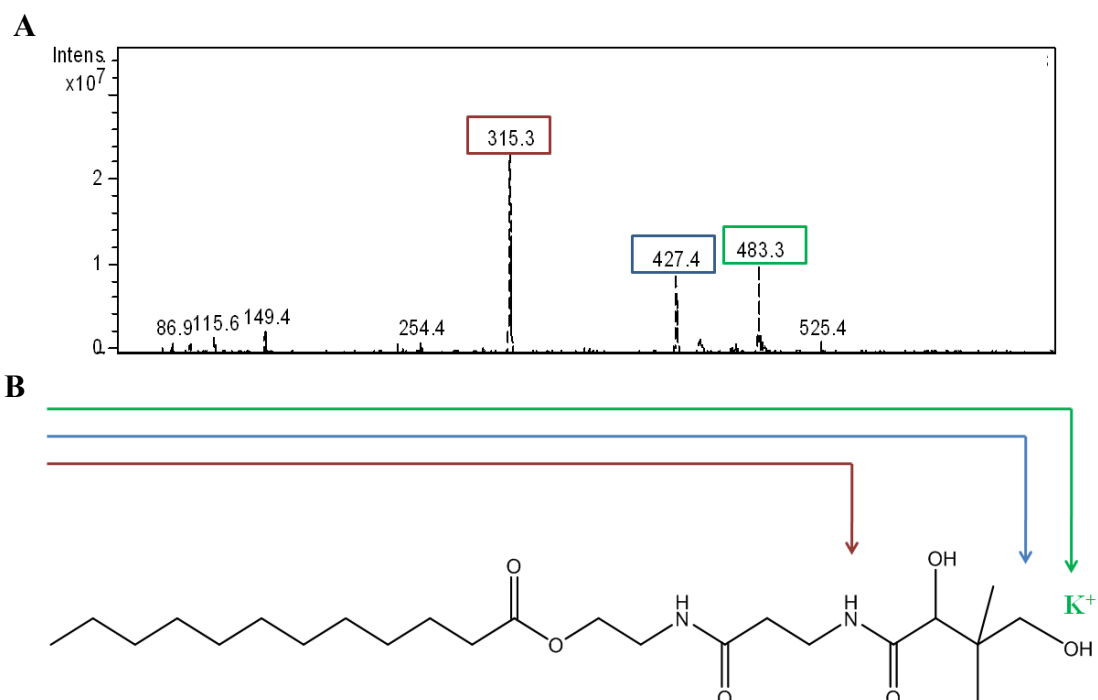


**Figure 3.5. Results of ESI-MS for C12 crypto-substrate (cC12).** **A.** A 10  $\mu\text{M}$  sample of cC12 in 50% ACN, 0.1 % formic acid (FA) was prepared from a 20 mM stock solution of cC12 in DMSO. The strongest mass peaks are outlined in colored squares. **B.** Chemical structure of cC12 with corresponding arrows identifying the chemical species represented in panel A. **Note:** The  $m/z$  peak at 427 is 17  $m/z$  less than expected mass of 444.3  $m/z$  for the full length substrate. This mass differs by a hydroxide moiety, and I arbitrarily chose the terminal hydroxide as the missing component.

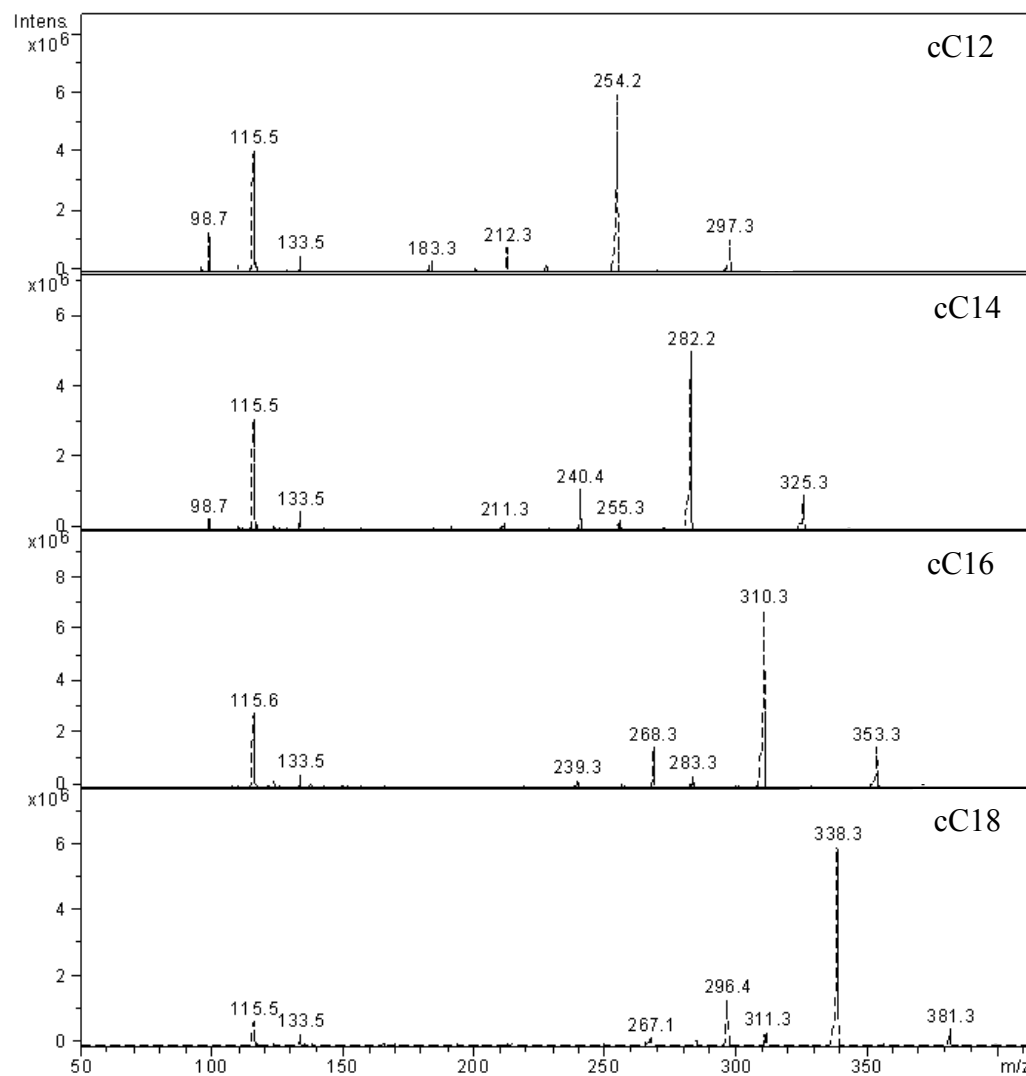


**Figure 3.6. Comparison of ESI-MS/MS fragmentation analyses of the cC12 315 m/z species and related species for cC14-cC18.**

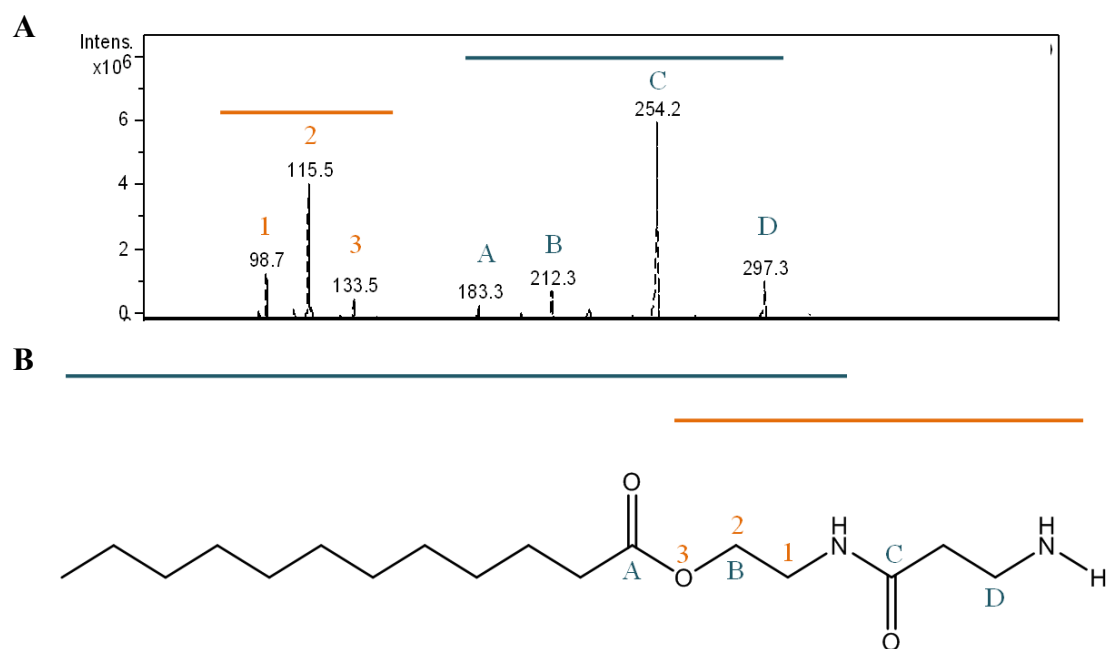


**Figure 3.7. Analyses of ESI-MS/MS fragmentation of the 315 m/z species from cC12.** **A.** Seven species were detected for the 315 m/z MS/MS experiment. The orange bar/numbers and teal bar/letters match the identified masses to the chemical structure. **B.** Proposed chemical structure representing the 315 m/z peak. The orange and teal bars outline the portions of the structure which match the fragments seen in the spectrum below. The orange numbers and maroon letters correspond to each site of fragmentation. **Note:** The 254.2 m/z peak matches the proposed fragmentation site with the corresponding loss of the carbonyl oxygen.

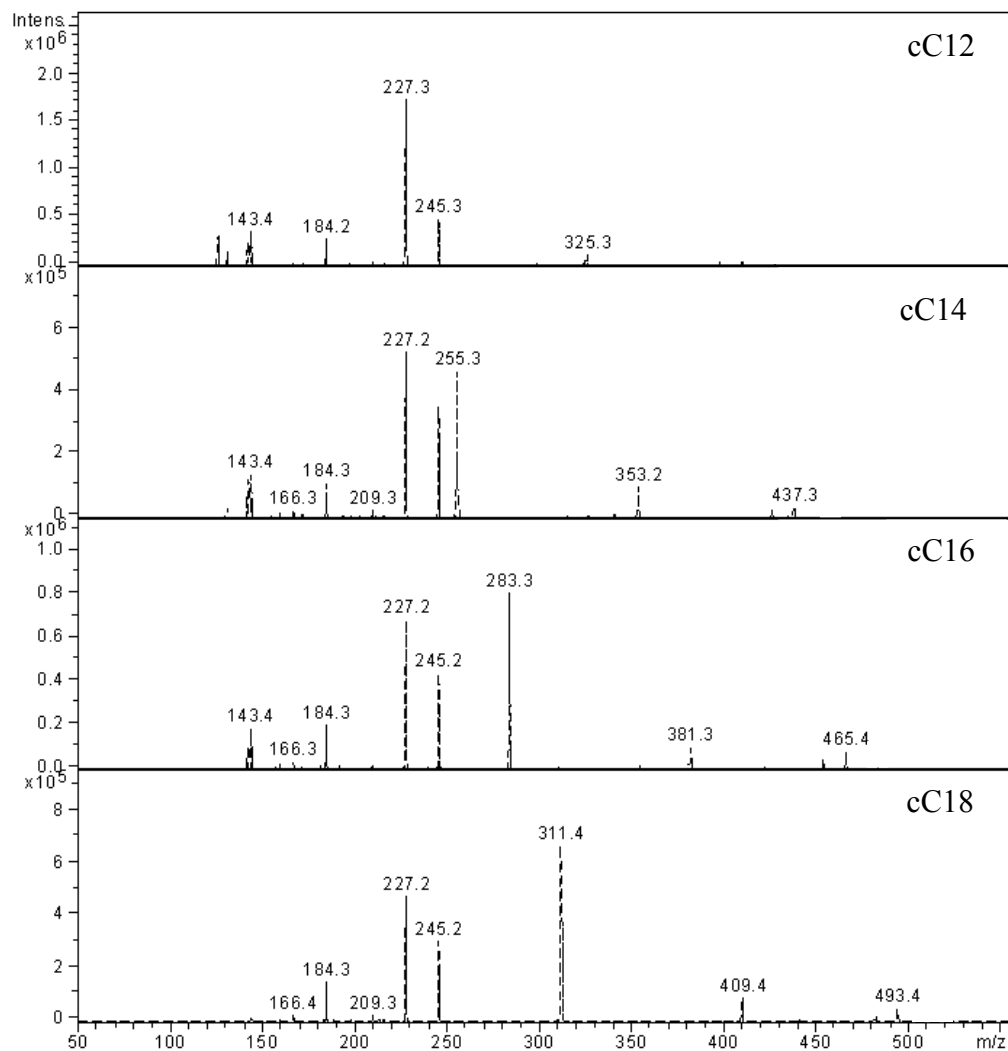


**Figure 3.8. Comparison of ESI-MS/MS fragmentation analyses of the cC12 427 m/z species and related species for cC14-cC18.**



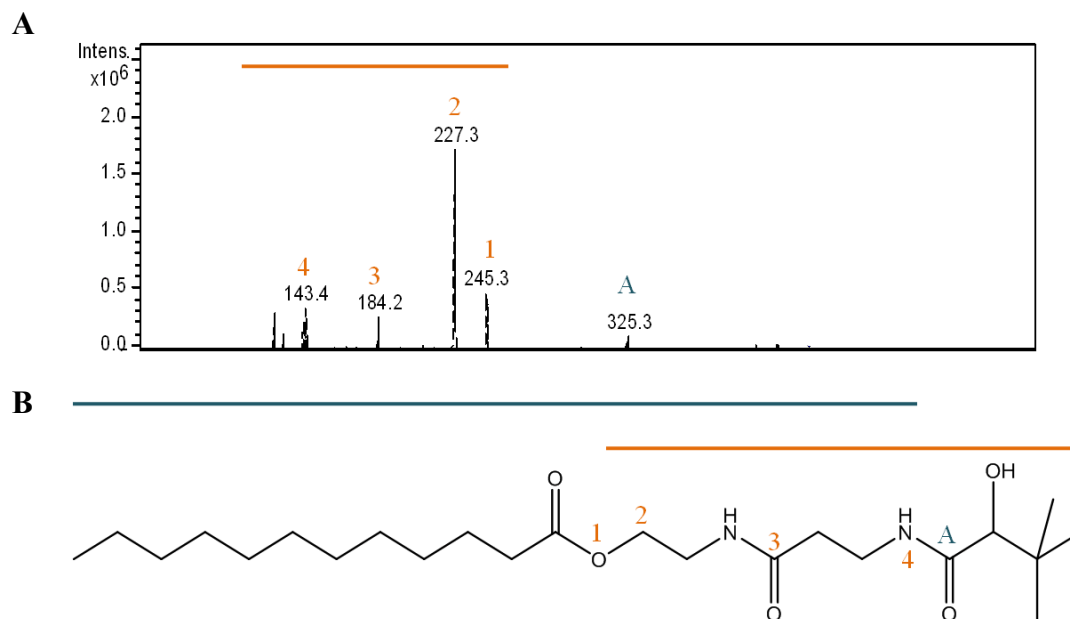


**Figure 3.9. Analyses of the MS/MS fragmentation of the 427 m/z species from cC12.** **A.** Five species were detected for the 427 m/z MS/MS experiment. The orange bar/numbers and teal bar/letters match the identified masses to the chemical structure. **B.** Proposed chemical structure representing the 427 m/z peak. The orange and teal bars outline the portion of the structure which matches the fragments seen in the spectrum below. The orange numbers and maroon letter correspond to each site of fragmentation.

### 3.3.3 Kinetic evaluation of TE1 and TE2 against C14-<sup>AA</sup>ACP and C16-<sup>AA</sup>ACP

As mentioned in the methods section, acyl-<sup>AA</sup>ACP substrates were originally prepared so that DTNB quantitation of thioesterase activity could be measured (Figure 3.10). Moreover, blocking Cys2202 of ACP prohibits the formation of intermolecular dimers, which could severely affect thioesterase activity. Therefore, the quantitative MALD-TOF MS methods for evaluating TE1 and TE2 activity were developed. Ten nM TE2 and 25 nM TE1 were assayed against 20  $\mu$ M C14-<sup>AA</sup>ACP or C16-<sup>AA</sup>ACP in 20 mM HEPES pH 7.5 and 100 mM NaCl at room temperature. Quantitative MALDI-TOF MS methods described in Chapter 2 were used to measure thioesterase activity. Surprisingly, no hydrolysis of substrate was observed after 10 minutes for either TE1 or TE2. When enzyme concentrations were supplemented to 1  $\mu$ M, minimal substrate hydrolysis was observed at 10 minutes (data not shown). These substrates were abandoned for any further kinetic evaluation.

### 3.3.4 WT and SeMet TE2-MBP crystal data

WT and SeMet TE2-MBP crystals were optimized for size and diffraction quality. Several optimizations for cryo-protecting the crystals prior to data collection were performed. Optimized crystals were grown at 4 °C, and it was critical to perform cryoprotection at 4 °C. The sum of optimizations produced crystals with medium diffraction quality to 3.0 Å resolution (Figure 3.11). Home source X-ray data and synchrotron data were collected on WT and SeMet TE2-MBP, respectively. WT or SeMet TE2-MBP crystallized in the I4 space group with equal unit cell parameters (Table 3.3). WT TE2-MBP data scaled to 3.2 Å and SeMet TE2-MBP scaled to 3.4 Å.

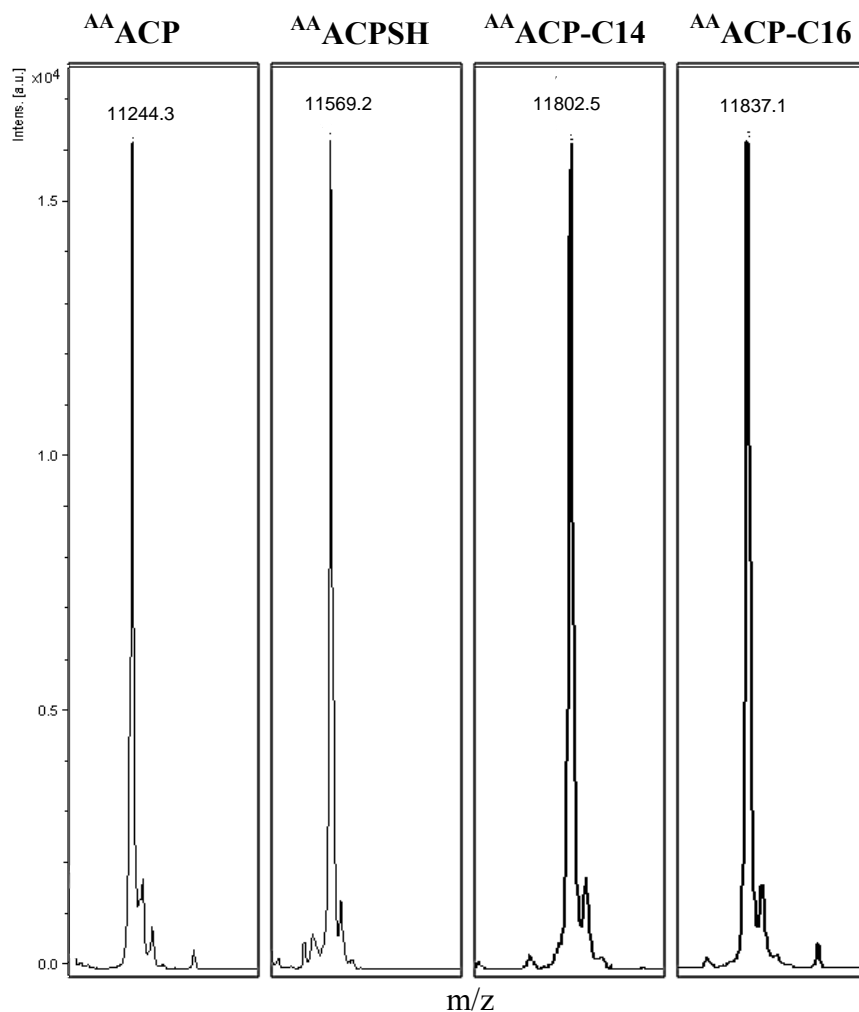


**Figure 3.10. MALDI-TOF results of IAA-treated ACP and synthesis of *S*-acyl- $^{AA}ACP$  substrates.** MALDI-TOF MS analyses confirmed ACP modifications with IAA, 4'PP and fatty acids. A single peak at 11244.3 m/z confirmed 100 % conversion of ACP to  $^{AA}ACP$ .  $^{AA}ACP$  was readily loaded with 4'PP ( $^{AA}ACPSH$ ) and myristate and palmitate substrates.

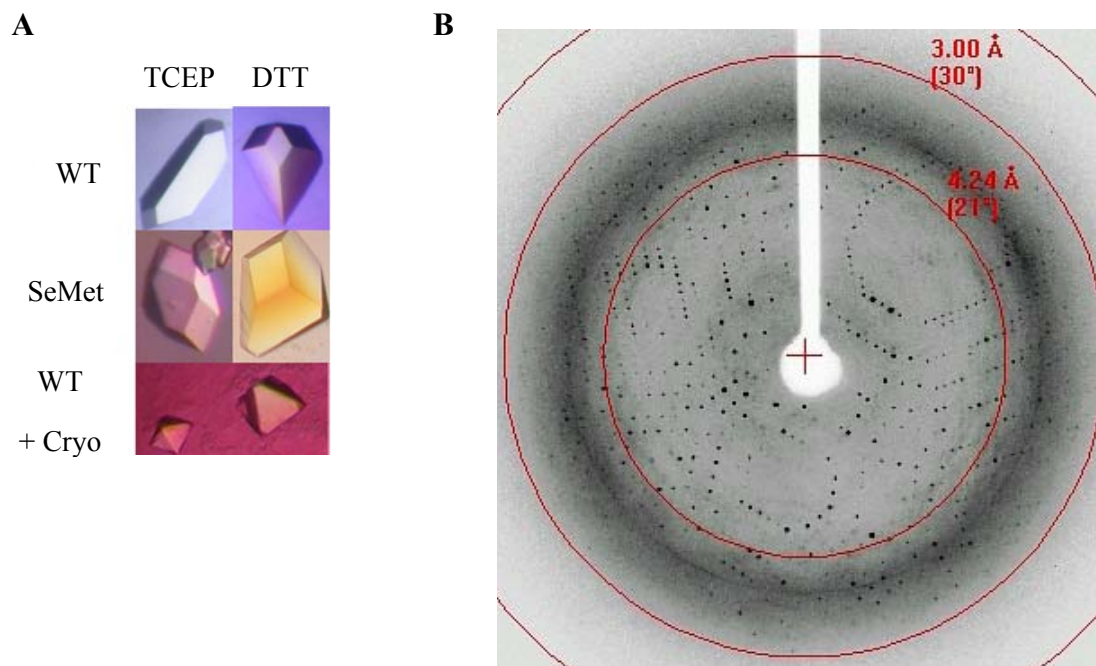


**Figure 3.11. Representative TE2-MBP crystals and sample diffraction image to 3.0 Å resolution.** Crystallization conditions were optimized to produce large, single crystals with diffraction to medium resolution. **A. Images of WT or SeMet TE2-MBP crystals.** Slight variation in crystal morphology was observed for WT TE2-MBP crystals grown with either DTT or TCEP. **B. X-ray diffraction pattern of the crystal screened from crystal tray MR230\_A3.** This protein construct and crystallization condition produced merohedrally twinned data.

**Table 3.3. Summary of data collection statistics**

Spacegroup	I4		
Unit cell dimensions (Å)	112.6	112.6	203.5
	90.0	90.0	90.0
Mosaicity	1.12		
Resolution (Å)	42.9-3.20	(3.31-3.20)	
Total number of reflections	59635		
Number of unique reflections	20398		
Average redundancy	2.9	(3.0)	
% completeness	97.7	(98.0)	
$R_{\text{merge}}$	0.049	(0.300)	
$R_{\text{meas}}$	0.060	(0.365)	
$\langle I \rangle / \sigma \langle I \rangle$	12.0	(3.1)	

Twinning analyses performed using Todd Yeates' on-line server revealed both data sets were approximately 35% merohedrally twinned (71). The high degree of merohedral twinning (the maximum value for twinning is 50%) is not resolvable by available software. Thus, the data could not be used for structure solution, and the crystallization condition as well as protein construct were abandoned for any further optimization experiments.

### 3.3.5 Co-crystallization experiments

TE1 substrate interactions represent an attractive target for FASN drug development. In an effort to provide detailed structural evidence for substrate, 4'PP cofactor and ACP binding interactions, co-crystallization experiments with the S2308A-H2481A double mutants of TE1 and ACP-TE1 and myristoyl- or palmitoyl-CoA substrates were set up. Two co-crystallization experiments produced crystals with poor morphology. The TE1 DM with myristoyl-CoA or palmitoyl-CoA formed tiny, needle-like crystals grown in well solution composed of 40% MPD and 100 mM Bicine pH 8.5 (Figure 3.12A). ATE DM with palmitoyl-CoA also produced crystals of needle morphology from well solution composed of 40% PEG 400, 100 mM Tris 8.5 and 200 mM Li<sub>2</sub>SO<sub>4</sub> (Figure 3.12B). These initial crystallization conditions will require further optimization.

nTE2 also produced clusters of needles grown in well solution composed of 1.8 M (NH<sub>4</sub>)<sub>2</sub>SO<sub>4</sub> and 100 mM NaOAc pH 5.5 (Figure 3.12C). Subsequent optimizations were unsuccessful in improving the crystal morphology. This crystal optimization was abandoned upon obtaining the 2.62 Å data set for WT TE2 crystals described in Chapter

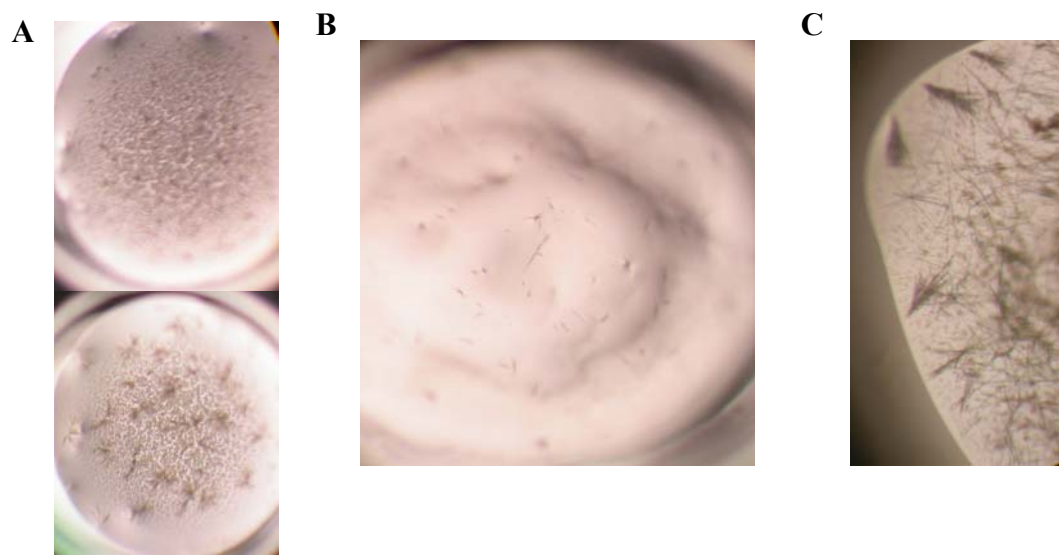


**Figure 3.12. Initial crystal hits from co-crystallization experiments.** A. TE1 DM with C14-CoA (Top) or C16-CoA (Bottom). B. ATE DM with C16-CoA. C. nTE2

2. However, the nTE2 construct may still provide utility in identifying co-crystal complexes with acyl-CoA substrates or acyl-ACP substrates.

### 3.4 Discussion

Optimization strategies achieved full conversion of ACP/nACP to acyl-<sub>crypto</sub>ACP/nACP in approximately 3 hours. However, the inability to stabilize the ester-linked acyl chain to the ACP cofactor is puzzling. The energetic difference in non-enzymatic ester hydrolysis versus thioester hydrolysis should favor the stability of the crypto acyl substrates over the natural substrates. Moreover, correspondence with our collaborators at UCSD provided only reassurance of the stability of the crypto substrates. They readily demonstrated stable conversion of *E. coli* ACP to acyl-<sub>crypto</sub>ACP; however, they only used low-resolution native Urea-PAGE analyses to confirm product synthesis (data not published). It should be noted that expression and purification of nACP produced much lower yields than full-length ACP. In addition, the stability of nACP was comprised, as the protein stock suffered severe precipitation when concentrated above 12-13 mg/mL; full-length ACP is readily concentrated to upwards of 100 mg/mL.

The comprehensive ESI-MS analyses did not provide a clear, alternative explanation for the additional peak observed from MALDI-TOF MS analyses in Figures 2 and 4. It was anticipated that pantothenic acid would be a contaminant to explain the enzymatic synthesis of the aberrant product formed. In fact, two chemical species were identified in each provided crypto substrate, but the chemical composition was not relevant to the observed loading result in Figure 2. Based on the results presented, it is



reasoned that the acyl-<sub>crypto</sub>ACP substrates are not as stable as was anticipated, and that non-enzymatic hydrolysis occurs.

The ability of ACP to sequester the acyl chain may explain the observed instability of either *O*- or *S*-acyl-ACP. The crystal structure of *E. coli* C10-ACP revealed the acyl chain was buried between  $\alpha$ -helix II and III (50). In contrast, an NMR structure of rat acyl- ACP supported that the acyl chain was solvent exposed (72). Acyl-chain sequestration may be an important feature in the type II FASN systems. The dissociative nature of type II ACPs requires diffusion within the cytosol in order to deliver the acyl substrate to the various functional enzymes; acyl-chain sequestration would protect the substrate from non-enzymatic hydrolysis of the thioester bond due to solvent exposure. In contrast, the human type I FASN ACP is tethered between the ER and TE1 domains; therefore diffusion from the enzymatic complex is not relevant. Moreover, the reaction kinetics for human FASN is quite rapid, so the necessity for acyl-chain sequestration is debatable. In fact, acyl-chain sequestration for type I FASN may decrease the catalytic efficiency of product turnover. Alternatively, acyl-chain sequestration may provide a means to regulate FASN product distribution. It may be possible for human ACP to sequester small to medium chain-length fatty acids, ensuring that TE1 only gains access to palmitate or stearate fatty acids (73). The latter argument seems unlikely since TE2 readily modulates FASN product distribution to favor medium chain length fatty acids. The high efficiency of FASN product turnover likely limits the time of solvent exposure for the acyl substrate tethered to ACP, overcoming the issue of thioester bond stability. Nevertheless, the observed hydrolysis of C14- and C16-<sub>crypto</sub>ACP/nACP substrates may suggest a chain-length limitation for human ACP to sequester fatty acids.

Blocking Cys2202 of ACP with IAA had no effect on the ability of Loader+His nor HAAS+His to catalyze cofactor and acyl substrate loading, respectively (Figure 10). This strategy was originally proposed in order to generate an acyl-ACP substrate that could be treated with a thiol modifying agent to be used for kinetic evaluation of acyl-ACP hydrolysis by TE1 or TE2. Moreover, blocking the only cysteine of the ACP construct would limit formation of dimers. Acyl-<sup>AA</sup>ACP substrates proved to be unsuitable for TE1 or TE2 hydrolysis using kinetic concentrations of enzyme and substrate. Equimolar concentrations of enzyme and substrate were marginally effective for observing acyl-<sup>AA</sup>ACP hydrolysis. This is an interesting result, as it appears the carboxyamidomethyl modification severely limits TE1 or TE2 ability to associate productively with ACP for hydrolysis. It is proposed in the literature that the human ACP-TE interactions are facilitated primarily through hydrophobic interactions. However, the residues upstream and downstream of Cys2202 are mostly acidic, and this C-terminal region is unstructured. It does not appear that acetamide is disrupting a hydrophobic region of ACP. Thus, it remains unclear why this modified ACP substrate is protected from TE1 or TE2 hydrolysis.

Crystallization of TE2 was achieved with early success; optimization for crystal size and diffraction quality required several months of processing. No optimizations were sufficient to improve diffraction quality beyond 3.0 Å resolution. SeMet TE2-MBP crystallized very well in equivalent conditions as WT TE2-MBP. Home source WT TE2-MBP data or SeMet TE2-MBP synchrotron data were processed, and were revealed to be 35 % merohedrally twinned. Because the diffraction patterns of merohedral twins are superimposed, and the TE2 crystals had a high degree of twinning, the data was not

resolvable. All crystallization optimizations for this TE2 clone were abandoned, and re-screening of available TE2 constructs immediately followed. To supplement crystallization strategies, an N-terminal truncation at Thr9 was introduced, and the mutant nTE2 was expressed, purified and screened for initial crystallization conditions. Initial nTE2 crystals of needle morphology were identified within the same time-frame WT TE2-His rod-shaped crystals were identified (Chapter 2). Both conditions were optimized in parallel. Whereas TE2-His rod-shaped crystal optimizations produced nice, single crystals of high diffraction quality, nTE2 crystal optimizations failed to reduce the showers of needle-like crystals.

In addition to re-screening alternative TE2 constructs, several co-crystallization experiments were set up. Enzyme:substrate co-crystal experiments were targeted in order to identify the putative 4'PP binding surface for TE1 and TE2. Utilization of the tethered ACP-TE1 construct could allow for the dual identification of substrate/4'PP binding as well as ACP-TE1 interactions. TE1 with TE2 crystallization trials were aimed at identifying potential interactions, given the proximity of TE1 to the ACP domain when TE2 hydrolysis occurs. To aid in these strategies, the active site double mutant TE1 and ATE constructs were cloned, expressed, purified, and screened for crystals in the presence of myristoyl-CoA and palmitoyl-CoA. As seen in Figures 12A,B, tiny needle crystals resulted from TE1 DM with myristoyl-CoA or palmitoyl-CoA substrates and from ATE DM with palmitoyl-CoA. Optimization of these conditions needs to be performed in order to generate crystals large enough to analyze by MADLI-TOF and SDS-PAGE to validate whether these are protein crystals and/or if substrate is present.

### 3.5 Conclusions

Synthesis of *O*-acyl-ACP substrates does not appear to provide stabilized substrates for utility in co-crystallization experiments. Moreover, the limitation for scaling-up the substrate syntheses will severely limit any utility of these substrates for future experiments. While we were grateful to collaborate with Dr. Burkart on this project, it is unlikely this synthetic strategy will prove useful.

The interactions between TE1 or TE2 and ACP remain poorly understood. The synthesis of acyl-<sup>AA</sup>ACP substrates revealed one potential region of interest in the C-terminal linker region between ACP and TE1. Co-crystallography experiments designed to provide experimental evidence for the interactions between these thioesterases and ACP are still underway. The crystal hits described above show promise toward advancing this research goal.

## References

1. Wakil, S. J. (1962) Enzymatic synthesis of fatty acids. *Comp Biochem Physiol* **4**, 123-158
2. Barnes, E. M., Jr., and Wakil, S. J. (1968) Studies on the mechanism of fatty acid synthesis. XIX. Preparation and general properties of palmitoyl thioesterase. *J Biol Chem* **243**, 2955-2962
3. Stoops, J. K., Arslanian, M. J., Aune, K. C., and Wakil, S. J. (1978) Further evidence for the multifunctional enzyme characteristic of the fatty acid synthetases of animal tissues. *Arch Biochem Biophys* **188**, 348-359
4. Mattick, J. S., Zehner, Z. E., Calabro, M. A., and Wakil, S. J. (1981) The isolation and characterization of fatty-acid synthetase mRNA from rat mammary gland. *Eur J Biochem* **114**, 643-651
5. Wakil, S. J., Stoops, J. K., and Mattick, J. S. (1981) The fatty acid synthetase-structure-function relationship and mechanism of palmitate synthesis. *Cardiovasc Res Cent Bull* **20**, 1-23
6. Wakil, S. J. (1989) Fatty acid synthase, a proficient multifunctional enzyme. *Biochemistry* **28**, 4523-4530
7. Chirala, S. S., and Wakil, S. J. (2004) Structure and function of animal fatty acid synthase. *Lipids* **39**, 1045-1053
8. Maier, T., Jenni, S., and Ban, N. (2006) Architecture of mammalian fatty acid synthase at 4.5 Å resolution. *Science* **311**, 1258-1262
9. Leibundgut, M., Maier, T., Jenni, S., and Ban, N. (2008) The multienzyme architecture of eukaryotic fatty acid synthases. *Curr Opin Struct Biol* **18**, 714-725

10. Shurbaji, M. S., Kalbfleisch, J. H., and Thurmond, T. S. (1996) Immunohistochemical detection of a fatty acid synthase (OA-519) as a predictor of progression of prostate cancer. *Hum Pathol* **27**, 917-921
11. Swinnen, J. V., Esquenet, M., Goossens, K., Heyns, W., and Verhoeven, G. (1997) Androgens stimulate fatty acid synthase in the human prostate cancer cell line LNCaP. *Cancer Res* **57**, 1086-1090
12. Pizer, E. S., Pflug, B. R., Bova, G. S., Han, W. F., Udan, M. S., and Nelson, J. B. (2001) Increased fatty acid synthase as a therapeutic target in androgen-independent prostate cancer progression. *Prostate* **47**, 102-110
13. Swinnen, J. V., Roskams, T., Joniau, S., Van Poppel, H., Oyen, R., Baert, L., Heyns, W., and Verhoeven, G. (2002) Overexpression of fatty acid synthase is an early and common event in the development of prostate cancer. *Int J Cancer* **98**, 19-22
14. Pflug, B. R., Pecher, S. M., Brink, A. W., Nelson, J. B., and Foster, B. A. (2003) Increased fatty acid synthase expression and activity during progression of prostate cancer in the TRAMP model. *Prostate* **57**, 245-254
15. Rossi, S., Graner, E., Febbo, P., Weinstein, L., Bhattacharya, N., Onody, T., Bubley, G., Balk, S., and Loda, M. (2003) Fatty acid synthase expression defines distinct molecular signatures in prostate cancer. *Mol Cancer Res* **1**, 707-715
16. Baron, A., Migita, T., Tang, D., and Loda, M. (2004) Fatty acid synthase: a metabolic oncogene in prostate cancer? *J Cell Biochem* **91**, 47-53

17. Menendez, J. A., and Lupu, R. (2004) Fatty acid synthase-catalyzed de novo fatty acid biosynthesis: from anabolic-energy-storage pathway in normal tissues to jack-of-all-trades in cancer cells. *Arch Immunol Ther Exp (Warsz)* **52**, 414-426
18. Wang, Y. Y., Kuhajda, F. P., Li, J., Finch, T. T., Cheng, P., Koh, C., Li, T., Sokoll, L. J., and Chan, D. W. (2004) Fatty acid synthase as a tumor marker: its extracellular expression in human breast cancer. *J Exp Ther Oncol* **4**, 101-110
19. Menendez, J. A., and Lupu, R. (2007) Fatty acid synthase and the lipogenic phenotype in cancer pathogenesis. *Nat Rev Cancer* **7**, 763-777
20. Liu, H., Liu, Y., and Zhang, J. T. (2008) A new mechanism of drug resistance in breast cancer cells: fatty acid synthase overexpression-mediated palmitate overproduction. *Mol Cancer Ther* **7**, 263-270
21. Wang, K. F., and Wu, B. (2008) [Fatty acid synthase and prostate cancer]. *Zhonghua Nan Ke Xue* **14**, 740-742
22. Mashima, T., Seimiya, H., and Tsuruo, T. (2009) *De novo* fatty-acid synthesis and related pathways as molecular targets for cancer therapy. *Brit J Cancer* **100**, 1369-1372
23. Migita, T., Ruiz, S., Fornari, A., Fiorentino, M., Priolo, C., Zadra, G., Inazuka, F., Grisanzio, C., Palescandolo, E., Shin, E., Fiore, C., Xie, W., Kung, A. L., Febbo, P. G., Subramanian, A., Mucci, L., Ma, J., Signoretti, S., Stampfer, M., Hahn, W. C., Finn, S., and Loda, M. (2009) Fatty acid synthase: a metabolic enzyme and candidate oncogene in prostate cancer. *J Natl Cancer Inst* **101**, 519-532
24. Uddin, S., Hussain, A. R., Ahmed, M., Abubaker, J., Al-Sanea, N., AbdulJabbar, A., Ashari, L. H., Alhomoud, S., Al-Dayel, F., Bavi, P., and Al-Kuraya, K. S.

- (2009) High Prevalence of Fatty Acid Synthase Expression in Colorectal Cancers in Middle Eastern Patients and Its Potential Role as a Therapeutic Target. *Am J Gastroenterol* **104**, 1790-1801
25. Flavin, R., Peluso, S., Nguyen, P. L., and Loda, M. (2010) Fatty acid synthase as a potential therapeutic target in cancer. *Future Oncol* **6**, 551-562
26. Pizer, E. S., Thupari, J., Han, W. F., Pinn, M. L., Chrest, F. J., Frehywot, G. L., Townsend, C. A., and Kuhajda, F. P. (2000) Malonyl-coenzyme-A is a potential mediator of cytotoxicity induced by fatty-acid synthase inhibition in human breast cancer cells and xenografts. *Cancer Res* **60**, 213-218
27. Thupari, J. N., Pinn, M. L., and Kuhajda, F. P. (2001) Fatty acid synthase inhibition in human breast cancer cells leads to malonyl-CoA-induced inhibition of fatty acid oxidation and cytotoxicity. *Biochem Biophys Res Commun* **285**, 217-223
28. Liu, B., Wang, Y., Fillgrove, K. L., and Anderson, V. E. (2002) Triclosan inhibits enoyl-reductase of type I fatty acid synthase in vitro and is cytotoxic to MCF-7 and SKBr-3 breast cancer cells. *Cancer Chemother Pharmacol* **49**, 187-193
29. Brusselmans, K., De Schrijver, E., Heyns, W., Verhoeven, G., and Swinnen, J. V. (2003) Epigallocatechin-3-gallate is a potent natural inhibitor of fatty acid synthase in intact cells and selectively induces apoptosis in prostate cancer cells. *Int J Cancer* **106**, 856-862
30. De Schrijver, E., Brusselmans, K., Heyns, W., Verhoeven, G., and Swinnen, J. V. (2003) RNA interference-mediated silencing of the fatty acid synthase gene



- attenuates growth and induces morphological changes and apoptosis of LNCaP prostate cancer cells. *Cancer Res* **63**, 3799-3804
31. Qiao, S., Pennanen, P., Nazarova, N., Lou, Y. R., and Tuohimaa, P. (2003) Inhibition of fatty acid synthase expression by 1 $\alpha$ -25-dihydroxyvitamin D3 in prostate cancer cells. *J Steroid Biochem Mol Biol* **85**, 1-8
  32. Yeh, C. W., Chen, W. J., Chiang, C. T., Lin-Shiau, S. Y., and Lin, J. K. (2003) Suppression of fatty acid synthase in MCF-7 breast cancer cells by tea and tea polyphenols: a possible mechanism for their hypolipidemic effects. *Pharmacogenomics J* **3**, 267-276
  33. Menendez, J. A., Mehmi, I., Verma, V. A., Teng, P. K., and Lupu, R. (2004) Pharmacological inhibition of fatty acid synthase (FAS): a novel therapeutic approach for breast cancer chemoprevention through its ability to suppress Her-2/neu (erbB-2) oncogene-induced malignant transformation. *Mol Carcinog* **41**, 164-178
  34. Qiao, S., and Tuohimaa, P. (2004) Vitamin D3 inhibits fatty acid synthase expression by stimulating the expression of long-chain fatty-acid-CoA ligase 3 in prostate cancer cells. *FEBS Lett* **577**, 451-454
  35. Murata, S., Yanagisawa, K., Fukunaga, K., Oda, T., Kobayashi, A., Sasaki, R., and Ohkohchi, N. (2010) Fatty acid synthase inhibitor cerulenin suppresses liver metastasis of colon cancer in mice. *Cancer Sci* **101**, 1861-1865
  36. Pandey, P. R., Okuda, H., Watabe, M., Pai, S. K., Liu, W., Kobayashi, A., Xing, F., Fukuda, K., Hirota, S., Sugai, T., Wakabayashi, G., Koeda, K., Kashiwaba, M., Suzuki, K., Chiba, T., Endo, M., Fujioka, T., Tanji, S., Mo, Y. Y., Cao, D.,

- Wilber, A. C., and Watabe, K. (2011) Resveratrol suppresses growth of cancer stem-like cells by inhibiting fatty acid synthase. *Breast Cancer Res Treat* **130**, 387-398
37. Heath, R. J., White, S. W., and Rock, C. O. (2001) Lipid biosynthesis as a target for antibacterial agents. *Prog Lipid Res* **40**, 467-497
38. Campbell, J. W., and Cronan, J. E., Jr. (2001) Bacterial fatty acid biosynthesis: targets for antibacterial drug discovery. *Annu Rev Microbiol* **55**, 305-332
39. Kridel, S. J., Axelrod, F., Rozenkrantz, N., and Smith, J. W. (2004) Orlistat is a novel inhibitor of fatty acid synthase with antitumor activity. *Cancer Res* **64**, 2070-2075
40. Browne, C. D., Hindmarsh, E. J., and Smith, J. W. (2006) Inhibition of endothelial cell proliferation and angiogenesis by orlistat, a fatty acid synthase inhibitor. *FASEB J* **20**, 2027-2035
41. Ma, G., Zancanella, M., Oyola, Y., Richardson, R. D., Smith, J. W., and Romo, D. (2006) Total synthesis and comparative analysis of orlistat, valilactone, and a transposed orlistat derivative: Inhibitors of fatty acid synthase. *Org Lett* **8**, 4497-4500
42. Carvalho, M. A., Zecchin, K. G., Seguin, F., Bastos, D. C., Agostini, M., Rangel, A. L., Veiga, S. S., Raposo, H. F., Oliveira, H. C., Loda, M., Coletta, R. D., and Graner, E. (2008) Fatty acid synthase inhibition with Orlistat promotes apoptosis and reduces cell growth and lymph node metastasis in a mouse melanoma model. *Int J Cancer* **123**, 2557-2565

43. Zhang, W., Richardson, R. D., Chamni, S., Smith, J. W., and Romo, D. (2008) Beta-lactam congeners of orlistat as inhibitors of fatty acid synthase. *Bioorg Med Chem Lett* **18**, 2491-2494
44. Dowling, S., Cox, J., and Cenedella, R. J. (2009) Inhibition of fatty acid synthase by Orlistat accelerates gastric tumor cell apoptosis in culture and increases survival rates in gastric tumor bearing mice *in vivo*. *Lipids* **44**, 489-498
45. Chuang, H. Y., Chang, Y. F., and Hwang, J. J. (2011) Antitumor effect of orlistat, a fatty acid synthase inhibitor, is via activation of caspase-3 on human colorectal carcinoma-bearing animal. *Biomed Pharmacother* **65**, 286-292
46. Kant, S., Kumar, A., and Singh, S. M. (2012) Fatty acid synthase inhibitor orlistat induces apoptosis in T cell lymphoma: role of cell survival regulatory molecules. *Biochim Biophys Acta* **1820**, 1764-1773
47. Seguin, F., Carvalho, M. A., Bastos, D. C., Agostini, M., Zecchin, K. G., Alvarez-Flores, M. P., Chudzinski-Tavassi, A. M., Coletta, R. D., and Graner, E. (2012) The fatty acid synthase inhibitor orlistat reduces experimental metastases and angiogenesis in B16-F10 melanomas. *Brit J Cancer* **107**, 977-987
48. Sankaranarayanapillai, M., Zhang, N., Baggerly, K. A., and Gelovani, J. G. (2013) Metabolic shifts induced by fatty acid synthase inhibitor orlistat in non-small cell lung carcinoma cells provide novel pharmacodynamic biomarkers for positron emission tomography and magnetic resonance spectroscopy. *Mol Imaging Biol* **15**, 136-147

49. Pemble, C. W. t., Johnson, L. C., Kridel, S. J., and Lowther, W. T. (2007) Crystal structure of the thioesterase domain of human fatty acid synthase inhibited by Orlistat. *Nat Struct Mol Biol* **14**, 704-709
50. Chan, D. I., and Vogel, H. J. (2010) Current understanding of fatty acid biosynthesis and the acyl carrier protein. *Biochem J* **430**, 1-19
51. Libertini, L. J., and Smith, S. (1978) Purification and properties of a thioesterase from lactating rat mammary gland which modifies the product specificity of fatty acid synthetase. *J Biol Chem* **253**, 1393-1401
52. Lin, C. Y., and Smith, S. (1978) Properties of the thioesterase component obtained by limited trypsinization of the fatty acid synthetase multienzyme complex. *J Biol Chem* **253**, 1954-1962
53. Libertini, L. J., and Smith, S. (1979) Synthesis of long chain acyl-enzyme thioesters by modified fatty acid synthetases and their hydrolysis by a mammary gland thioesterase. *Arch Biochem Biophys* **192**, 47-60
54. Smith, S., and Libertini, L. J. (1979) Specificity and site of action of a mammary gland thioesterase which releases acyl moieties from thioester linkage to the fatty acid synthetase. *Arch Biochem Biophys* **196**, 88-92
55. Nolin, J. M., Thompson, B. J., and Smith, S. (1982) Localization of thioesterase II, the chain-length regulatory enzyme of milk fatty acid synthesis, in rat mammary gland epithelial cells. *J Endocrinol* **94**, 251-256
56. Witkowski, A., and Smith, S. (1985) Inhibition of the functional interaction between fatty acid synthetase and thioesterase II by modification of a single cysteine thiol on the thioesterase. *Arch Biochem Biophys* **243**, 420-426

57. Mikkelsen, J., Witkowski, A., and Smith, S. (1987) Interaction of rat mammary gland thioesterase II with fatty acid synthetase is dependent on the presence of acyl chains on the synthetase. *J Biol Chem* **262**, 1570-1574
58. Naggert, J., Witkowski, A., Wessa, B., and Smith, S. (1991) Expression in *Escherichia coli*, purification and characterization of two mammalian thioesterases involved in fatty acid synthesis. *Biochem J* **273 ( Pt 3)**, 787-790
59. Tai, M. H., Chirala, S. S., and Wakil, S. J. (1993) Roles of Ser101, Asp236, and His237 in catalysis of thioesterase II and of the C-terminal region of the enzyme in its interaction with fatty acid synthase. *Proc Natl Acad Sci USA* **90**, 1852-1856
60. Heathcote, M. L., Staunton, J., and Leadlay, P. F. (2001) Role of type II thioesterases: evidence for removal of short acyl chains produced by aberrant decarboxylation of chain extender units. *Chem Biol* **8**, 207-220
61. Chakravarty, B., Gu, Z. W., Chirala, S. S., Wakil, S. J., and Quijcho, F. A. (2004) Human fatty acid synthase: Structure and substrate selectivity of the thioesterase domain. *Proc Natl Acad Sci USA* **101**, 15567-15572
62. Joshi, A. K., Witkowski, A., Berman, H. A., Zhang, L., and Smith, S. (2005) Effect of modification of the length and flexibility of the acyl carrier protein-thioesterase interdomain linker on functionality of the animal fatty acid synthase. *Biochemistry* **44**, 4100-4107
63. Haushalter, R. W., Worthington, A. S., Hur, G. H., and Burkart, M. D. (2008) An orthogonal purification strategy for isolating crosslinked domains of modular synthases. *Bioorg Med Chem Lett* **18**, 3039-3042

64. Meier, J. L., Mercer, A. C., Rivera, H., Jr., and Burkart, M. D. (2006) Synthesis and evaluation of bioorthogonal pantetheine analogues for *in vivo* protein modification. *J Am Chem Soc* **128**, 12174-12184
65. Mandel, A. L., La Clair, J. J., and Burkart, M. D. (2004) Modular synthesis of pantetheine and phosphopantetheine. *Org Lett* **6**, 4801-4803
66. Bunkoczi, G., Pasta, S., Joshi, A., Wu, X., Kavanagh, K. L., Smith, S., and Oppermann, U. (2007) Mechanism and substrate recognition of human *holo* ACP synthase. *Chem Biol* **14**, 1243-1253
67. Zhang, Y. (2008) I-TASSER server for protein 3D structure prediction. *Bmc Bioinformatics* **9**, 40-51
68. Zhang, Y. (2009) I-TASSER: Fully automated protein structure prediction in CASP8. *Proteins-Structure Function and Bioinformatics* **77**, 100-113
69. Roy, A., Kucukural, A., and Zhang, Y. (2010) I-TASSER: a unified platform for automated protein structure and function prediction. *Nat Protoc* **5**, 725-738
70. Gassner, N. C., and Matthews, B. W. (1999) Use of differentially substituted selenomethionine proteins in X-ray structure determination. *Acta Crystallogr D Biol Crystallogr* **55**, 1967-1970
71. Padilla, J. E., and Yeates, T. O. (2003) A statistic for local intensity differences: robustness to anisotropy and pseudo-centering and utility for detecting twinning. *Acta Crystallogr D Biol Crystallogr* **59**, 1124-1130
72. Ploskon, E., Arthur, C. J., Evans, S. E., Williams, C., Crosby, J., Simpson, T. J., and Crump, M. P. (2008) A mammalian type I fatty acid synthase acyl carrier protein domain does not sequester acyl chains. *J Biol Chem* **283**, 518-528

73. Zornetzer, G. A., Tanem, J., Fox, B. G., and Markley, J. L. (2010) The length of the bound fatty acid influences the dynamics of the acyl carrier protein and the stability of the thioester bond. *Biochemistry* **49**, 470-477

## **Chapter 4: Conclusions and Future Directions**



## 4.1 Conclusions

The *de novo* biosynthesis of medium and long chain fatty acids by FASN represents an essential function to the maintenance of normal cell biology and homeostasis, and also for the survival and progression of several cancers (1-8). Normal tissues absorb dietary sources of lipids, and therefore the role of FASN in normal cell biology is delegated to converting excess acetyl-CoA into LCFAs for energy storage. Palmitate is the primary product synthesized by FASN, and this preference in acyl product is determined by the selectivity of the endogenous TE1 domain (9-11). In lactating breast, FASN produces mostly MCFAs which are essential components for breast milk lipids (12-13). Modulation of FASN product distribution is achieved by the intervention of TE2 (14-17). Expression levels of FASN in normal tissues are insignificant, with the exception of the lipogenic liver, adipose and lactating breast tissues. In contrast, cancer cells upregulate FASN expression and are critically dependent on *de novo* lipid sources for survival (18-30). The differential expression of FASN in normal versus cancer tissues favors a large therapeutic window for cancer treatment.

FASN has become an attractive target for cancer drug development. Several studies have established FASN inhibition to have cytotoxic and anti-tumor effects (18-20,31-56). Moreover, FASN represents a single enzymatic system to target. Importantly, FASN inactivation via TE1 inhibition has demonstrated a promising drug discovery strategy. The weight-loss drug Orlistat was identified to inhibit TE1 with high potency ( $IC_{50} \sim 100$  nM). In addition, the crystal structure of Orlistat covalently bound to the TE1 active site provided molecular insights for acyl chain length specificity as well as specific

surface features with which to design novel inhibitors. Several studies on various cancer cell lines clearly demonstrated the cytotoxic effect of Orlistat-mediated FASN inhibition.

TE1 and TE2 interactions with ACP represent an additional factor for FASN drug discovery. In lactating breast, TE2 modulates the activity of FASN in the presence of active TE1. It is important to consider TE2 interactions with ACP since it is a discrete enzyme, and harbors the ability to rescue TE1-inhibited FASN if upregulated in cancer cells. Given that both thioesterases interact with ACP to hydrolyze the acyl substrate, the interface between ACP and TE1 or TE2 may be an alternative target for pharmaceutical intervention.

Kinetic evaluation of TE1 and TE2 activity in Chapter 2 provides the first activity profile of these enzymes using a biologically relevant substrate and highlighted the importance of ACP interactions for catalysis and maintenance of cellular lipid distributions. TE1 maintained high selectivity for palmitate regardless of the presence of the ACP domain, which was demonstrated by similar values for specific activity against C16-CoA and C16-ACP. In contrast, TE2 hydrolase activity was dramatically enhanced when the acyl substrate was tethered to the ACP domain instead of Coenzyme A. The fact that TE2 is 5-10 fold less active against acyl-CoA substrates compared to TE1 further implicated the requirement for ACP interactions to facilitate comparable rates of hydrolysis which would allow TE2 to modulate FASN activity in the presence of active TE1. TE2 did show slight preference for C14-CoA compared to the other substrates; however, it remains unclear whether TE2 is selective for specific acyl chain lengths or if ACP interactions facilitate acyl chain selection. Residence within the FASN peptide effectively sequesters the high efficiency and selectivity of TE1 for palmitate; TE1 access

to cellular acyl-CoA lipid pools would be detrimental to cellular homeostasis. Equally, the discrete nature of TE2, coupled with its attenuated ability to hydrolyze acyl-CoA substrates, enables its function to modulate FASN product distribution without perturbing the homeostasis of acyl-CoA lipid pools.

The 2.62 Å crystal structure of human TE2 provides the first three-dimensional model of any type II thioesterases associated with the type I FASN system. Determination of the WT TE2 crystal structure provides clarity for the 20-fold increase in TE2 hydrolase activity toward C16-ACP. Classification of TE2 as a  $\alpha/\beta$  serine hydrolase based on sequence identity to TE1, RedJ and RifR was confirmed structurally. Mutational analysis also confirmed that Ser101 is the active site nucleophile. Moreover, the loop insertion observed in the TE2 protein sequence was observed as a capping domain comprised of  $\alpha$ -helices. Surprisingly, TE2 exhibited the closest relationship to the type II thioesterases, RedJ and RifR, from PKS and NRPS modular assemblies. As was discussed in Chapter 1, type II thioesterases are described as editing thioesterases and function to hydrolyze aberrant extender units on stalled PKS or NRPS modules. Therefore, it is reasoned that type II thioesterases require high selection for ACP interactions to facilitate rescuing of natural product biosynthetic pathways. The homology of human TE2 to the PKS and NRPS type II thioesterases, combined with 20-fold improvement in hydrolase activity against the C16-ACP substrate, suggests an ancestral relationship between TE2, RedJ and RifR. Sequence and structural divergence have produced unique thioesterases with complimentary function to each respective modular synthase assembly.

Additional TE2 structural features explain the novel observation of the magnitude difference for TE1 and TE2 specific activities against acyl-CoA substrates as well as differential inhibition. A portion of the TE2 capping domain extends over the active site region and makes contact with the hydrolase core. These surfaces clearly block access of substrate or inhibitor to the active site. Differences in active site architectures were also demonstrated by the observed differential inhibition for TE1 and TE2 when treated with Orlistat or Ebelactone B compounds. Both Orlistat and Ebelactone B achieved 100% TE1 inhibition, with Orlistat showing a higher degree of potency. In contrast, TE2 showed resistance to inactivation, as seen by the inability to achieve full TE2 inhibition even when treated with 100X molar excess of either compound.

Measurement of hydrogen bonding distances of TE2 active site residues determined that Ser101 and His237 are 3.6 Å apart and are not optimally positioned for catalysis. This is a common feature of catalytic triads, including trypsin, chymotrypsin and subtilisin (57). The interaction between the catalytic aspartate and histidine residues confers unfavorable geometry between the catalytic histidine and serine residues. Substrate binding relieves the geometric restraint and allows for efficient catalysis.

A blocked active site with sub-optimally positioned catalytic residues explains the attenuated TE2 activity against acyl-CoA substrates compared to TE1 activity, as well as resistance to inhibitor inactivation. Repositioning of the capping domain to allow substrate access must occur, and three possible mechanisms are possible. First, the capping domain may exist in a two-state equilibrium between open and closed conformations, and the crystal structure captured the closed conformation. Second, interaction with only the acyl substrate facilitates capping domain movements. Third,

TE2 interactions with the ACP domain facilitate movement of the capping domain to allow substrate binding and hydrolysis. The ability of TE2 to hydrolyze acyl-CoA substrates, albeit at a much lower rate, suggests some coordination between substrate and ACP binding to facilitate capping domain reorganization.

As mentioned earlier, it is unclear whether TE2 elicits acyl chain length specificity. The TE2 crystal structure revealed a putative substrate binding pocket adjacent to the active site. Importantly, this pocket is comprised mostly of small hydrophobic residues which would readily accommodate an acyl substrate. In contrast, an abundance of bulky, aromatic residues line the TE1 substrate specificity channel and directly coordinate a palmitic substrate, as was demonstrated by the TE1-Orlistat co-crystal structure.

In contrast to the kinetic evidence presented, crystallographic evidence for TE1 and TE2 interactions with acyl-ACP has yet to be determined. Several strategies for obtaining stable, acyl-ACP substrates for kinetic evaluation and crystallography experiments were developed. Suitable *S*-acyl-ACP substrates for kinetic evaluation of TE1 and TE2 were generated using a two-step synthetic strategy, and were stabilized with the addition of detergent and by lowering the pH of dialysis buffer to 5.5. However, given the inherent ability for non-enzymatic hydrolysis of the acyl moiety of acyl-ACP substrates over time, these substrates were not utilized for co-crystallographic experiments. Collaboration with Dr. Burkart at UCSD provided an alternative strategy to synthesize the ester-linked, *O*-acyl-ACP substrates (58-60). Two ACP constructs were used in parallel optimizations for crypto substrate loading. In summary, crypto loading conditions were optimized and achieved full conversion of ACP/nACP to acyl-

crypto-ACP/nACP within 3 hours at room temperature; however, hydrolysis of the acyl chain was observed for the C14 and C16 crypto substrates. The loading of crypto-C18 was not achievable due to the insolubility of the substrate. Non-enzymatic hydrolysis of an ester-linked acyl substrate on ACP was entirely unexpected, given the order of magnitude increase in stability of an ester bond compared to a thioester bond. These results may provide an important observation to the ambiguity of acyl chain sequestration by ACP.

Another surprising result from acyl-ACP syntheses was observed with the IAA-derivatized C14-<sup>AA</sup>ACP and C16-<sup>AA</sup>ACP substrates. Although the CAM moiety on Cys 2202 of ACP was of no detriment to the loading enzymes, the ability of TE1 or TE2 to hydrolyze the acyl substrate was severely compromised. Even with 1  $\mu$ M enzyme treated against 20  $\mu$ M acyl-<sup>AA</sup>ACP substrate, marginal hydrolysis was observed (data not shown). Cys2202 may represent a region of interest for pharmaceutical intervention of TE1 or TE2 activity.

#### **4.2 Future Directions**

Optimization of synthetic strategies which produced high milligram quantities of stably acylated ACP substrates and the development of the novel discontinuous assay using MALDI-TOF MS analyses will allow for further kinetic evaluations of TE1 and TE2 against biologically relevant substrates. To date, only the C16-ACP substrate was assayed with TE1 and TE2. Future kinetic experiments using C12-, C14-, and C18-ACP substrates will provide a direct complement to the established TE1 and TE2 specific activities against acyl-CoA substrates. Importantly, the full panel of acyl-ACP substrates

will provide kinetic evidence for the potential specificity of TE2 for the ACP domain regardless of the acyl substrate present.

Moreover, the results of TE1 and TE2 specific activities toward acyl-ACP substrates should refine our current understanding of acyl chain length specificity. Current evidence strongly supports the high selectivity of TE1 for palmitate substrates independent of the presence of ACP. Similarly, TE2 showed slight preference for C14-CoA. However, the dramatic improvement in TE2 hydrolase activity when presented with an acyl-ACP substrate may suggest a lack of chain length selection

Continued optimization of WT TE2 crystal conditions will provide future datasets with improved resolution. The current 2.62 Å TE2 model is not optimally refined, with  $R_{\text{free}}$  statistics still well above 30%. Improved data resolution will allow for improved atomic positioning of the model in the electron density map, and may provide additional electron density for missing regions of the model.

In addition, future efforts to obtain crystals of TE2 active site mutants in complex with substrate are needed to clearly establish the molecular mechanism of substrate selection ACP domain binding, and catalysis. As described in Chapter 3, several crystallization experiments to this effect have been set up. All variables, including protein concentration, substrate concentration, drop size, temperature, reducing agent, and others, need to be tested. Moreover, cloning and purification of the TE2 S101A and H237A double mutant should be pursued as an additional strategy to obtain crystals of TE2 in complex with an intact acyl-CoA or acyl-ACP substrate. Removal of two catalytic residues may reduce any enzyme-mediated instability of the substrate thioester

bond. Co-crystal structures of TE1 active site mutants (S2308A and H2481A) with acyl-CoA will compliment the TE2 co-crystal structure by allowing for identification of the putative 4'PP cofactor specificity channel. Differences in molecular recognition of cofactor may explain the differences in TE1 and TE2 activity toward acyl-ACP substrates.

With the three component crystal structures of interest at hand (ACP, TE1 and TE2), future crystallographic experiments are needed to provide experimental evidence for thioesterase-ACP interactions as well as capping domain dynamics. Co-crystallization of acyl-ACP with TE1 active site mutants will provide the first structural model for the C-terminal region of FASN; the inherent mobility of these domains did not allow determination of their positions within the context of the FASN crystal structure. In addition, this crystal complex will provide the first structural model of TE1 in complex with its biological substrate. Co-crystallization of acyl-ACP with TE2 active site mutants will also provide the first structural model of TE2 in complex with its biological substrate. Furthermore, the TE2: acyl-ACP crystal complex will provide experimental evidence for the similarities and differences in ACP interactions between TE1 and TE2.

The critical contacts at the interface between ACP and TE1 or TE2 could be further tested by mutating residues on TE1 or TE2 and performing both acyl-CoA and acyl-ACP kinetic evaluations. Complete loss or severe attenuation of activity will validate critical interface contacts. In addition, the degree to which, if at all, the capping domain 'opens' may be dependent on both substrate and ACP interactions. Therefore, comparison of co-crystal structures of TE2 with acyl-CoA and acyl-ACP substrates will



be necessary to provide comprehensive evidence for the mechanism of capping domain re-organization.

In summary, the proposed future experiments will further expand our current understanding of FASN structural organization and molecular mechanisms of catalysis. Comprehensive kinetic evaluations of TE1 and TE2 with the novel acyl-ACP substrates will report the first analyses of any FASN domains using a biologically relevant substrate. Structural analyses of acyl-ACP-TE1 complexes will provide the first evidence for the C-terminal domain organization of FASN. Importantly, experimental evidence for the novel modulation of FASN product distribution by TE2 will demonstrate the molecular signature favoring TE2 interactions with ACP compared to TE1. Moreover, the explicit detailing of TE1 and TE2 interactions with both acyl substrates and ACP will provide additional molecular blueprints for advancing FASN drug development. Enabling the development of novel FASN inhibitor will aid in current treatment strategies for a variety of cancers and improve the outcome of many patients afflicted with this disease.

## References

1. Smith, S., and Abraham, S. (1975) Fatty acid synthase from lactating rat mammary gland. *Methods Enzymol* **35**, 65-74
2. Huxtable, R. J., and Wakil, S. J. (1971) Comparative mitochondrial oxidation of fatty acids. *Biochim Biophys Acta* **239**, 168-177
3. Smith, S., and Abraham, S. (1970) Fatty acid synthetase from lactating rat mammary gland. I. Isolation and properties. *J Biol Chem* **245**, 3209-3217
4. Wolken, J. J. (1968) Cellular organelles and lipids. *J Am Oil Chem Soc* **45**, 241-246
5. Smith, S., and Dils, R. (1964) Factors Effecting the Chain-Length of Fatty Acids Synthesised by Lactating-Rabbit Mammary Glands. *Biochim Biophys Acta* **84**, 776-778
6. Wakil, S. J. (1962) Enzymatic synthesis of fatty acids. *Comp Biochem Physiol* **4**, 123-158
7. Wakil, S. J. (1962) Lipid metabolism. *Annu Rev Biochem* **31**, 369-406
8. Mahler, H. R., Wakil, S. J., and Bock, R. M. (1953) Studies on fatty acid oxidation. I. Enzymatic activation of fatty acids. *J Biol Chem* **204**, 453-468
9. Wakil, S. J., Stoops, J. K., and Mattick, J. S. (1981) The fatty acid synthetase-structure-function relationship and mechanism of palmitate synthesis. *Cardiovasc Res Cent Bull* **20**, 1-23
10. Lin, C. Y., and Smith, S. (1978) Properties of the thioesterase component obtained by limited trypsinization of the fatty acid synthetase multienzyme complex. *J Biol Chem* **253**, 1954-1962

11. Smith, S., Agradi, E., Libertini, L., and Dileepan, K. N. (1976) Specific release of the thioesterase component of the fatty acid synthetase multienzyme complex by limited trypsinization. *Proc Natl Acad Sci U S A* **73**, 1184-1188
12. Jensen, R. G. (1999) Lipids in human milk. *Lipids* **34**, 1243-1271
13. Thompson, B. J., and Smith, S. (1985) Biosynthesis of fatty acids by lactating human breast epithelial cells: an evaluation of the contribution to the overall composition of human milk fat. *Pediatr Res* **19**, 139-143
14. Mikkelsen, J., Witkowski, A., and Smith, S. (1987) Interaction of rat mammary gland thioesterase II with fatty acid synthetase is dependent on the presence of acyl chains on the synthetase. *J Biol Chem* **262**, 1570-1574
15. Nolin, J. M., Thompson, B. J., and Smith, S. (1982) Localization of thioesterase II, the chain-length regulatory enzyme of milk fatty acid synthesis, in rat mammary gland epithelial cells. *J Endocrinol* **94**, 251-256
16. Smith, S., and Libertini, L. J. (1979) Specificity and site of action of a mammary gland thioesterase which releases acyl moieties from thioester linkage to the fatty acid synthetase. *Arch Biochem Biophys* **196**, 88-92
17. Libertini, L. J., and Smith, S. (1978) Purification and properties of a thioesterase from lactating rat mammary gland which modifies the product specificity of fatty acid synthetase. *J Biol Chem* **253**, 1393-1401
18. Lee, J. S., Sul, J. Y., Park, J. B., Lee, M. S., Cha, E. Y., Song, I. S., Kim, J. R., and Chang, E. S. (2013) Fatty Acid Synthase Inhibition by Amentoflavone Suppresses HER2/neu (erbB2) Oncogene in SKBR3 Human Breast Cancer Cells. *Phytother Res* **27**, 713-720

19. Tomek, K., Wagner, R., Varga, F., Singer, C. F., Karlic, H., and Grunt, T. W. (2011) Blockade of fatty acid synthase induces ubiquitination and degradation of phosphoinositide-3-kinase signaling proteins in ovarian cancer. *Mol Cancer Res* **9**, 1767-1779
20. Saati, G. E., and Archer, M. C. (2011) Inhibition of fatty acid synthase and Sp1 expression by 3,3'-diindolylmethane in human breast cancer cells. *Nutr Cancer* **63**, 790-794
21. Nguyen, P. L., Ma, J., Chavarro, J. E., Freedman, M. L., Lis, R., Fedele, G., Fiore, C., Qiu, W., Fiorentino, M., Finn, S., Penney, K. L., Eisenstein, A., Schumacher, F. R., Mucci, L. A., Stampfer, M. J., Giovannucci, E., and Loda, M. (2010) Fatty acid synthase polymorphisms, tumor expression, body mass index, prostate cancer risk, and survival. *J Clin Oncol* **28**, 3958-3964
22. Flavin, R., Peluso, S., Nguyen, P. L., and Loda, M. (2010) Fatty acid synthase as a potential therapeutic target in cancer. *Future Oncol* **6**, 551-562
23. Uddin, S., Hussain, A. R., Ahmed, M., Abubaker, J., Al-Sanea, N., AbdulJabbar, A., Ashari, L. H., Alhomoud, S., Al-Dayel, F., Bavi, P., and Al-Kuraya, K. S. (2009) High Prevalence of Fatty Acid Synthase Expression in Colorectal Cancers in Middle Eastern Patients and Its Potential Role as a Therapeutic Target. *Am J Gastroenterol* **104**, 1790-1801
24. Migita, T., Ruiz, S., Fornari, A., Fiorentino, M., Priolo, C., Zadra, G., Inazuka, F., Grisanzio, C., Palescandolo, E., Shin, E., Fiore, C., Xie, W., Kung, A. L., Febbo, P. G., Subramanian, A., Mucci, L., Ma, J., Signoretti, S., Stampfer, M., Hahn, W.

- C., Finn, S., and Loda, M. (2009) Fatty acid synthase: a metabolic enzyme and candidate oncogene in prostate cancer. *J Natl Cancer Inst* **101**, 519-532
25. Mashima, T., Seimiya, H., and Tsuruo, T. (2009) De novo fatty-acid synthesis and related pathways as molecular targets for cancer therapy. *Brit J Cancer* **100**, 1369-1372
26. Ogino, S., Nosho, K., Meyerhardt, J. A., Kirkner, G. J., Chan, A. T., Kawasaki, T., Giovannucci, E. L., Loda, M., and Fuchs, C. S. (2008) Cohort study of fatty acid synthase expression and patient survival in colon cancer. *J Clin Oncol* **26**, 5713-5720
27. Menendez, J. A., and Lupu, R. (2007) Fatty acid synthase and the lipogenic phenotype in cancer pathogenesis. *Nat Rev Cancer* **7**, 763-777
28. Lu, S., and Archer, M. C. (2005) Fatty acid synthase is a potential molecular target for the chemoprevention of breast cancer. *Carcinogenesis* **26**, 153-157
29. Baron, A., Migita, T., Tang, D., and Loda, M. (2004) Fatty acid synthase: a metabolic oncogene in prostate cancer? *J Cell Biochem* **91**, 47-53
30. Pizer, E. S., Pflug, B. R., Bova, G. S., Han, W. F., Udan, M. S., and Nelson, J. B. (2001) Increased fatty acid synthase as a therapeutic target in androgen-independent prostate cancer progression. *Prostate* **47**, 102-110
31. Sankaranarayananpillai, M., Zhang, N., Baggerly, K. A., and Gelovani, J. G. (2013) Metabolic shifts induced by fatty acid synthase inhibitor orlistat in non-small cell lung carcinoma cells provide novel pharmacodynamic biomarkers for positron emission tomography and magnetic resonance spectroscopy. *Mol Imaging Biol* **15**, 136-147

32. Seguin, F., Carvalho, M. A., Bastos, D. C., Agostini, M., Zecchin, K. G., Alvarez-Flores, M. P., Chudzinski-Tavassi, A. M., Coletta, R. D., and Graner, E. (2012) The fatty acid synthase inhibitor orlistat reduces experimental metastases and angiogenesis in B16-F10 melanomas. *Brit J Cancer* **107**, 977-987
33. Pellinen, J., and Szentirmai, E. (2012) The effects of C75, an inhibitor of fatty acid synthase, on sleep and metabolism in mice. *PLoS One* **7**, e30651
34. Puig, T., Aguilar, H., Cufi, S., Oliveras, G., Turrado, C., Ortega-Gutierrez, S., Benhamu, B., Lopez-Rodriguez, M. L., Urruticoechea, A., and Colomer, R. (2011) A novel inhibitor of fatty acid synthase shows activity against HER2+ breast cancer xenografts and is active in anti-Her2 drug-resistant cell lines. *Breast Cancer Res* **13**, R131
35. Pandey, P. R., Okuda, H., Watabe, M., Pai, S. K., Liu, W., Kobayashi, A., Xing, F., Fukuda, K., Hirota, S., Sugai, T., Wakabayashi, G., Koeda, K., Kashiwaba, M., Suzuki, K., Chiba, T., Endo, M., Fujioka, T., Tanji, S., Mo, Y. Y., Cao, D., Wilber, A. C., and Watabe, K. (2011) Resveratrol suppresses growth of cancer stem-like cells by inhibiting fatty acid synthase. *Breast Cancer Res Treat* **130**, 387-398
36. Notarnicola, M., Messa, C., Refolo, M. G., Tutino, V., Miccolis, A., and Caruso, M. G. (2011) Polyunsaturated fatty acids reduce Fatty Acid Synthase and Hydroxy-Methyl-Glutaryl CoA-Reductase gene expression and promote apoptosis in HepG2 cell line. *Lipids Health Dis* **10**
37. Mansour, M., Schwartz, D., Judd, R., Akingbemi, B., Braden, T., Morrison, E., Dennis, J., Bartol, F., Hazi, A., Napier, I., and Abdel-Mageed, A. B. (2011)

- Thiazolidinediones/PPARgamma agonists and fatty acid synthase inhibitors as an experimental combination therapy for prostate cancer. *Int J Oncol* **38**, 537-546
38. Chuang, H. Y., Chang, Y. F., and Hwang, J. J. (2011) Antitumor effect of orlistat, a fatty acid synthase inhibitor, is via activation of caspase-3 on human colorectal carcinoma-bearing animal. *Biomed Pharmacother* **65**, 286-292
39. Oliveras, G., Blancafort, A., Urruticoechea, A., Campuzano, O., Gomez-Cabello, D., Brugada, R., Lopez-Rodriguez, M. L., Colomer, R., and Puig, T. (2010) Novel anti-fatty acid synthase compounds with anti-cancer activity in Her2+ breast cancer. *Ann N Y Acad Sci* **1210**, 86-92
40. Murata, S., Yanagisawa, K., Fukunaga, K., Oda, T., Kobayashi, A., Sasaki, R., and Ohkohchi, N. (2010) Fatty acid synthase inhibitor cerulenin suppresses liver metastasis of colon cancer in mice. *Cancer Sci* **101**, 1861-1865
41. Liu, H., Liu, J. Y., Wu, X., and Zhang, J. T. (2010) Biochemistry, molecular biology, and pharmacology of fatty acid synthase, an emerging therapeutic target and diagnosis/prognosis marker. *Int J Biochem Mol Biol* **1**, 69-89
42. Dowling, S., Cox, J., and Cenedella, R. J. (2009) Inhibition of fatty acid synthase by Orlistat accelerates gastric tumor cell apoptosis in culture and increases survival rates in gastric tumor bearing mice *in vivo*. *Lipids* **44**, 489-498
43. Rae, C., and Graham, A. (2008) Fatty acid synthase inhibitor, C75, blocks resistin-induced increases in lipid accumulation by human macrophages. *Diabetes Obes Metab* **10**, 1271-1274
44. Weng, M. S., Ho, C. T., Ho, Y. S., and Lin, J. K. (2007) Theanaphthoquinone inhibits fatty acid synthase expression in EGF-stimulated human breast cancer

- cells via the regulation of EGFR/ErbB-2 signaling. *Toxicol Appl Pharmacol* **218**, 107-118
45. Vazquez-Martin, A., Colomer, R., Brunet, J., and Menendez, J. A. (2007) Pharmacological blockade of fatty acid synthase (FASN) reverses acquired autoresistance to trastuzumab (Herceptin by transcriptionally inhibiting 'HER2 super-expression' occurring in high-dose trastuzumab-conditioned SKBR3/Tzb100 breast cancer cells. *Int J Oncol* **31**, 769-776
46. Schmidt, L. J., Ballman, K. V., and Tindall, D. J. (2007) Inhibition of fatty acid synthase activity in prostate cancer cells by dutasteride. *Prostate* **67**, 1111-1120
47. Pan, M. H., Lin, C. C., Lin, J. K., and Chen, W. J. (2007) Tea polyphenol (-)-epigallocatechin 3-gallate suppresses heregulin-beta1-induced fatty acid synthase expression in human breast cancer cells by inhibiting phosphatidylinositol 3-kinase/Akt and mitogen-activated protein kinase cascade signaling. *J Agric Food Chem* **55**, 5030-5037
48. Kridel, S. J., Lowther, W. T., and Pemble, C. W. t. (2007) Fatty acid synthase inhibitors: new directions for oncology. *Expert Opin Investig Drugs* **16**, 1817-1829
49. Ho, T. S., Ho, Y. P., Wong, W. Y., Chi-Ming Chiu, L., Wong, Y. S., and Eng-Choon Ooi, V. (2007) Fatty acid synthase inhibitors cerulenin and C75 retard growth and induce caspase-dependent apoptosis in human melanoma A-375 cells. *Biomed Pharmacother* **61**, 578-587
50. Menendez, J. A., Mehmi, I., Verma, V. A., Teng, P. K., and Lupu, R. (2004) Pharmacological inhibition of fatty acid synthase (FAS): a novel therapeutic



- approach for breast cancer chemoprevention through its ability to suppress Her-2/neu (erbB-2) oncogene-induced malignant transformation. *Mol Carcinog* **41**, 164-178
51. Kridel, S. J., Axelrod, F., Rozenkrantz, N., and Smith, J. W. (2004) Orlistat is a novel inhibitor of fatty acid synthase with antitumor activity. *Cancer Res* **64**, 2070-2075
52. Kim, E. K., Miller, I., Aja, S., Landree, L. E., Pinn, M., McFadden, J., Kuhajda, F. P., Moran, T. H., and Ronnett, G. V. (2004) C75, a fatty acid synthase inhibitor, reduces food intake via hypothalamic AMP-activated protein kinase. *J Biol Chem* **279**, 19970-19976
53. Yeh, C. W., Chen, W. J., Chiang, C. T., Lin-Shiau, S. Y., and Lin, J. K. (2003) Suppression of fatty acid synthase in MCF-7 breast cancer cells by tea and tea polyphenols: a possible mechanism for their hypolipidemic effects. *Pharmacogenomics J* **3**, 267-276
54. Qiao, S., Pennanen, P., Nazarova, N., Lou, Y. R., and Tuohimaa, P. (2003) Inhibition of fatty acid synthase expression by 1alpha,25-dihydroxyvitamin D3 in prostate cancer cells. *J Steroid Biochem Mol Biol* **85**, 1-8
55. Brusselmans, K., De Schrijver, E., Heyns, W., Verhoeven, G., and Swinnen, J. V. (2003) Epigallocatechin-3-gallate is a potent natural inhibitor of fatty acid synthase in intact cells and selectively induces apoptosis in prostate cancer cells. *Int J Cancer* **106**, 856-862

56. Liu, B., Wang, Y., Fillgrove, K. L., and Anderson, V. E. (2002) Triclosan inhibits enoyl-reductase of type I fatty acid synthase in vitro and is cytotoxic to MCF-7 and SKBr-3 breast cancer cells. *Cancer Chemother Pharmacol* **49**, 187-193
57. Dodson, G., and Wlodawer, A. (1998) Catalytic triads and their relatives. *Trends Biochem Sci* **23**, 347-352
58. Haushalter, R. W., Worthington, A. S., Hur, G. H., and Burkart, M. D. (2008) An orthogonal purification strategy for isolating crosslinked domains of modular synthases. *Bioorg Med Chem Lett* **18**, 3039-3042
59. Meier, J. L., Mercer, A. C., Rivera, H., Jr., and Burkart, M. D. (2006) Synthesis and evaluation of bioorthogonal pantetheine analogues for *in vivo* protein modification. *J Am Chem Soc* **128**, 12174-12184
60. Mandel, A. L., La Clair, J. J., and Burkart, M. D. (2004) Modular synthesis of pantetheine and phosphopantetheine. *Org Lett* **6**, 4801-4803

## CURRICULUM VITAE

Melissa Kay Ritchie  
Wake Forest School of Medicine (WFSM)  
Department of Biochemistry  
Center for Structural Biology  
Winston-Salem, NC 27157  
E-mail:[mritchie@wakehealth.edu](mailto:mritchie@wakehealth.edu)

### EDUCATION

Doctorate of Philosophy, Wake Forest School Of Medicine, Department of Biochemistry, Center for Structural Biology, Winston-Salem, NC 27106 (August 2013)

Uncovering the Molecular Basis for Fatty Acid Synthase Product Specificity: Structural and Kinetic Evaluation of Thioesterase 1 and Thioesterase 2. Dissertation Research Project (2007-2013), Dr. W. Todd Lowther, Department of Biochemistry, Center for Structural Biology.

B.S. Biochemistry with Minor in Chemistry, Virginia Polytechnic and State University, Blacksburg, VA (Fall 2006) *Cum Laude*

Synthesis and Crystallization of Iridium Hydride Amino Acid Complexes, Undergraduate Research Project (2005-2006), Dr. Joseph Merola, Department of Chemistry.

### EMPLOYMENT

Lab Technician, Nanosonic, Inc., Blacksburg, VA 24060 (January-July 2007)

Undergraduate Teaching Assistant, Virginia Polytechnic and State University, Blacksburg, VA (2006) Dr. Michael Berg, Department of Chemistry

### PROFESSIONAL MEMBERSHIPS

Virginia Academy of Science (2006)

### HONORS AND AWARDS

John Lee Pratt Foundation – Scholarship (2005-06) \$3,000, College of Agriculture and Life Sciences, Virginia Polytechnic and State University.

Sandy Lee Cowgill Memorial Scholarship Fund (2009) - \$2,500, Department of Biochemistry, Wake Forest School of Medicine.

Outstanding Oral Presentation (2013) – \$250, 43<sup>rd</sup> Mid-Atlantic Macromolecular Crystallography Meeting, Duke University

## SCIENTIFIC PRESENTATIONS

Synthesis and Crystallization of Iridium Hydride Amino Acid Complexes (Undergraduate Student Research Day, Virginia Tech, April 2006)

Consequences of TREX I Mutations in Autoimmune Disease (Departmental Seminar, WFSM April 2008)

Human Thioesterase II, A Novel Serine Hydrolase that Modifies the Acyl Product Distribution of Fatty Acid Synthase (Departmental Seminar, WFSM September 2008; Poster Session, WFSM Biochemistry Research Day, September 2009)

Characterization of Recombinant and Endogenous Human Thioesterase II and Its Relevance in Cancer Biology (Departmental Seminar, WFSM November 2009)

Characterization of Human Thioesterase II and Its Implications in Breast Cancer Drug Discovery (Poster Session, WFUSM Graduate Student Research Day, March 2010; Poster Session, AACR 101<sup>st</sup> Annual Meeting April 2010)

Characterization of Thioesterase I and II Interactions with an Acylated Acyl Carrier Protein Substrate: An Additional Strategy for Fatty Acid Synthase Drug Discovery (Poster Session, WFSM Graduate Student Research Day, March 2011; Biochemistry Research Day, September 2012)

Characterization of Thioesterase I and II Interactions with an Acylated Acyl Carrier Protein Substrate: An Additional Strategy for Fatty Acid Synthase Drug Discovery (Departmental Seminar, WFSM, November 2012)

Crystal Structure of Human Thioesterase 2: Insights into the Molecular Basis for the Novel Modulation of Fatty Acid Synthase Activity (Selected Presentation, 43<sup>rd</sup> Mid-Atlantic Macromolecular Crystallography Meeting, Duke University, June 2013)

## PUBLICATIONS

Berg, M., Ritchie, M. and Joseph Merola. Synthesis and crystals of 3-alkyl-2,4-pentanedionates and 3-phenyl-2,4-pentanedionate of palladium. *Polyhedron*, Vol. 38, No. 1. (May 2012), pp. 126-130

Ritchie, M., Clodfelter, J., Johnson, L. and Lowther, W. T. Crystal Structure of Human Thioesterase 2: Insights into the Molecular Basis for the Novel Modulation of Fatty Acid Synthase Activity (Manuscript to be published Summer 2013)

## **ADDITIONAL ACTIVITIES & ACCOMPLISHMENTS**

Mentor/Running Coach for Girls On The Run, El Buen Pastor, Winston-Salem, NC 27106 (Spring 2010)

Community outreach program sponsored by The Junior League. This program is designed to build the foundation of health and exercise, as well as healthy body image, social interactions, and self esteem as it relates not only inward but outward in everyday situations. This program is specific for elementary girls, grades 3<sup>rd</sup> through 5<sup>th</sup>. The end of each term is seeded with participation in a local 5K race.

Science Fair Mentor, Cook Elementary, Winston-Salem, NC 27106 (Fall 2012)

We are given the opportunity to mentor a family who has a child with a desire to participate in the school-sponsored science fair. This program provides education, one-on-one engagement between students and parents and their respective mentor. All materials are provided at no cost, and the only requirement is for the student to willingly participate and follow through with presenting their project at the science fair

Group Fitness Instructor, Les Mills Body Pump, Gold's Gym Winston-Salem (March 2012 to present)

As a group fitness instructor, I regularly engage participants and lead them through total body weight training exercises. For each hour-long class, I prepare a set list of music, memorize choreography and practice coaching and motivational cues so that my participants receive consistent and effective direction throughout their workouts. My effectiveness as a leader and role model for endurance and performance of all the exercises provides an atmosphere which motivates participants to consistently engage in exercise activity.